# Application of Force Actuators and Variable Stiffness Systems with Base Isolation

by

Phillip M. Lavallee

MBA
Colorado State University, 2006

B. S. Civil Engineering
Syracuse University, 1997

SUBMITTED TO THE DEPARTMENT OF CIVIL AND ENVIRONMENTAL ENGINEERING IN PARTIAL FULFILLMENT OF THE REQUIREMENTS FOR THE DEGREE OF

MASTER OF ENGINEERING IN CIVIL AND ENVIRONMENTAL ENGINEERING
AT THE
MASSACHUSETTS INSTITUTE OF TECHNOLOGY

JUNE 2008

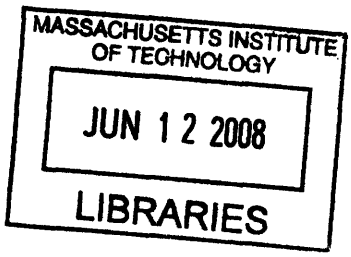






Signature of Author: _____
Department of Civil and Environmental Engineering
May 05, 2008

Certified by: _____
Jerome J. Connor
Professor of Civil and Environmental Engineering
Thesis Supervisor

Accepted by: _____
Daniele Veneziano
Chairman, Departmental Committee for Graduate Students

# Application of Force Actuators and Variable Stiffness Systems with Base Isolation

by

Phillip M. Lavallee

Submitted to the Department of Civil and Environmental Engineering on May 05, 2008 in Partial Fulfillment of the Requirements for the Degree of Master of Engineering in Civil and Environmental Engineering

ABSTRACT

Recent developments have occurred that limit the effectiveness of conventional strength-based structural design. First, there has been a trend towards designing more flexible structures that require increased emphasis on structural motion and serviceability. Next, motion has become more important for the design of new facilities that house very sensitive manufacturing and operating equipment. This equipment can only operate properly under extremely low movement conditions. Third, advances in material science and engineering have led to developing materials with significantly increased strengths, but the stiffness of these materials have not increased at the same rate. Motion parameters control the design for these high-strength materials. Finally, recent earthquake responses have shown that repair costs from structural damage due to inelastic deformation that was much greater than anticipated. This has led to a trend in reducing the reliance on inelastic deformation in the structure to dissipate energy, and designing control of the response with other energy dissipation and absorption devices. Motion-based design is more effective to address the developments mentioned above. To control the motion of civil structures from earthquake excitations, base isolation systems have become more common to uncouple the structure from the ground. Base isolation reduces the lateral stiffness of the bottom floor to allow large movement of the structure as a rigid body for earthquake excitations. For lower service loads such as wind, the lateral stiffness of the isolation bearings is insufficient to prevent the structure from large movement and uplift. Variable stiffness systems have been used to adjust lateral stiffness based on the size of the load experienced. This thesis proposes using force actuators to increase and decrease lateral stiffness by clipping and unclipping horizontal members when the ground acceleration reaches preset threshold limits. When clipped, the structure responds as a conventional strength-based designed structure. When unclipped, the structure responds as a base isolated structure. After an event is complete, the actuators re-clip and the structure is prepared for the next event.

Thesis Supervisor: Jerome J. Connor
Title: Professor of Civil and Environmental Engineering

## Acknowledgements

To Shelley and Gavin: You are the inspiration for everything I do. I could not have completed this document or degree without having you to come home to every night to give me the support and drive to get up and work on it again the next day. "Daddy's home!" will forever be ringing in my ears. You are my life, and I love you very much.

To Mom and Dad: I cannot thank you enough for watching Gavin on countless weekends to afford me the time required to complete my work. This is just one additional amazing show of support that you have provided for me for the past 32 years. I am thankful everyday for having the best parents in the world. I love you.

To Creighton and Carmella: I also cannot thank you enough for welcoming us into your home for a year, and the incredible support you have provided to Shelley, Gavin and I. There is no way that I could have made it through without your assistance and help with raising Gavin. We will miss being with you daily and are lucky to have such wonderful, supportive parents.

To Simon Lafalmme: Thank you for giving me direction and focus for this thesis. I could not have completed this without your guidance and continuous review of my work. I have learned a lot from this exercise and most of it is due to your interest and guidance.

To Professor Connor: It has been a true honor and privilege to have learned from such an amazing educator. Your enthusiasm towards the field of structural engineering and teaching others to carry it on in the future cannot be matched. Thank you for your guidance and assistance with completing this demanding and rewarding program.

Finally, to the MEng Class of 2008: Thank you for dragging the old guy through this long, difficult year. Your support with bringing me back up to speed with the mathematics and learning new complex subjects were essential to me completing this degree. It has been an honor working with you and good luck with everything you do. You are some of the most intelligent, amazing people I have ever met. Go out and perform great things. I will never forget this year.

## Table of Contents

## List of Figures

## List of Tables

# 1.0 INTRODUCTION

## 1.1 Conventional Strength-Based Design vs. Motion-Based Design

Conventional structural design for buildings is based on the strength of the structure and its capacity to support gravity and applied vertical and lateral loads, and to dissipate earthquake-induced energy. The main two requirements for the design procedures are safety and serviceability. Safety is related to extreme loads that have a very low 2% probability of occurrence during the structure's life (Connor, 2003). Typical concerns regarding safety are significant structural damage, collapse, and loss of life. Serviceability is related to medium to large loads that have a higher 10-50% probability of occurrence during the structure's life (Connor, 2003). For serviceability, the motion experienced by the structure should allow operational capabilities to continue, and be below the comfort levels for humans and sensitive equipment.

Strength-based design requires the resistance of the individual structural elements to be greater than the extreme loads expected to act on the structure. Stiffness properties are determined for the structure after it is proportioned, and serviceability constraints are then checked for adequacy. This approach to design is appropriate when strength is the dominant design requirement, as typically has been the case in the past.

As explained in Connor 2003, four recent developments have occurred that tend to limit the effectiveness of strength-based design. First, there has been a trend towards designing more flexible structures that require increased emphasis to be placed on

structural motion and serviceability. Next, motion has also become more important for the design of new facilities that house very sensitive manufacturing and operating equipment. This equipment can only operate properly under extremely low movement conditions. Third, advances in material science and engineering have led to developing materials with significantly increased strengths, but the stiffness of these materials have not increased at the same rate. Motion parameters control the design for these high-strength materials. Finally, recent earthquake responses have shown that the repair costs from structural damage due to inelastic deformation was much greater than anticipated. This has led to a trend in reducing the reliance on inelastic deformation in the structure to dissipate energy, and designing control of the response with other energy dissipation and absorption devices.

Motion-based design is more effective to address the developments mentioned above. Engineers must optimize the materials, motion control devices, and deployment locations, to achieve the desired design for motion, while still meeting the strength constraints.

## 1.2 Economics of Motion Controlled Structures

As discussed above, the repair costs of structures damaged in recent earthquakes has been significantly greater than estimated. The traditional strength-based design mainly considers only elastic behavior and limiting life safety issues. The performance of structures in recent earthquakes has resulted in limited loss of life, proving that the strength-based design has performed well in that respect. The

economic results from the earthquakes have not been as favorable by only considering the strength of the structure. One example is the 1994 Northridge earthquake where at least $20 billion in damage resulted from the excitation (Celikbas, 1999). These large dollar values have become extremely important to building owners and operators, and have increased the importance of cost as a major factor in the design and construction process.

Connor et al, 1997 illustrate the potential economic benefit of using a motion-based design approach to reduce the damage caused during earthquake events. Figure 1 shows the relationship between the repair cost and the earthquake intensity level for conventional and motion controlled designs (Iwata, 1994). Based on this plot, motion-based design is most effective for moderately large earthquakes.

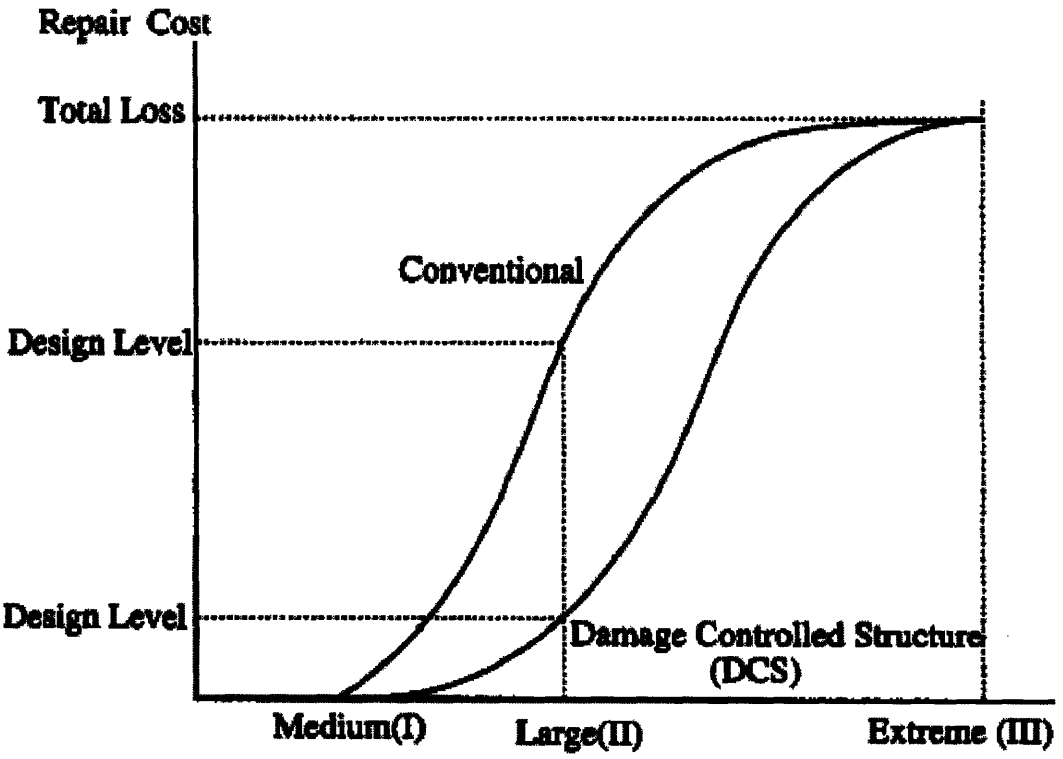


**Figure 1: Repair Cost versus Earthquake Intensity (Connor et al, 1997)**

## 2.0 BASE ISOLATION SYSTEMS

Over the past several decades, isolation design has been frequently used to isolate systems for vibrating machinery. The main benefits to isolating the machinery or sensitive equipment are to reduce the effect of the load that is transmitted to the support floor or structure, or to reduce the effect on the equipment from the movement of the support. The later example is typical for buildings that are located next to railroad tracks or other sources of ground disturbance.

Although this design strategy has been used for a long period of time for machinery isolation, only recently has the concept been seriously considered for civil structures subjected to ground motion (Connor, 2003). Ground isolation is beneficial since ground motion interacts directly with the foundation of the structure, and the force generated is then transmitted up throughout the structure. The idea of seismic isolation dates back to the late nineteenth century, but the lack of capable commercial isolation components delayed the application. Substantial development began in the 1980's and continues today (Naeim and Kelly, 1999). The seismic engineering community now considers base isolation for some civil structures a viable option for moderate to extreme seismic excitation (Wada, 1998).

Horizontal ground motion during earthquakes causes the most damage to structures. Isolation systems installed at the base uncouple the buildings from the ground motion, and allow the entire structure to move independent of the earthquake. This isolation layer reduces the fundamental frequency of the structure to a value lower than its fixed-base

frequency and the predominant frequencies of the ground motion. The first dynamic mode of the isolated structure involves deformation only in the isolation system and the structure above remains rigid and moves as a unit. The higher modes that will produce deformation in the structure are orthogonal to the first mode and to the ground motion. These higher modes do not participate in the motion, so that if there is high energy in the ground motion at these higher frequencies, this energy cannot be transmitted into the structure. The isolation system does not absorb the earthquake energy, but rather deflects it through the dynamics of the system (Kelly, 1998).

When base isolation systems are used the structure moves as a rigid body due to the reduced absolute motion of the structure and the associate inertia forces. The story shear forces decrease and the loads on the structure and it occupants and contents are reduced. Reducing the interstory drift results in less structural damage, and less damage to nonstructural components and internal equipment, as illustrated in Figure 2.

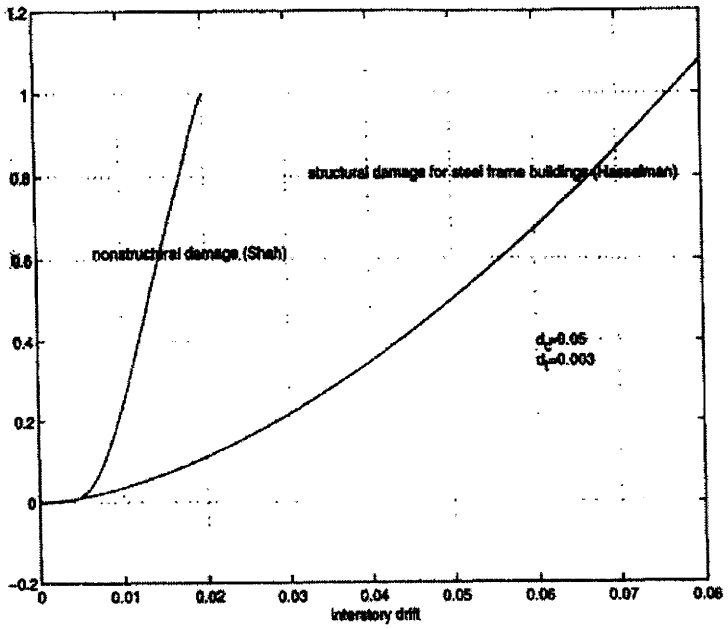


**Figure 2: Interstory Drift versus Damage (Celikbas, 1999)**

## 2.1 Isolation Bearings

Connection of base isolation systems between the foundation and the structure is accomplished through the use of some type of bearings to constrain against motion relative to a support plane. The bearings resist against vertical displacements caused by gravity and vertical applied loads, and against horizontal displacement caused by lateral loads through shear capacity over the height of the bearing. The vertical motion is resisted by axial bearings, such as spring and rubber cushions with axial stiffness. The horizontal motion is resisted by shear bearings, such as laminated rubber cushions or inverted pendulum-type sliding devices with shearing stiffness. Typically, the shearing or lateral stiffness is low for the bearings relative to the stiffness of the structure to enable large movement. When designing against seismic excitation, the horizontal motion is more significant because it leads to horizontal loading. The vertical motion due to the earthquake is supported by structures that are typically designed for the vertical loads. These additional loads can usually be supported by the original design since they are equivalent to adding vertical loads.

Various types of bearings are used for base isolation systems, including air spring/damper bearings for vertical excitations, sleeved piles, inverted pendulum bearings, laminated rubber bearings, natural rubber bearings (NRB), lead rubber bearings (LRB), and other combinations of these. Appendix C includes photos of various bearing examples.

## 2.2 Basic Design Issues

When designing base isolation systems, the simplified single-degree-of-freedom (SDOF) model shown Figure 3 can be used for rigid structures. A similar model can be developed for flexible structures as a multiple-degree-of-freedom (MDOF) system. The model used for this analysis of force actuators in conjunction with base isolation is explained in Section 3.

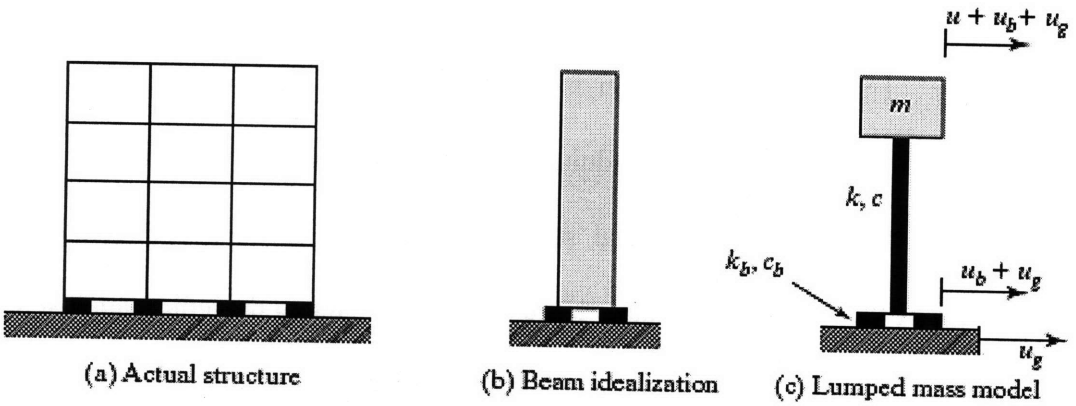


**Figure 3: Base isolation model (Connor, 2003)**

Isolation system design consists of flexibility, rigidity under low-level lateral loading, and energy dissipation. The flexible supports are designed to ensure that the natural period of vibration of the isolated structure is greater than the dominant period of the excitation. This is accomplished by the various bearings mentioned in Section 2.1. The most common system used to date is the rubber bearing isolation system. These bearings have layers of natural rubber sheets bonded to steel plates as shown in Figure 4. The steel plates are required to restrict the rubber from exploding out horizontally due to the large vertical loads. The lateral stiffness of the bearings depends on the size and number of rubber sheets. Rubber is favored in these designs

because of its very large deformation capabilities. The rubber can deform up to 300% without permanent damage. A typical strain for used design is on the order of 100%.

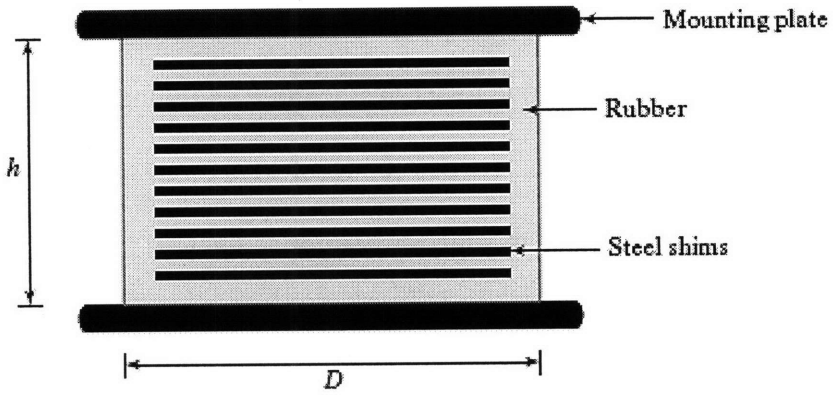


**Figure 4: Typical NRB (Connor 2003)**

As explained by Kelly, the shear stiffness of this rubber is high for small strains but decreases by a factor of about four or five as the strain increases, reaching a minimum value at a shear strain of 50%. For strains greater than 100%, the stiffness begins to increase again, providing a fail-safe action under a very high load. The damping follows the same pattern but less dramatically, decreasing from an initial value of 20% to a minimum of 10% and then increasing again. The design of the system assumes minimum values of stiffness and damping and a linear response. The high initial stiffness is invoked only for wind load design and the large strain response only for fail-safe action (Kelly, 1998).

Rigidity under low-level lateral loads is what VSS and force actuators improve. The lateral flexibility of the isolation system allows large relative motion between the structure and the support, but it significantly reduces the absolute structural motion for uncoupling purposes. Other service lateral loads, such as wind, cause very

different results. The low lateral stiffness results in large lateral displacement of the structure relative to the support, which is undesirable. Significant moments that develop at the base due to wind loading can cause the bearings to move into tension. To control the lateral motion due to service loading, additional stiffness is required at the base that will function for the service-level loads, but not for high-level loads. Systems have been developed to support the service loads elastically, but then deform inelastically and yield for the high-level loads. Steel and lead dampers combined with rubber bearings have been used and are illustrated in Figure 5 and Figure 6. The rods are designed to provide initial stiffness up to a prescribed threshold, and yield after the threshold is met or exceeded. VSS and force actuators are being proposed as an alternative to the rods described above as a stiffness mechanism. Damping will need to be provided by some other devices, such as viscous dampers.

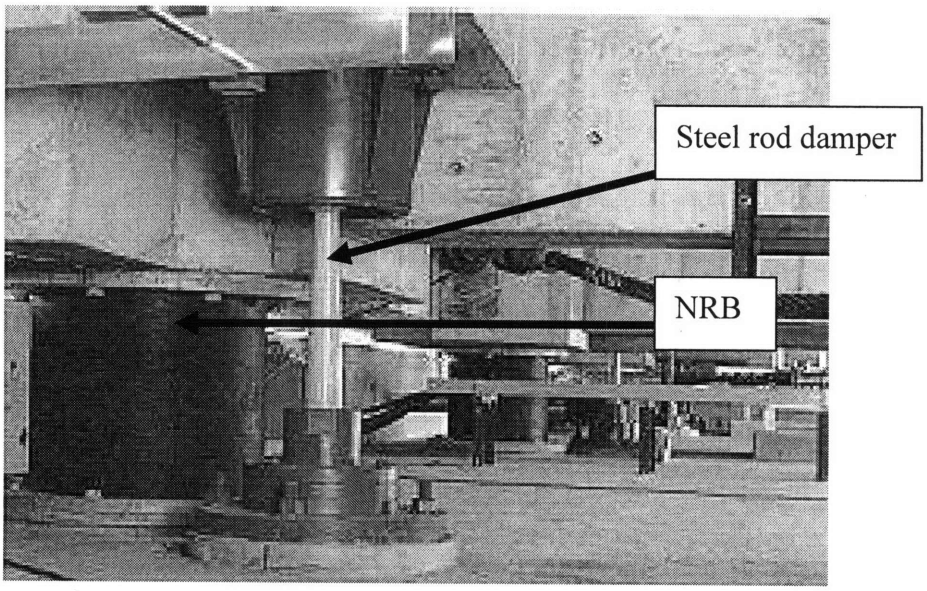


**Figure 5: Steel rod damper with NRB (Connor, 2003)**

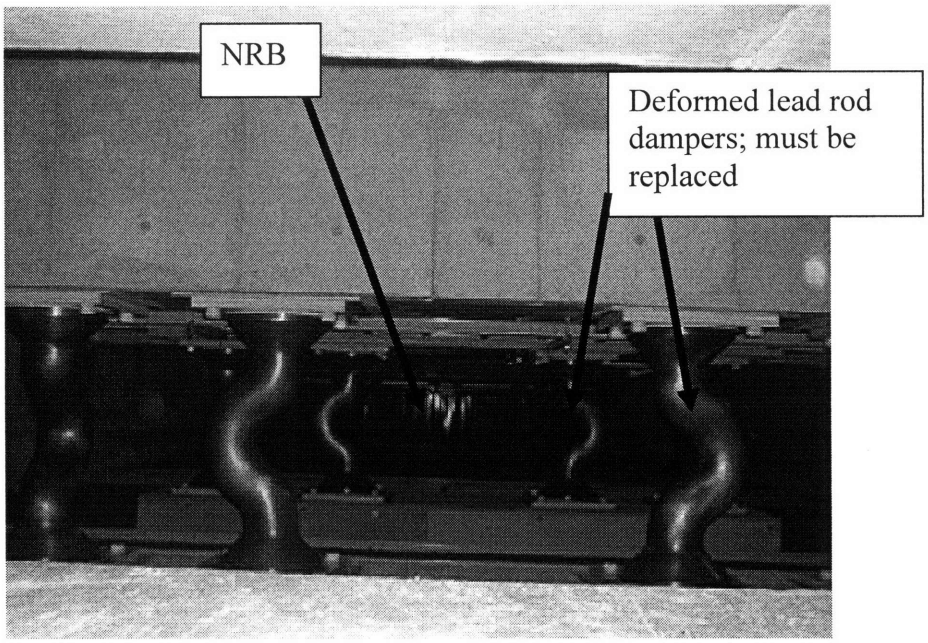


**Figure 6: Lead rod damper with NRB (Connor, 2003)**

The bearing systems used for isolation do have some energy dissipation capacity, but not enough to reduce the effect on the structure. Additional devices are often provided in conjunction with the bearings to increase the energy dissipation capacity of the system. The rods described above that increase the initial lateral stiffness also serve as energy dissipation devices once yielding occurs. The yielding is called hysteretic damping, and only occurs during high level loading events. Since hysteretic damping only occurs for high-level loads, viscous and friction damping devices are also used to dissipate energy. Figure 7 shows a system with these devices used in combination in the Bridgestone Toranomon Building. Additional information regarding hysteretic damping is described in Section 6.

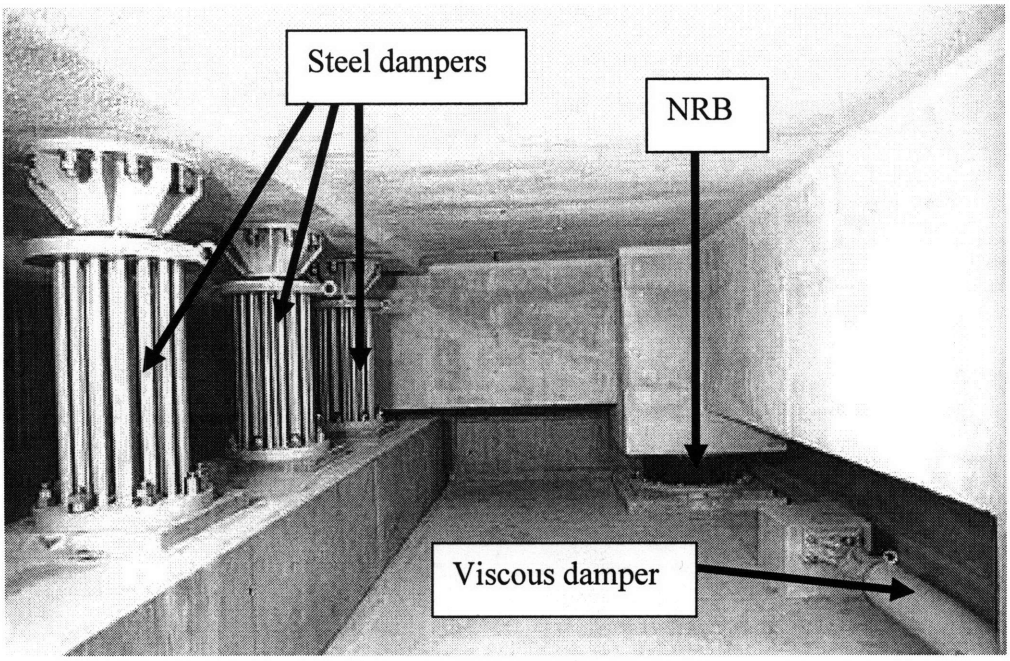


**Figure 7: Combination of NRBs, steel dampers, and viscous dampers used in the Bridgestone Toranomon Building (Connor, 2003)**

## 2.3 Applicability of Base Isolation Systems

The use of base isolation depends on two main factors. First is the suitability of the structure. A structure is said to be suitable if subsoil conditions do not produce motions with long period input to the structure, the height of the structure is 10-15 stories, the height-to-width ratio prevents overturning, the site allows the required base motion capacity relative to the ground, and the non-seismic lateral loads are less than 10% of the structure weight (Connor, 2003). Although the typical application of base isolation is for structures below 15 stories, there have been systems used on taller structures. An example is the Los Angeles City Hall seismic retrofit on the 32-story structure.

The second major factor in determining whether or not to use base isolation is the cost effectiveness. Cost analysis must consider the total life cycle cost, including the initial design and construction costs, the long-term maintenance costs, and the estimated structural repair costs due to seismic induced damage. Reduction in structural damage is the key reason to isolate a structure. Historically, the most significant costs have been in the repair and replacement of the structure and the contents of the building. The ultimate cost saving is in the loss of life, and this is difficult to put an actual price tag on. A tradeoff analysis must be conducted early in the design process to determine if the facility can withstand any disruption in operations. If it can be disrupted without significant consequences, then the higher cost of isolation may not be appropriate. If the building is essential and must remain operational, then the cost would be worth it.

## 2.4 Base Isolation Systems in the United States

### 2.4.1 Foothill Communities Law & Justice Center

**Figure 8: Foothill Communities Law and Justice Center (Kelly, 1998; Photo: I. D. Aiken)**

Constructed in 1985, this was the first base-isolated building in the United States. It is a $30 million legal services center located about 60 miles (97 km) east of downtown Los Angeles, 12 miles (20 km) from the San Andreas fault. The building is four stories with a full basement and sub-basement for the isolation system. The isolation system consists of 98 NRB bearings reinforced with steel plates. The superstructure of the building has a structural steel frame stiffened by braced frames in some bays. San Bernardino was the first county in the U.S. to have a thorough earthquake preparedness program, and asked that this building be designed for a Richter magnitude 8.3 earthquake, the maximum credible earthquake for that site. The design selected for the isolation system, which accounted for possible torsion, incorporated a maximum horizontal displacement demand of 380 mm (15 in.) in the isolators at the corners of the building. Tests of full-scale sample bearings verified this capacity (Kelly, 1998).

### 2.4.2 University of Southern California (USC) Hospital

**Figure 9: USC Hospital (Kelly, 1998; Photo: P. W. Clark)**

The USC Teaching Hospital in eastern Los Angeles is an eight-story concentrically braced steel frame supported on 68 lead rubber isolators and 81 elastomeric isolators. The California Strong Motion Instrumentation Program instrumented the building soon after its completion in 1991. The foundation system consists of spread footings and grade beams on rock. The plan shown in Figure 10 and the elevation of the building are irregular due to functional requirements. The two wings on each side of the building are connected by the "necked-down" portion of the building, and in the original fixed-base design the irregular configuration led to both coupling between the lateral and torsional vibration modes and very large shear force demands in the slender region between the two rings. Even in the isolated design steel trusses are required to carry the shears in the necked-down region. These were two of the main reasons that seismic isolation was eventually chosen for this structure. The structure was 23 miles (36 km) from the epicenter of the $M_w$ 6.8 1994 Northridge earthquake. The peak ground acceleration outside the building was 0.49 g, and the accelerations

inside the building were around 0.10 to 0.13 g. In this earthquake the structure was effectively isolated from ground motions strong enough to cause significant damage to other buildings in the medical center. The records obtained from the USC hospital are particularly encouraging in that they represent the most severe test of an isolated building to date (Kelly, 1998).

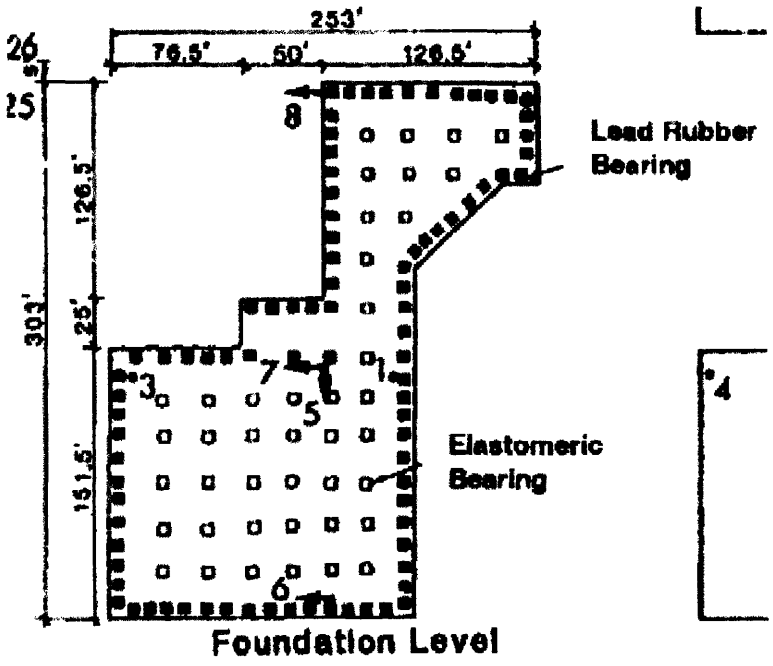


**Figure 10: USC Plan & Base-Isolation System (Nagarajaiah, Xiaohong, 2000)**

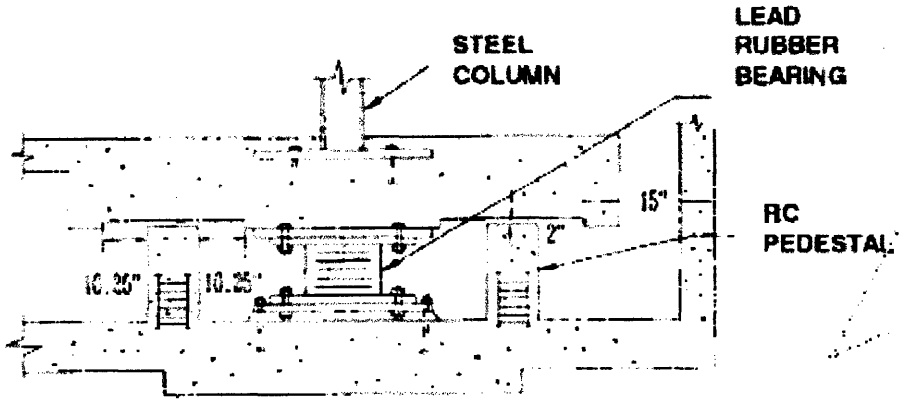


**Figure 11: USC Isolation System Detail (Nagarajaiah, Xiaohong, 2000)**

### 2.4.3 Los Angeles City Hall

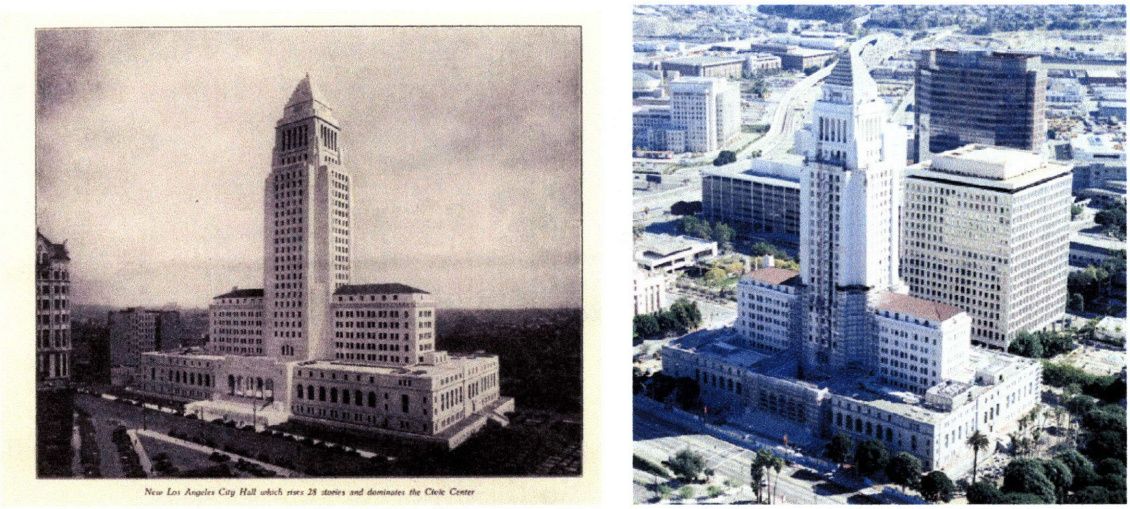


**Figure 12: LA City Hall in 1931(Wikipedia) and 2001 (Bovis, 2001)**

This landmark building is 32 stories (454 feet) tall, and was completed in 1928. Although the structure survived hundreds of earthquakes throughout its history, a major seismic retrofit was completed in 2001. Over 526 isolators and sliders were inserted into the columns and under the walls just below the existing foundations. The rubber isolators allow movement of 22 inches in any direction. 52 viscous dampers were also installed in the basement and 12 were installed in the tower. A moat was created around the structure to permit 2.5 feet of movement in any lateral direction (Bovis, 2001).

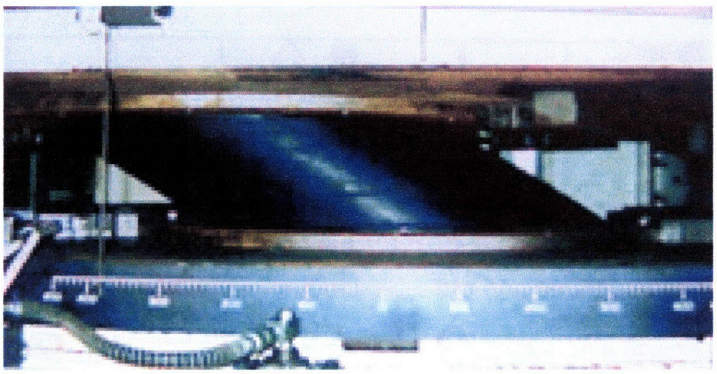

**Figure 13: NRB being tested for LA City Hall (LA DPW)**

### 2.4.4 Los Angeles County Fire Command & Control Facility (FCCF)

**Figure 14: LA County Fire Command & Control Facility (Kelly, 1998)**

Completed in 1990, a high-damping rubber base-isolation system was installed for the Los Angeles County (LAC) Fire Command & Control Facility. The building houses the computer systems for the emergency services of the county and is required to remain functional after an extreme event. The decision to use base isolation for this project was reached by comparing conventional and isolation schemes designed to provide the same degree of protection. In most projects, the isolation design costs 5% more. Not only was the isolation design estimate 6% less in this case, but also it is less for any building when equivalent levels of protection are considered. These estimates are for the initial costs. Once life-cycle costs are added, it becomes even more favorable (Kelly, 1998).

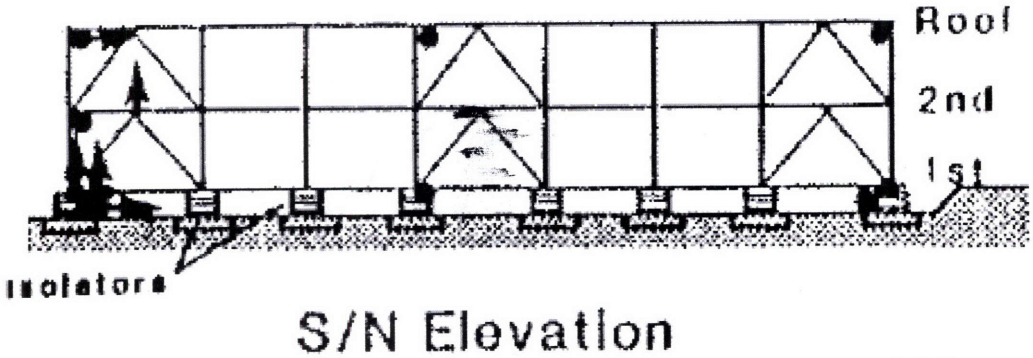


**Figure 15: LAC FCCF Elevation, Isolator Locations (Nagarajaiah, Xiaohong, 2001)**

## 3.0 HYSTERETIC DAMPING

Conventional structural design relies on the primary structural system to dissipate the energy induced by earthquakes by inelastic deformation of the members. The strong-column-weak-beam approach allows plastic deformation to occur at the beam-ends and contributes to the ductility of the building. As mentioned previously, this deformation is permanent and may require significant structural repairs to maintain operability.

Hysteretic damping is the introduction of a secondary structural system or damping devices that are capable of undergoing inelastic deformation before the primary structure yields. This would maintain the integrity of the structure, improve life safety, and ultimately reduce the cost of repair.

The lead and steel rods mentioned previously are examples of hysteretic damping. Another commonly used device is the Unbonded Brace developed by Nippon Steel Corporation illustrated in Figure 16. These members have a low-strength steel core that is encased in a concrete filled steel tube. A material is applied to the member that ensures no bond develops between the core and the encasement. The steel is allowed to yield independently of the support. The goal is to select material to ensure the buckling load of the brace equals the yield force of the core. These devices have been used in many building applications in the U. S. and around the world.

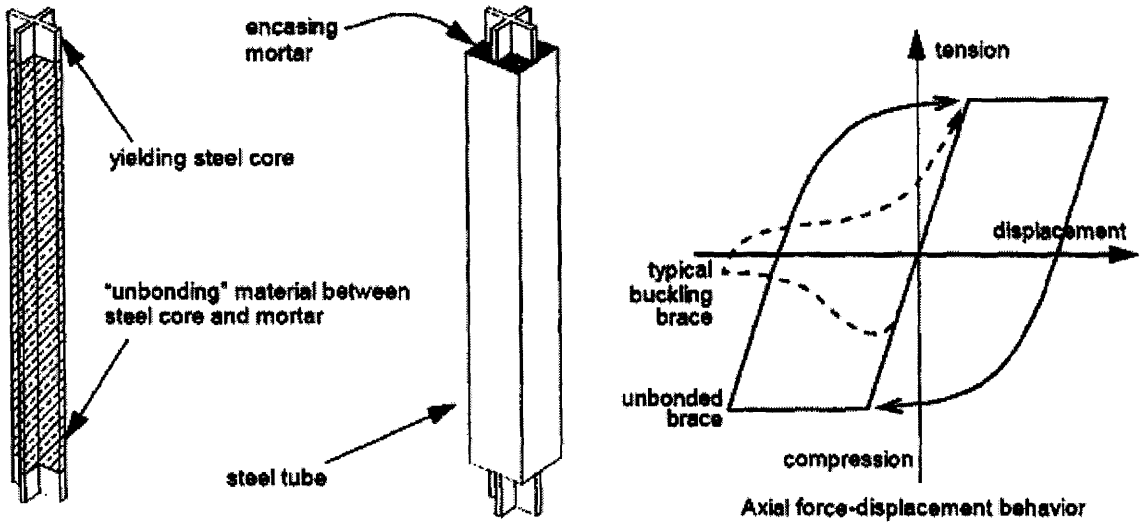


**Figure 16: Unbonded brace (Aiken et al, 1999)**

## 4.0 ACTIVE VARIABLE STIFFNESS SYSTEM

Yang, Li and Wu 1994 presents an evaluation of the performance of an active variable stiffness system (AVS) used in conjunction with control methods based on the theory of variable structure system or sliding mode control. Active control of buildings has received a lot of attention in the past two decades. Variable stiffness systems are one type of control system that has been researched and tested.

The AVS system consists of braces that are installed in selected locations throughout a structure on various stories with locking and unlocking devices. When an earthquake excitation is sensed, some of the bracings may be locked at certain times to increase the stiffness of the corresponding story. A control algorithm regulates the locking and unlocking of different braces at each time to reduce the structural response due to the earthquake.

An 8-story building model was evaluated based on the El Centro earthquake (NS component) excitation scaled to the maximum ground acceleration of 0.3g. Constant mass, stiffness and damping were assumed for each story in the model.

Table 1 shows the results of the evaluation. Columns 2 and 3 show the maximum interstory drifts and maximum floor accelerations without control or the use of AVS; columns 4 and 5 show the results with the control algorithm for the AVS used; and columns 6 and 7 show the results with all of the braces locked continuously. Based on these results, the AVS is effective in reducing the building response.

**Table 1: Maximum Response Quantities of an 8-Story Building (Yang, Li, Wu 1994)**

| ST. NO (1) | No Control | | AVS | | Passive | |
|---|---|---|---|---|---|---|
| | $x_i$ (2)* | $\ddot{x}_{ai}$ (3)* | $x_i$ (4) | $\ddot{x}_{ai}$ (5) | $x_i$ (6) | $\ddot{x}_{ai}$ (7) |
| 1 | 2.80 | 240 | 1.40 | 1556 | 1.94 | 267 |
| 2 | 2.78 | 349 | 1.37 | 1356 | 1.87 | 366 |
| 3 | 2.69 | 386 | 1.31 | 1464 | 1.76 | 481 |
| 4 | 2.52 | 404 | 1.20 | 1440 | 1.62 | 551 |
| 5 | 2.24 | 450 | 1.04 | 1309 | 1.42 | 612 |
| 6 | 1.84 | 533 | 0.93 | 1193 | 1.17 | 686 |
| 7 | 1.32 | 624 | 0.74 | 1103 | 0.86 | 786 |
| 8 | 0.69 | 680 | 0.41 | 820 | 0.46 | 912 |

* $x_i$ in cm and $\ddot{x}_{ai}$ in cm/s$^2$

## 5.0 SEMI-ACTIVE HYBRID ISOLATION SYSTEM

Agrawal and Yang 2000 proposes and analyzes the use of a resetting or switching semi-active stiffness damper (RSASD or SSASD) to reduce the structural response due to earthquake excitations. The semi-active stiffness properties of the device are similar to the proposed use of the force actuators analyzed in this thesis. Just as the force actuators, the RSASD and SSASD can be installed between the base isolation system and the foundation as shown in Figure 17.

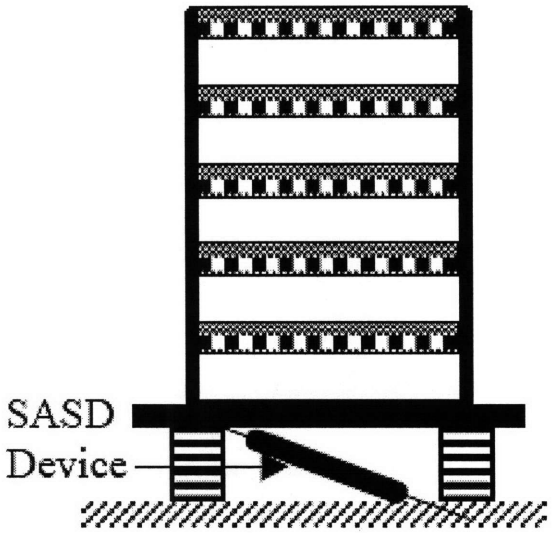


**Figure 17: Base-Isolated Model with SASD Damper (Agrawal & Yang, 2000)**

The hydraulic damper shown in Figure 18 was proposed as an energy dissipation device (Thai et al, 1997; Yang et al, 1999a, b, c). It consists of a piston-cylinder system with a valve in the bypass pipe connecting two sides of the cylinder. With the valve closed, the device provides stiffness by the bulk modulus of the fluid in the cylinder. With the valve open, the piston moves freely and the device provides a small amount of damping with no stiffness.

The device can be operated in a resetting mode or in a switching mode. For the resetting mode, the valve remains closed at all times and potential energy is stored in the hydraulic damper. At the appropriate time, the valve is pulsed open and closed quickly and the piston at this time is located at the resetting position. The energy stored in the damper is released and converted into heat energy. Pulsing the valve at the right times allow energy to be extracted from the vibrating system to reduce the structural response. The

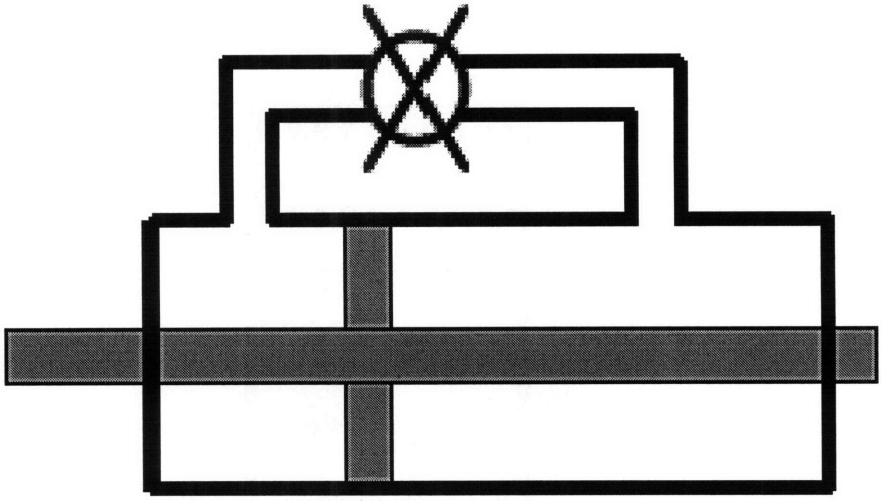

**Figure 18: Schematic Diagram of the Semi-Active Stiffness Damper (SASD) (Agrawal & Yang, 2000)**

For the switching mode, the valve is open for a certain time interval and closed for a different time interval. This on-off SSASD is the same as the active variable stiffness system proposed by Kobori and Kamagata, 1992.

The performance of the RSASD and SSASD were evaluated for the following earthquake excitations: El Centro NS (PGA = 0.314g), Kobe NS (1995, PGA = 0.818g), Kobe EW (1995, PGA = 0.619g), Northridge (Santa Monica, PGA = 0.884g), Northridge (Sylmar County, PGA = 0.605g), Takatori (Kobe) EW (PGA = 0.65g) and Takatori (Kobe) NS

(PGA = 0.612g). Table 2 summarizes the results from the investigation. $x_b$ is the peak drift of the rubber bearings, $\ddot{x}_b$ is the absolute acceleration of the base, and $\ddot{x}_5$ is the absolute acceleration of the 5th (top) floor. The results show that there are significant reductions in the peak drifts for all of the earthquake excitations for both the RSASD and the SSASD. The results also show that the absolute accelerations for the base and the top floor increase significantly. These issues with acceleration increases must be addressed in the future.

**Table 2: Peak Response Quantities of the Base-Isolated Building Subjected to Near-Field Earthquakes Using Resetting and Switching SASD's (Agrawal & Yang, 2000)**

| Earthq. | Passive Isolation | | | Resetting SASD | | | Switching SASD | | |
|---|---|---|---|---|---|---|---|---|---|
| (1) | $x_b$ (cm) (2) | $\ddot{x}_b$ (g) (3) | $\ddot{x}_5$ (g) (4) | $x_b$ (cm) (5) | $\ddot{x}_b$ (g) (6) | $\ddot{x}_5$ (g) (7) | $x_b$ (cm) (8) | $\ddot{x}_b$ (g) (9) | $\ddot{x}_5$ (g) (10) |
| El Centro | 28.53 | 0.186 | 0.191 | 9.63 | 0.420 | 0.267 | 9.61 | 0.516 | 0.220 |
| Kobe NS | 36.59 | 0.232 | 0.246 | 17.03 | 0.851 | 0.593 | 26.12 | 1.167 | 0.660 |
| Kobe EW | 26.92 | 0.179 | 0.192 | 13.06 | 0.710 | 0.499 | 14.57 | 0.829 | 0.454 |
| Takatori NS | 80.46 | 0.518 | 0.534 | 43.15 | 2.192 | 1.333 | 60.27 | 2.750 | 1.293 |
| Takatori EW | 94.73 | 0.612 | 0.624 | 38.70 | 1.733 | 1.031 | 50.61 | 2.205 | 1.062 |
| Northridge Santa Mo. | 36.15 | 0.235 | 0.241 | 9.12 | 0.547 | 0.342 | 14.82 | 0.715 | 0.321 |
| Northridge Syl. Co. | 62.40 | 0.400 | 0.416 | 16.15 | 1.00 | 0.661 | 26.48 | 1.517 | 0.553 |

## 6.0 MODEL SIMULATION

The objective of this thesis is to analyze the use of variable stiffness systems (VSS) in conjunction with building base isolation systems to control the displacement between floors during earthquake excitations. Force actuators are proposed to control the clipping and unclipping of the VSS. Controlling interstory displacement reduces the structural damage to the building, and ultimately, lowers the total repair costs to the owners.

While the interstory drift is reduced for all stories, the total displacement of the ground floor will be significantly increased with the isolation system installed. This must be addressed in the design and construction and will result in increased costs to the owner. The increased costs are due to the connection requirements for utilities and other systems that normally do not move independent of the structure. The tradeoff of all costs must be considered by the owner to determine if the use of isolation and VSS are worth the expense.

Although base isolation is good for earthquake loading, it is usually not adequate for wind loading due to its low lateral stiffness properties. This is where VSS are required. They can be installed at the base of the building in conjunction with the isolation system to provide the additional lateral stiffness required to support other lateral loads, mainly wind. Ground accelerometers can be installed next to the building and set to obtain acceleration data in order to monitor for a specific threshold that would necessitate unclipping the VSS. This would allow the base isolation system to operate as designed, and the building will begin to move with the ground. A low-level acceleration limit will

also be set on the ground accelerometers to ensure the VSS will "clip" back to the structure upon completion of the excitation. Once clipped, the structure will be ready for the next loading cycle to occur

Other systems have been developed to support the lateral stiffness by use of members that have adequate elastic capacity for low stiffness, but then deform inelastically and yield for high stiffness requirements. These members are designed to provide initial stiffness up to a prescribed threshold, and yield after the threshold is met or exceeded. Inelastic deformation serves the design purpose of adding lateral stiffness, but requires replacement of the deformed members after the event is over. VSS with force actuators are being proposed as an alternative to the hysteretic systems described above for the increased stiffness because they will not yield and will not require replacement.

It is assumed that the structure will respond in a similar manner to a base-isolated structure once the force actuator unclips and the stiffness is significantly reduced. The main concern is whether an instantaneous reduction in lateral stiffness combined with the ground acceleration will cause the structure to respond in a negative manner. If this impulse load does amplify the response, an alternative approach can be analyzed to reduce the lateral stiffness in stages.

## 6.1 Building Design Properties and Description

### 6.1.1 Plan and Elevation Design

To evaluate the response due wind and earthquake loading with the proposed force actuator and base isolation system, a basic structural model was designed based on assumed properties of the mass, fundamental period and damping. The model is a lumped mass model of a shear beam with eleven degrees of freedom. It consists of ten stories and the base floor connected to the isolation system. The 1st floor is the base isolation system. Figure 19 illustrates a schematic building model design. The actual model extends from $F_b$ to $F_{11}$, the base floor to the 11th floor and u is not included in this model.

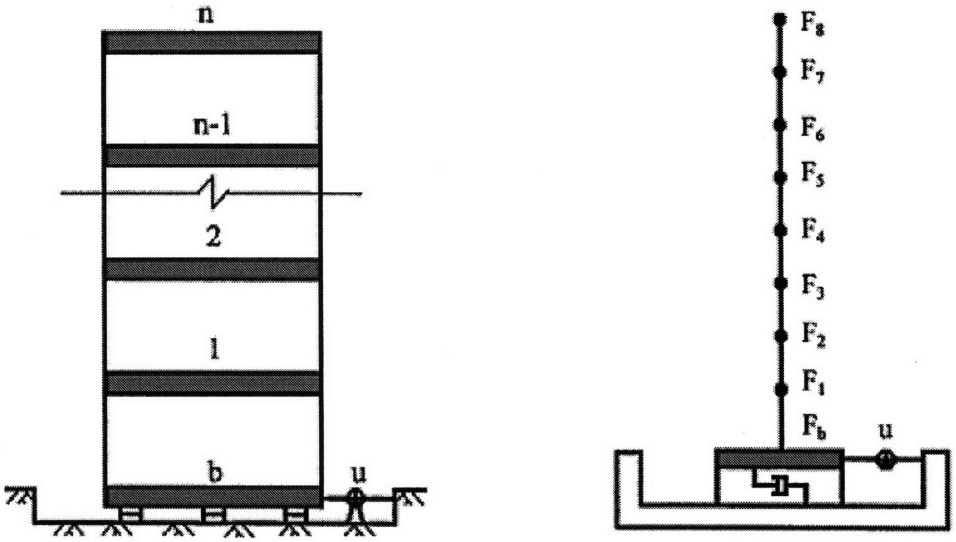


**Figure 19: Building with base-isolation and force actuator (Zhao et al, 2000)**

As is typical for most buildings, the fundamental period of the structure was assumed to be 1/10 of the number of stories and the critical damping was assumed to be 10% (0.1). The length and width of the structure were selected to be equal

at 50 meters. The total height was selected as 40 meters based on 10 stories at a 4-meter story height.

### 6.1.2 Mass distribution

The mass per floor was calculated based on the above dimensions and the following parameters: concrete unit weight = 2400 $kg/m^3$ ; concrete floor depth = 0.1 meter; steel structure weight per square meter of floor = 40 $kg/m^2$ ; equipment weight = 100 $kg/m^2$ . Table 3 shows the calculations.

**Table 3: Total mass per floor calculations**

| | | |
|---|---|---|
| Concrete Slab | $50m \times 50m \times 0.1m \times 2400 kg/m^3 =$ | 600,000 $kg$ |
| Steel Structure | $50m \times 50m \times 40 kg/m^2 =$ | 100,000 $kg$ |
| Equipment | $50m \times 50m \times 100 kg/m^2 =$ | 250,000 $kg$ |
| Total mass per floor, $m_i$ | | 950,000 $kg$ |

### 6.1.3 Stiffness distribution

The fundamental period $T_1$ for the structure is assumed to be 1.1 seconds, resulting in a fundamental frequency, $\omega_1$, of 5.71 rad/s. Assuming a fundamental mode shape that is linear, and based on the mass and the fundamental frequency above, the stiffness is calibrated for the structure based on the following process from Connor 2003:

The equilibrium equation for an undamped $n$th-order discrete system is:

$$\mathbf{M}\ddot{\mathbf{U}} + \mathbf{K}\mathbf{U} = \mathbf{P} \tag{1}$$

$$\mathbf{M} = \begin{bmatrix} m_1 & & & & \\ & m_2 & & & \\ & & \cdot & & \\ & & & \cdot & \\ & & & & m_n \end{bmatrix}$$

$$\mathbf{K} = \begin{bmatrix} k_1+k_2 & -k_2 & 0 & \cdots & 0 & 0 & 0 \\ -k_2 & k_2+k_3 & -k_3 & \cdots & 0 & 0 & 0 \\ \cdot & \cdot & \cdot & \cdot & \cdot & \cdot & \cdot \\ \cdot & \cdot & \cdot & \cdot & \cdot & \cdot & \cdot \\ \cdot & \cdot & \cdot & \cdot & \cdot & \cdot & \cdot \\ 0 & 0 & 0 & \cdots & -k_{n-1} & k_{n-1}+k_n & -k_n \\ 0 & 0 & 0 & \cdots & 0 & -k_n & k_n \end{bmatrix}$$

For $\mathbf{P} = 0$ and $\mathbf{U} = \Phi\cos(\omega t + \delta)$, equation 1 becomes

$$\mathbf{K}\Phi = \omega^2\mathbf{M}\Phi \tag{2}$$

Solutions for equation 2 define the frequencies, $\omega_j$, and the mode shapes, $\Phi_j$, for the specified **M** and **K** matrices. To calibrate stiffness, the inverse operation is required and the mode shape is specified to determine **K**.

Defining a scaled version of **K**,

$$\mathbf{K}' = \frac{1}{\omega^2}\mathbf{K} \tag{3}$$

Equation 2 reduces to

$$\mathbf{K}'\Phi = \mathbf{M}\Phi = \mathbf{P}' \tag{4}$$

This problem is statically determinate since there are $n$ equations for $n$ stiffness coefficients, $\mathbf{k}$.

$$\mathbf{k}' = \begin{bmatrix} k_1' \\ k_2' \\ . \\ . \\ k_n' \end{bmatrix} \qquad \mathbf{k}' = \begin{bmatrix} k_1' \\ k_2' \\ . \\ . \\ k_n' \end{bmatrix} \tag{5}$$

Equation 4 can then be written as

$$\mathbf{S}'\mathbf{k}' = \mathbf{P}' \tag{6}$$

Where $\mathbf{S}'(i,i) = \Phi_i - \Phi_{i-1}$

$\mathbf{S}'(i,i+1) = \Phi_i - \Phi_{i+1}$

$\mathbf{S}'(i,j) = 0$ for $j \neq i, i+1$

Next, solve equation 6 for $\mathbf{k}'$ with $\mathbf{k}' = \mathbf{S}'^{-1}\mathbf{P}'$ and

$$\mathbf{k} = \omega^2\mathbf{k}' \tag{7}$$

Table 4 lists the stiffness distribution for the structural model.

### 6.1.4 Damping distribution

The damping ratio for the fundamental mode, $\xi_1$, is assumed to be 0.1. The damping distribution for the structure is assumed to be proportional to the stiffness, $k_i$, based on the following relationships:

$$c_i = \alpha k_i$$

$$\alpha = \frac{2\xi_1}{\omega_1}$$

**Table 4: Structural model parameters**

| Floor | Mass (kg) | Stiffness (MN/m) | Damping (MNs/m) |
|---|---|---|---|
| 1 (Base) | 950,000 | 2046 | 7.16 |
| 2 | 950,000 | 2015 | 70.54 |
| 3 | 950,000 | 1953 | 68.37 |
| 4 | 950,000 | 1860 | 65.12 |
| 5 | 950,000 | 1736 | 60.78 |
| 6 | 950,000 | 1581 | 53.35 |
| 7 | 950,000 | 1395 | 48.84 |
| 8 | 950,000 | 1178 | 41.24 |
| 9 | 950,000 | 930 | 32.56 |
| 10 | 950,000 | 651 | 22.79 |
| 11 | 950,000 | 341 | 11.94 |

## 6.2 Load Conditions

### 6.2.1 Steady-State Wind

The steady state wind used in the analysis is 958 $N/m^2$ (20 $lb/ft^2$) based on a wind velocity of 100 miles per hour acting for a period of 50 seconds. This wind pressure is applied over the area of the building resulting in a total force of 1.9MN. To apply this to the building model the nodal forces are required. To determine the constant nodal force, divide the total force by the number of nodes above the ground floor (n-1). For this model, the steady state wind load applied to each node is 0.19 MN.

### 6.2.2 Wind Gust

The gust wind used in the analysis is 479 $N/m^2$ (10 $lb/ft^2$) based on a wind velocity of 50 miles per hour acting for a period of 5 seconds. The same procedure used for steady-state wind is used to determine the nodal force of 0.096 MN.

### 6.2.3 Earthquake

The earthquake load used in the analysis is the ground acceleration caused by the earthquake applied to the base floor of the structural model. For this analysis the El Centro, Mexico City, Kobe, and Pacoima earthquakes were investigated. Figure 20 is a plot of the El Centro ground acceleration. Observation shows that the excitation had a large, quick increase in acceleration very early in the event. This load is similar to an impulse load on the structure. After the large initial

shock, the acceleration then tapered off and was complete after about 40 seconds. In contrast to the El Centro earthquake, the Mexico City earthquake had a slow, gradual acceleration for about 40 seconds with long large accelerations later in time. The overall duration was over 180 seconds. Figure 21 below shows this acceleration plot. The Kobe and Pacoima earthquakes are both short duration excitations with large ground accelerations. The acceleration plots are shown in Figure 22 and Figure 23.

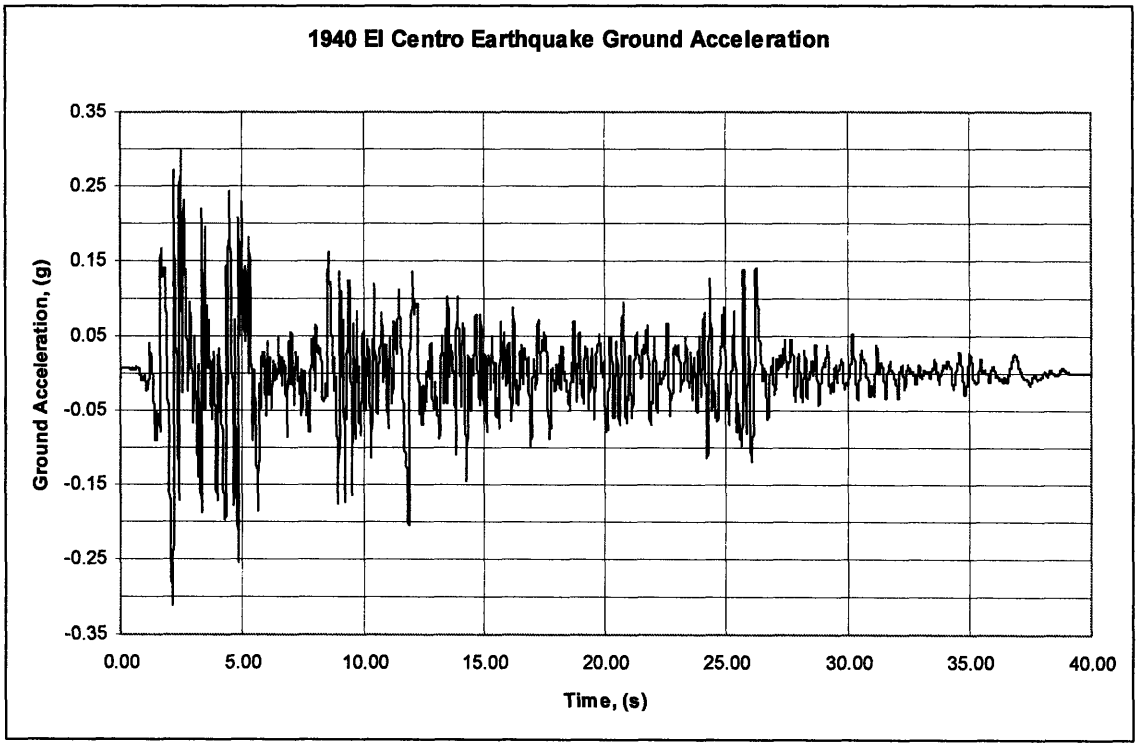


**Figure 20: El Centro earthquake acceleration**

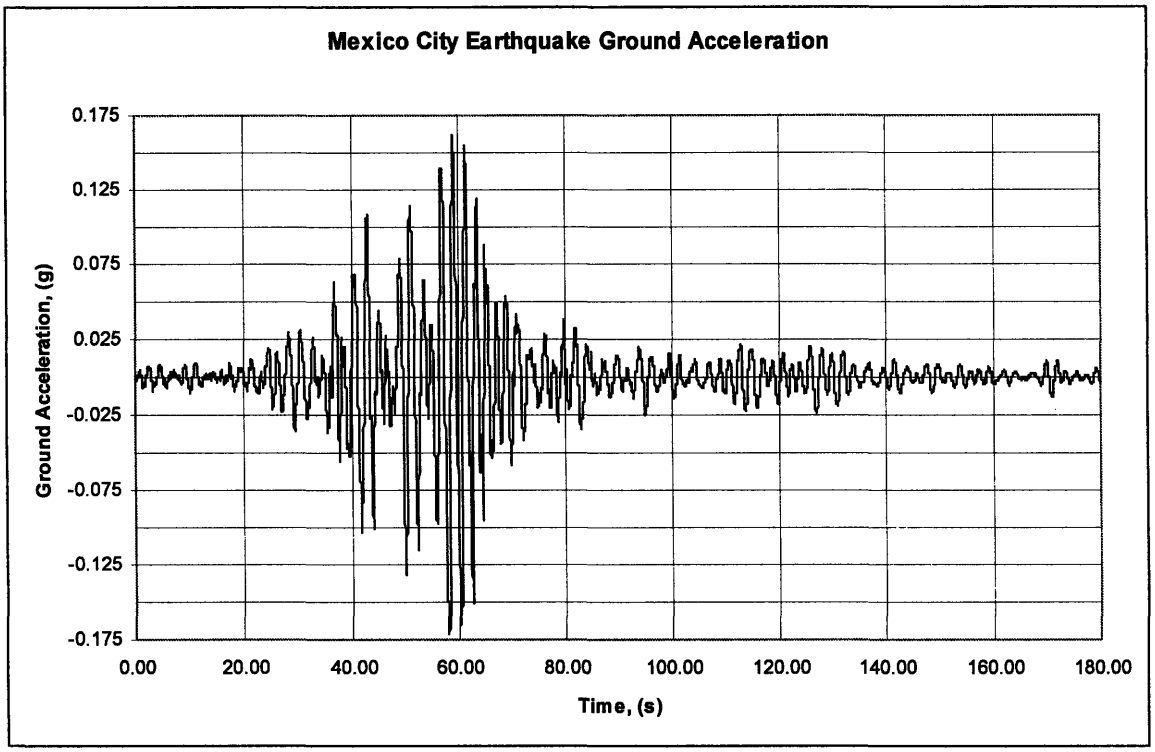


**Figure 21: Mexico City earthquake acceleration**

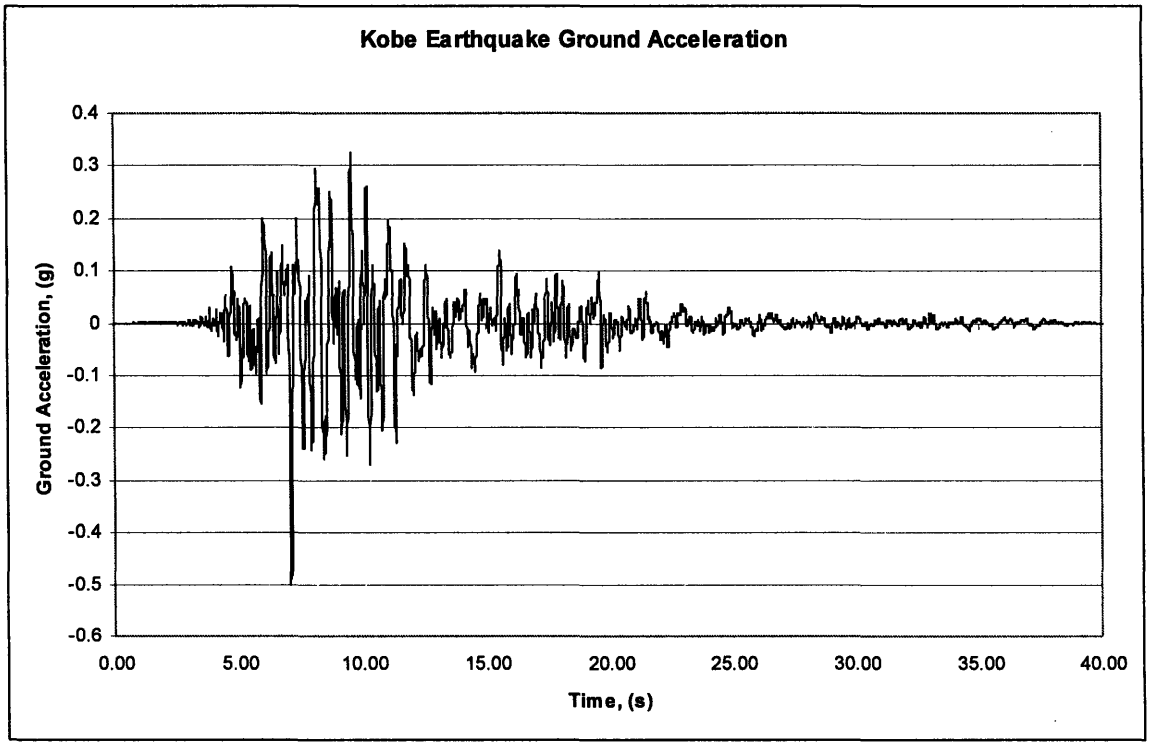


**Figure 22: Kobe earthquake acceleration**

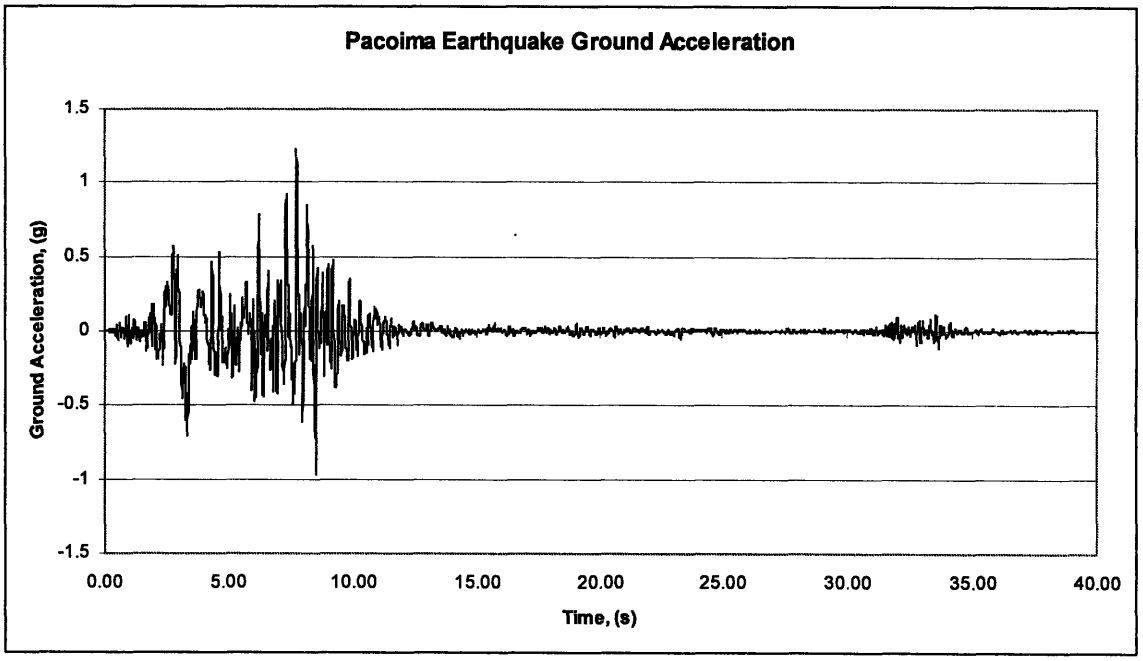


**Figure 23: Pacoima earthquake acceleration**

## 6.3 State-Space Representation

The dynamic response of systems requires working with a second order differential equation. This system of equations can be transformed to a set of first order equations based on defining state variables. This process is called state-space representation, and makes solving for the response much more convenient. The following state space formulation is from Connor, 2003.

### 6.3.1 State-Space Formulation for SDOF Systems:

Below is the second-order dynamic response of the SDOF system shown in Figure 24:

$$m\ddot{u} + c\dot{u} + ku = -ma_g + p + F \tag{8}$$

$p$ = the applied external loading

F = the active control force opposing motion

$m$ , $k$, $c$ = constant mass, stiffness, and damping system parameters

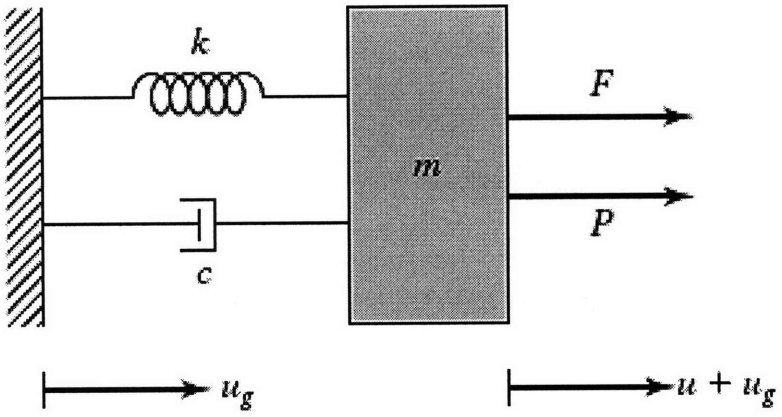


**Figure 24: Single degree of freedom system (Connor, 2003)**

The control force, $F$, in this analysis is taken to be zero since control of the structure is not being considered. The same benefits gained from active and passive control systems will still be realized when used in conjunction with the proposed actuator system.

The velocity and displacement can be determined by integrating equation 8 in time, and enforcing the initial conditions $u$ and $\dot{u}$ at $t = 0$. This is what characterizes the state of the system, and once $u$ and $\dot{u}$ are specified, the acceleration and internal forces can be determined by back-substitution. Following is the transformation to the first order, state-space representation equations involving the variables $u$ and $\dot{u}$.

$$\dot{u} = \frac{du}{dt}$$

$$\ddot{u} = \frac{d\dot{u}}{dt} = \left(-\frac{c}{m}\right)\dot{u} + \left(-\frac{k}{m}\right)u + (-1)a_g + \left(\frac{1}{m}\right)p + \left(\frac{1}{m}\right)F \tag{9}$$

It is more convenient to express the state-space equations in matrix form for evaluation. The state vectors are then defined as:

$$\mathbf{X} = \begin{bmatrix} u \\ \dot{u} \end{bmatrix} = \boldsymbol{X(t)} \tag{10}$$

$$\dot{\mathbf{X}} = \begin{bmatrix} \dot{u} \\ \ddot{u} \end{bmatrix}$$

The dynamic matrix equilibrium equation is then:

$$\frac{d\mathbf{X}}{dt} = \dot{\mathbf{X}} = \mathbf{A}\mathbf{X} + \mathbf{B}_f F + \mathbf{B}_g a_g + \mathbf{B}_p p \tag{11}$$

The constant coefficient matrices are defined as:

$$\mathbf{A} = \begin{bmatrix} 0 & 1 \\ -\frac{k}{m} & -\frac{c}{m} \end{bmatrix} \tag{12}$$

$$\mathbf{B}_f = \mathbf{B}_p = \begin{bmatrix} 0 \\ \frac{1}{m} \end{bmatrix} \tag{13}$$

$$\mathbf{B}_g = \begin{bmatrix} 0 \\ -1 \end{bmatrix} \tag{14}$$

The initial conditions at $t = 0$ are:

$$\mathbf{X}_o \equiv \mathbf{X}(0) = \begin{bmatrix} u(0) \\ \dot{u}(0) \end{bmatrix} \tag{15}$$

### 6.3.2 Discrete Time Formulation for SDOF Systems:

The continuous state-space formulation described above considers $\mathbf{X}$ and $F$ to be continuous functions of time that satisfy equation 11 and the initial conditions:

$$\mathbf{X}(t=0) = \mathbf{X}_o^* \tag{16}$$

Below is an approximate solution between two time points, such as, $t_j$ and $t_{j+1} = t_j + \Delta t$. Assumptions are introduced for the variation of the force during the time interval.

$$\mathbf{X}_{j+1} = \mathbf{e}^{\mathbf{A}\Delta t}\mathbf{X}_j + \mathbf{A}^{-1}\left(\mathbf{e}^{\mathbf{A}\Delta t} - \mathbf{I}\right)\left[\mathbf{B}_g a_{g,j} + \mathbf{B}_f F_j + \mathbf{B}_p p_j\right] \tag{17}$$

Equation 17 results in an estimate of $\mathbf{X}_{j+1}$ based on the information associated with the time point, $t_j$. The first term on the right side is the exact free vibration response at $t_{j+1}$, considering $\mathbf{X}_j$ being the initial state at $t_j$. The other terms on the right side are the contribution of the constant loading terms over the time interval, $\Delta t$. Starting at $t = 0$, which corresponds to $j = 0$, $\mathbf{X}_o$ is specified and $\mathbf{X}_1$ is computed. This process can be continued until the desired timeframe is reached.

### 6.3.3 State-Space Formulation for MDOF Systems:

The formulation for SDOF systems can be extended to MDOF systems by generalizing the definition equations for the matrices involved in the state-space

representation. The equations for an *n*th order linear system subjected to seismic excitation and a set of *r* applied control forces are:

$$\mathbf{M\ddot{U}} + \mathbf{C\dot{U}} + \mathbf{KU} = \text{-}\mathbf{ME}a_g + \mathbf{E}_f\mathbf{F} + \mathbf{P} \tag{18}$$

$\mathbf{E}$ = vector of ones

$\mathbf{E}_f = n \times r$ matrix locating control forces with respect to degrees of freedom

Figure 25 is representative of a four degree of freedom lumped mass model

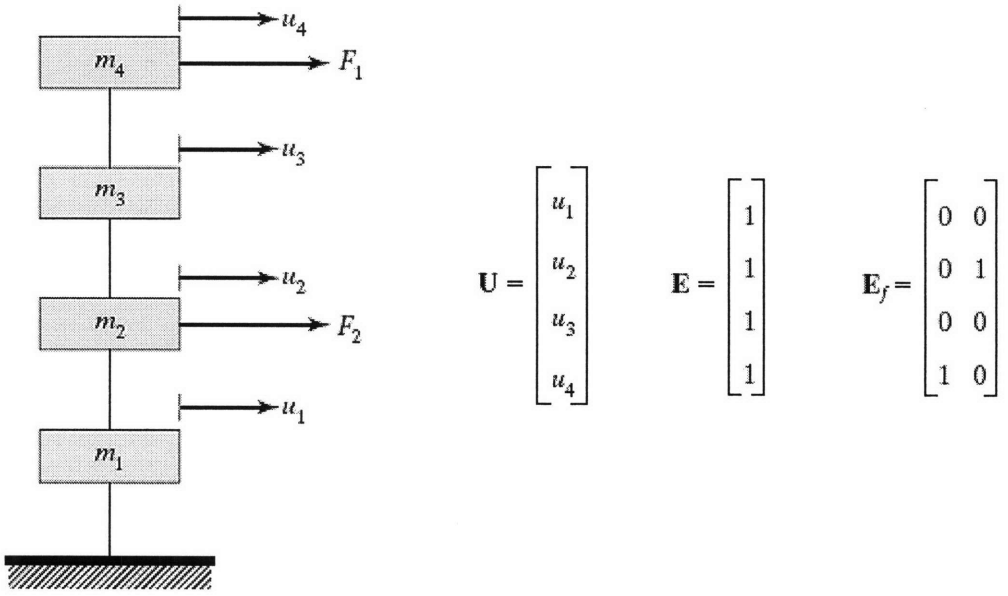


**Figure 25: 4DOF system with two control forces (Connor, 2003)**

The same transformation can be applied to the MDOF equations to obtain the first order, state-space representation equations involving the variable matrices $\mathbf{U}$ and $\dot{\mathbf{U}}$.

$$\dot{\mathbf{U}} = \frac{d\mathbf{U}}{dt}$$

$$\ddot{\mathbf{U}} = \frac{d\dot{\mathbf{U}}}{dt} = \left(\mathbf{M}^{-1}\mathbf{C}\right)\dot{\mathbf{U}} + \left(\mathbf{M}^{-1}\mathbf{K}\right)\mathbf{U} + \left(-\mathbf{E}\right)a_g + \left(\mathbf{M}^{-1}\right)p + \left(\mathbf{M}^{-1}\right)F \tag{19}$$

It is more convenient to express the state-space equations in matrix form for evaluation. The state vectors are then defined as:

$$\mathbf{X} = \begin{bmatrix} \mathbf{U} \\ \dot{\mathbf{U}} \end{bmatrix} = X(t) \tag{20}$$

$$\dot{\mathbf{X}} = \begin{bmatrix} \dot{\mathbf{U}} \\ \ddot{\mathbf{U}} \end{bmatrix}$$

$\mathbf{X}$ = vector with values 1 through $n$ equal to the displacements at the $n$th DOF and values $n + 1$ through $2n$ equal to the velocity at the $n$th DOF

$\dot{\mathbf{X}}$ = vector with values 1 through $n$ equal to the velocity at the $n$th DOF and values $n + 1$ through $2n$ equal to the acceleration at the $n$th DOF

The dynamic matrix equilibrium equation is then:

$$\frac{d\mathbf{X}}{dt} = \dot{\mathbf{X}} = \mathbf{A}\mathbf{X} + \mathbf{B}_f\mathbf{F} + \mathbf{B}_g a_g + \mathbf{B}_p\mathbf{P} \tag{21}$$

The constant coefficient matrices are defined as:

$$\mathbf{A} = \begin{bmatrix} \mathbf{0} & \mathbf{I} \\ -\mathbf{M}^{-1}\mathbf{K} & -\mathbf{M}^{-1}\mathbf{C} \end{bmatrix} \tag{22}$$

$$\mathbf{B}_f = \begin{bmatrix} \mathbf{0} \\ \mathbf{M}^{-1}\mathbf{E}_f \end{bmatrix} \tag{23}$$

$$\mathbf{B}_g = \begin{bmatrix} \mathbf{0} \\ -\mathbf{E} \end{bmatrix} \tag{24}$$

$$\mathbf{B}_p = \begin{bmatrix} \mathbf{0} \\ \mathbf{M}^{-1} \end{bmatrix} \tag{25}$$

The initial conditions at $t = 0$ are:

$$\mathbf{X}_o \equiv \mathbf{X}(0) = \begin{bmatrix} \mathbf{U}(0) \\ \dot{\mathbf{U}}(0) \end{bmatrix} \tag{26}$$

6.3.4 Discrete Time Formulation for MDOF Systems:

Below is an approximate general solution for an arbitrary loading between two time points.

$$\mathbf{X}_{j+1} = \mathbf{e}^{\mathbf{A}\Delta t}\mathbf{X}_j + \mathbf{A}^{-1}\left(\mathbf{e}^{\mathbf{A}\Delta t} - \mathbf{I}\right)\left[\mathbf{B}_g a_{g,j} + \mathbf{B}_f \mathbf{F}_j + \mathbf{B}_p \mathbf{P}_j\right] \tag{27}$$

Equation 27 again results in an estimate of $\mathbf{X}_{j+1}$ based on the information associated with the time point, $t_j$. The first term on the right side is the exact free vibration response at $t_{j+1}$, considering $\mathbf{X}_j$ being the initial state at $t_j$. The other terms on the right side are the contribution of the constant loading terms over the time interval, $\Delta t$. Starting at $t = 0$, which corresponds to $j = 0$, $\mathbf{X}_o$ is specified and $\mathbf{X}_1$ is computed. This process can be continued until the desired timeframe is reached.

## 6.4 Unclipping Scheme

### 6.4.1 Structural Frame

For base isolation systems to function properly the structure should be designed and construction on a structural frame system that is connected to the foundation through the isolation bearing system. The structural frame is required to provide a continuous floor to transmit loads and enable the structure to move as a single unit above the foundation during seismic activity.

### 6.4.2 Force Actuators

VSS and force actuators can be installed as a part of the base structural frame to act as stiffening members for the soft base isolation bearing system. One proposed system solution could be a smooth steel member that rides along the force actuator similar to a brake or clutch system. During normal day-to-day operations the force actuator would be activated and clamped down on the smooth steel member. Ground accelerometers installed adjacent to the structure in perpendicular and diagonal directions would be set to a desired ground acceleration threshold. Once the acceleration in any direction reaches the threshold, the actuators acting in the main direction of the accelerometer will release the smooth steel member and the structure will be allowed to move with the ground acceleration in that direction. If the accelerometers in the diagonal direction reach the set threshold, all actuators in all directions will be released and the building will move as the ground dictates.

To eliminate or reduce the effects of torsion and twisting, it is critical that the force actuators and the isolation system must be designed and constructed in a symmetric manner. By doing so, the center of stiffness and center of twist will remain constant no matter which actuators are released, and the torsion response of the structure will be minimized. This is essential due to the unknown nature of earthquake excitations.

The actuators may be either magnetic or electrically actuated. For magnetic actuators the clamp will induce a magnetic force that will squeeze the actuators together to hold the steel members by friction. Electric actuators would work in a similar manner, but may be combined with a mechanical clamp to hold the stiffened member. Both of these types of actuators would require a primary and backup power source. Battery backup may be an option, but the duration of the power outage could be an issue. If the system is not allowed to clamp back together after a seismic event, significant problems could result if a wind event occurs. An emergency manual override clamp could be designed to address this, but may also cause problems if aftershocks occur.

## 6.5 MATLAB Methodology

MATLAB was used to create a mathematical model to analyze the response due to the various earthquakes. First, a design scheme was developed to size the physical building structure, including the mass, stiffness, and damping properties. Next the earthquake data was loaded to be the forcing function to excite the model. The various material property matrices and state-space formulation matrices were established to carry out the mathematical analysis.

The first response analysis was for the clipped condition where the base floor horizontal stiffness remains as the optimal distribution from the entire structural design. This response sets the baseline from which the base isolation and VSS can be compared. After completing the clipped response, the ground acceleration threshold was set at 0.01g for which the force actuators would unclip and allow the structure to move with the base isolation system. The ground floor horizontal stiffness was reduced so that the new fundamental period of the structure would be approximately 3.0 seconds. This period was selected because history has shown that most earthquake excitations have a period of about 1.0 seconds. When the period of the structure is greater than the excitation period, the ground and the structure move independent of each other.

The response analysis was then evaluated for the unclipped condition. In this situation, the model begins with the original stiffness for the base floor until the earthquake acceleration reaches the threshold. At that instant in time, the model

unclips and the new soft stiffness is assigned to the base floor. From this point on the analysis maintained the soft stiffness. If this VSS were used for actual structures, the low threshold would have to be set so that the system would automatically clip back to increase the stiffness back to the original capacity.

Another analysis was conducted to allow the force actuators to continuously clip and unclip when the high and low thresholds were reached. The low limit was set at 0.005g and the stiffness continuously changed from soft to firm as the two limits were reached. The critical observation to make is whether the instantaneous acceleration that results from the unclipping actually makes the response worse than if there were no base isolation system. The final step in the process was to plot the results. Appendices B and C contain the code used for the design and analysis.

# 7.0 ANALYSIS RESULTS

## 7.1 Earthquake Response: Force Actuators Unclip and Remain Unclipped

When the force actuators unclip and remain unclipped, the analysis results show that the structure does actually behave very closely to a base isolated structure. The total displacements of each floor significantly increase as the soft stiffness takes control, and the interstory displacements, or drifts, are drastically reduced. Although the total displacements of all floors increase, they all do so in unison so that the structure actually does not feel the movement. The complete structure moves as one large rigid mass in a relatively straight line above the shaking ground. The base isolators allow the movement due to the very low stiffness. The absolute acceleration experienced at each floor is reduced to very low values resulting in low inertia forces and shear forces between floors. This is what will reduce the structural and nonstructural damage explained earlier in the document. One concern from the acceleration results is the instantaneous increase in acceleration caused by the unclipping of the force actuator. The displacement and drift results are favorable, but it must be noted that there will be some effect on the structure due to the quick spike in acceleration. The following tables and graphs for each earthquake illustrate the results explained above.

### 7.1.1 El Centro Earthquake

The El Centro earthquake acceleration reaches the unclipping threshold of 0.01g at just over one second. The unclipped stiffness of the first element reduces to 46 MN/m resulting in a new fundamental period for the structure of 3.13 seconds. Table 5 lists the maximum response summary showing the total displacement of each floor and the interstory drift between floors. The main goal of the proposed system was to reduce the interstory drift when the force actuators unclip. The results were very successful with a reduction in the drift of 75-80%. The very large drift between the first two floors is what was expected because this is where the base isolation system is installed. It is designed to handle this large deformation. For the model analyzed, the damping of the isolation bearing was assumed to be low. Increasing the damping of the base isolation system will result in lower total displacements and the same favorable interstory displacements.

Figure 26 illustrates the displacement profiles for the clipped and unclipped structural responses. Note the virtually straight line in the unclipped profile illustrating the rigid body motion that the structure will experience. Figure 27 shows the total displacement of the ground floor where it moves very little in the clipped mode and significantly in the unclipped mode. Figure 28 shows the total displacement of the top floor where there is significant movement for both modes. The favorable result shows the unclipped displacement of the top floor is close to the same as the ground floor. Figure 29 and Figure 30 clearly indicate the

reduction in the interstory displacements. Appendix D contains all of the analysis results for the El Centro earthquake.

**Table 5: El Centro Maximum Response Summary for T = 3 seconds**

| Floor | Total Disp (cm) | | | Interstory Drift (cm) | | |
|---|---|---|---|---|---|---|
| | Clipped | Unclipped | Change | Clipped | Unclipped | Change |
| 1 | 1.3 | 13.98 | 975% | 1.3 | 13.98 | |
| 2 | 2.43 | 14.28 | 488% | 1.22 | 0.31 | -75% |
| 3 | 3.61 | 14.56 | 303% | 1.22 | 0.28 | -77% |
| 4 | 4.81 | 14.83 | 208% | 1.22 | 0.27 | -78% |
| 5 | 6 | 15.07 | 151% | 1.23 | 0.26 | -79% |
| 6 | 7.17 | 15.29 | 113% | 1.23 | 0.26 | -79% |
| 7 | 8.33 | 15.49 | 86% | 1.23 | 0.25 | -80% |
| 8 | 9.47 | 15.67 | 65% | 1.23 | 0.25 | -80% |
| 9 | 10.58 | 15.84 | 50% | 1.24 | 0.25 | -80% |
| 10 | 11.65 | 15.99 | 37% | 1.25 | 0.25 | -80% |
| 11 | 12.71 | 16.13 | 27% | 1.27 | 0.26 | -80% |

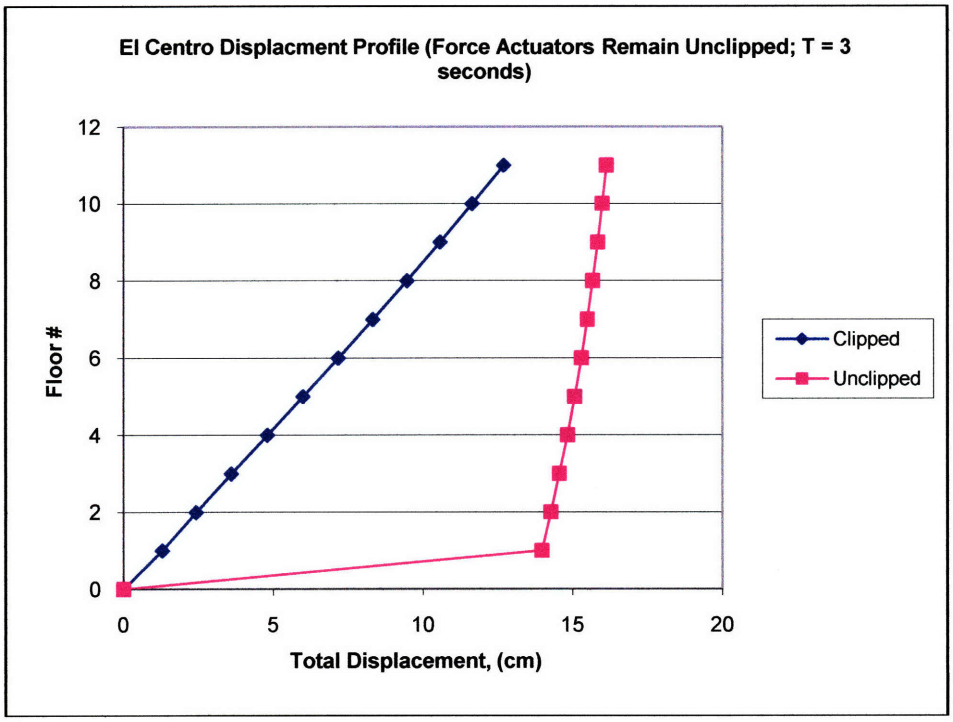


**Figure 26: El Centro Response Displacement Profiles for T = 3 seconds**

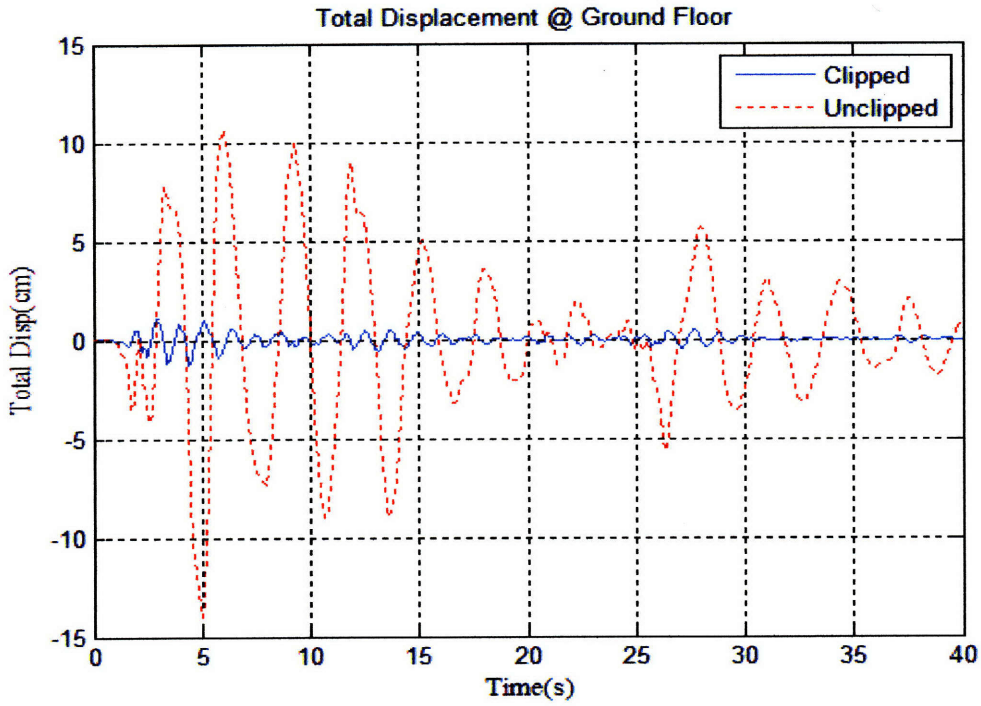


**Figure 27: Total Displacement at Floor 1 due to El Centro earthquake: Force actuators remain unclipped**

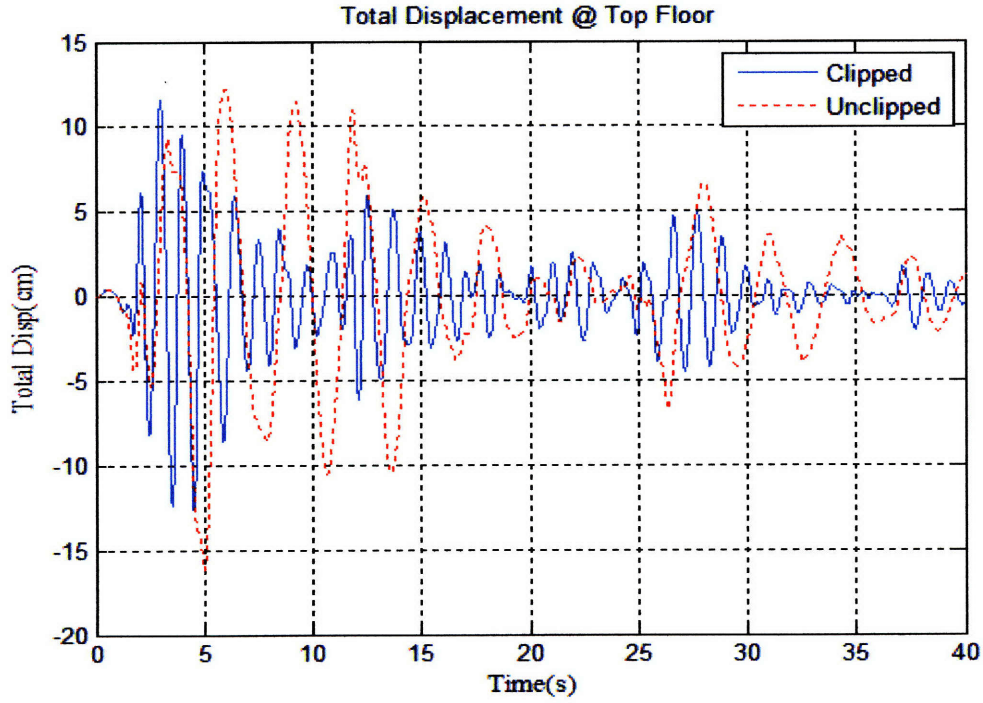


**Figure 28: Total Displacement at Floor 11 due to El Centro earthquake: Force actuators remain unclipped**

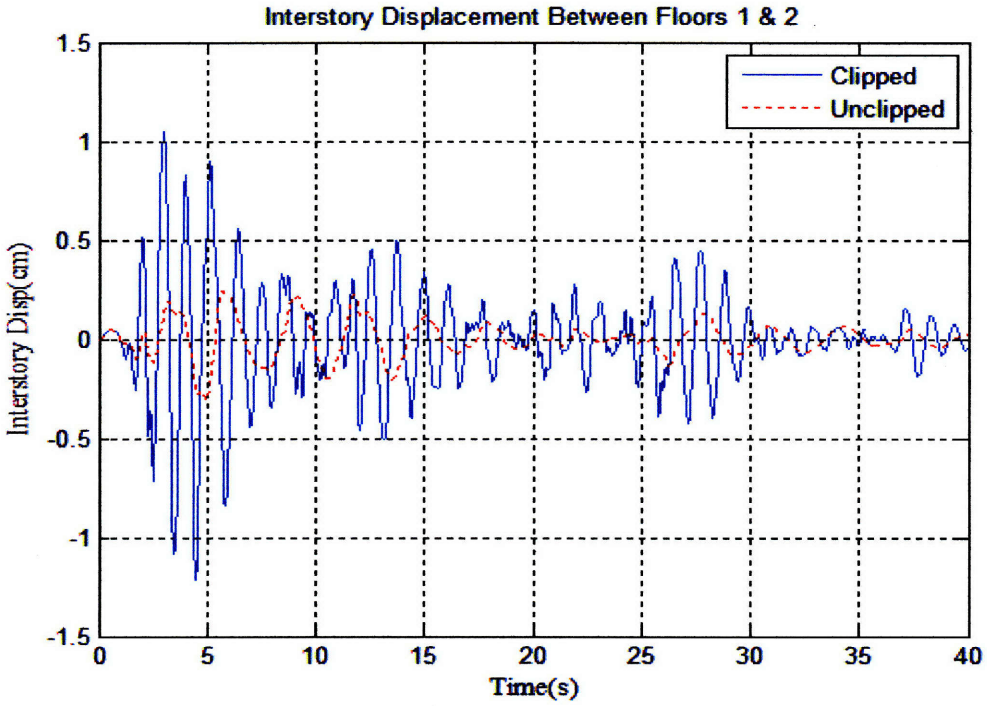


**Figure 29: Interstory Drift between Floors 1 & 2 due to El Centro earthquake: Force actuators remain unclipped**

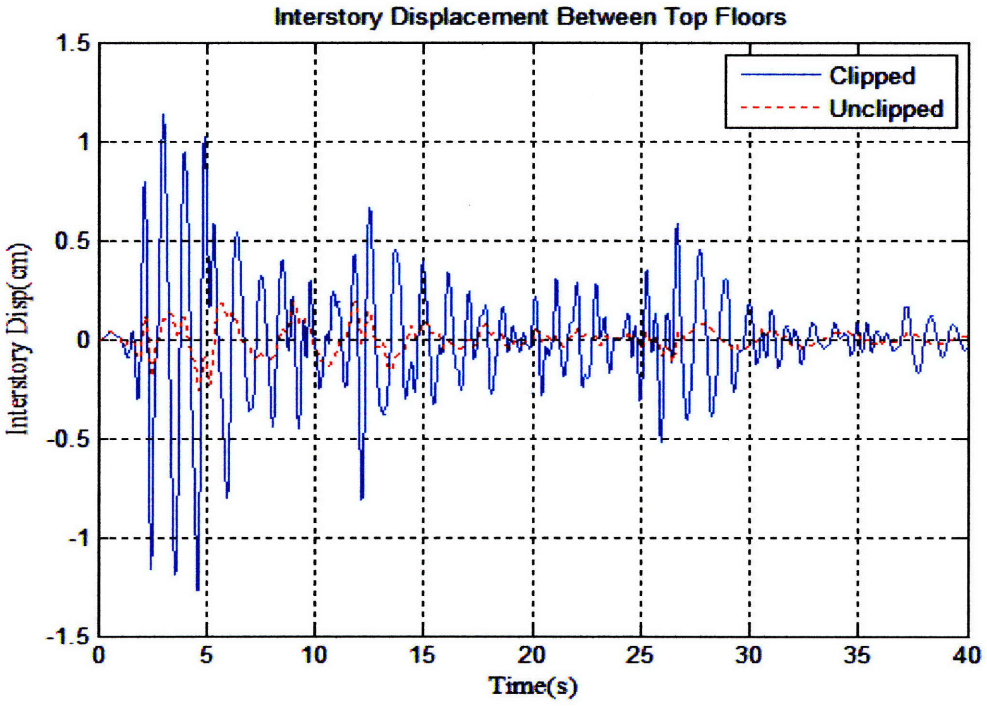


**Figure 30: Interstory Drift between Floors 10 & 11 due to El Centro earthquake: Force actuators remain unclipped**

### 7.1.2 Kobe Earthquake

The results for the Kobe earthquake are similar to El Centro. The earthquake acceleration reaches the unclipping threshold at 3.5 seconds and the unclipped stiffness and period are the same. Table 6 lists the maximum response summary and Figure 31 illustrates the displacement profiles for the structural response. Appendix F contains all of the analysis results for the Kobe earthquake.

**Table 6: Kobe Maximum Response Summary for T = 3 seconds**

| Floor | Total Disp (cm) | | | Interstory Drift (cm) | | |
|---|---|---|---|---|---|---|
| | Clipped | Unclipped | Change | Clipped | Unclipped | Change |
| 0 | 0 | 0 | | 0 | 0 | |
| 1 | 0.9 | 10.38 | 1053% | 0.9 | 10.38 | |
| 2 | 1.67 | 10.65 | 538% | 0.84 | 0.29 | -65% |
| 3 | 2.48 | 10.92 | 340% | 0.85 | 0.28 | -67% |
| 4 | 3.32 | 11.19 | 237% | 0.87 | 0.27 | -69% |
| 5 | 4.17 | 11.44 | 174% | 0.91 | 0.27 | -70% |
| 6 | 5.04 | 11.68 | 132% | 0.98 | 0.26 | -73% |
| 7 | 5.94 | 11.91 | 101% | 1.06 | 0.25 | -76% |
| 8 | 6.86 | 12.14 | 77% | 1.17 | 0.24 | -79% |
| 9 | 7.83 | 12.35 | 58% | 1.28 | 0.24 | -81% |
| 10 | 8.83 | 12.56 | 42% | 1.4 | 0.24 | -83% |
| 11 | 10.11 | 12.76 | 26% | 1.53 | 0.25 | -84% |

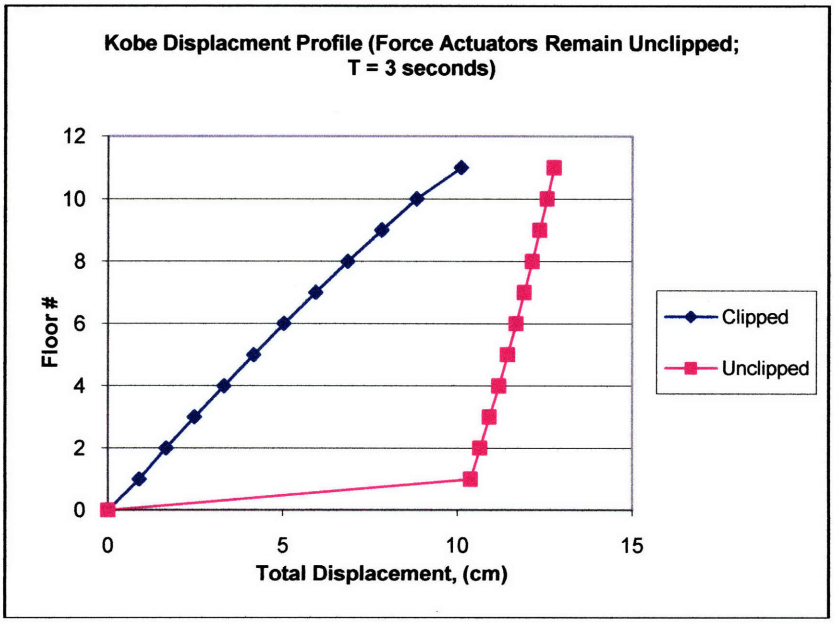


**Figure 31: Kobe Response Displacement Profiles for T = 3 seconds**

### 7.1.3 Pacoima Earthquake

The results for the Pacoima earthquake are similar to El Centro. The earthquake acceleration reaches the unclipping threshold of 0.01g at well under one second and the unclipped stiffness and period are the same. Table 7 lists the maximum response summary and Figure 32 illustrates the displacement profiles for the structural response. Appendix G contains the analysis results for the Pacoima earthquake.

**Table 7: Pacoima Maximum Response Summary for T = 3 seconds**

| Floor | Total Disp (cm) | | | Interstory Drift (cm) | | |
|---|---|---|---|---|---|---|
| | Clipped | Unclipped | Change | Clipped | Unclipped | Change |
| 0 | 0 | 0 | | 0 | 0 | |
| 1 | 4.2 | 37.24 | 787% | 4.2 | 37.24 | |
| 2 | 8.23 | 38.08 | 363% | 4.08 | 0.9 | -78% |
| 3 | 12.26 | 38.89 | 217% | 4.06 | 0.86 | -79% |
| 4 | 16.27 | 39.67 | 144% | 4.03 | 0.83 | -79% |
| 5 | 20.25 | 40.43 | 100% | 4 | 0.8 | -80% |
| 6 | 24.19 | 41.18 | 70% | 3.97 | 0.78 | -80% |
| 7 | 28.11 | 41.91 | 49% | 3.94 | 0.75 | -81% |
| 8 | 31.99 | 42.63 | 33% | 3.95 | 0.73 | -82% |
| 9 | 35.85 | 43.33 | 21% | 3.96 | 0.71 | -82% |
| 10 | 39.69 | 44.03 | 11% | 3.97 | 0.7 | -82% |
| 11 | 43.51 | 44.71 | 3% | 3.97 | 0.68 | -83% |

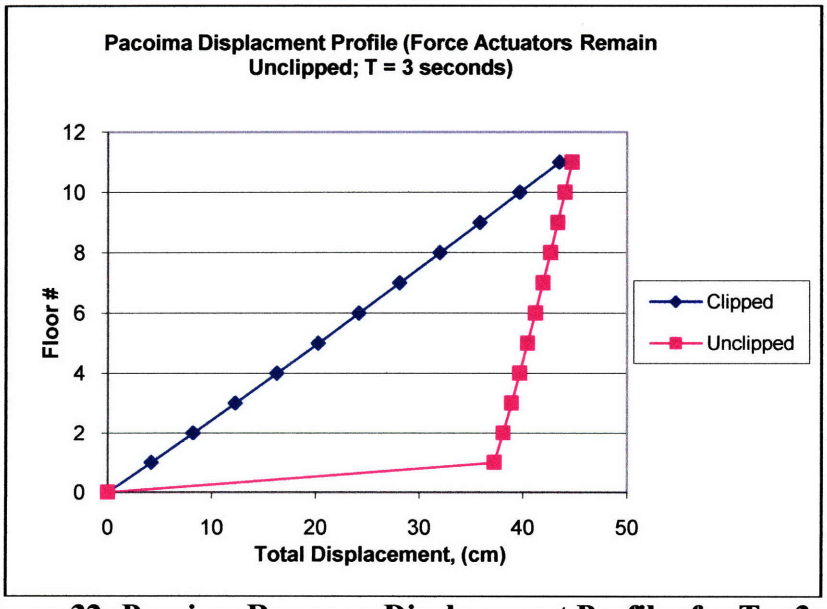


**Figure 32: Pacoima Response Displacement Profiles for T = 3 seconds**

### 7.1.4 Mexico City Earthquake with 3 Second Fundamental Period

The results for the Mexico City earthquake are not as favorable as other earthquakes. Table 8 lists the maximum response summary and Figure 33 illustrates the displacement profile for the structural response. Figure 34 and Figure 35 show the total displacements for the ground and top floors. The results for these are similar to the other earthquakes analyzed, but the unclipped displacements are very large. Figure 36 and Figure 37 show the drift between the bottom and top floors for both modes and unclipping does not reduce the value at all. The reason for this is the fact that the dominant fundamental period for this earthquake excitation is large compared to the others studied. To obtain a larger reduction in drift, the unclipped stiffness must be reduced even more as explained in the next section. Appendix E contains all of the analysis results for the Mexico City earthquake for a period of 3 seconds.

**Table 8: Mexico City Maximum Response Summary for T = 3 seconds**

| Floor | Total Disp (cm) | | | Interstory Drift (cm) | | |
|---|---|---|---|---|---|---|
| | Clipped | Unclipped | Change | Clipped | Unclipped | Change |
| 0 | 0 | 0 | | 0 | 0 | |
| 1 | 1.17 | 44.36 | 3691% | 1.17 | 44.36 | |
| 2 | 2.27 | 45.32 | 1896% | 1.1 | 1 | -9% |
| 3 | 3.32 | 46.22 | 1292% | 1.05 | 0.94 | -10% |
| 4 | 4.32 | 47.07 | 990% | 1 | 0.89 | -11% |
| 5 | 5.28 | 47.89 | 807% | 0.96 | 0.85 | -11% |
| 6 | 6.2 | 48.67 | 685% | 0.93 | 0.81 | -13% |
| 7 | 7.1 | 49.41 | 596% | 0.89 | 0.77 | -13% |
| 8 | 7.96 | 50.12 | 530% | 0.87 | 0.74 | -15% |
| 9 | 8.8 | 50.8 | 477% | 0.84 | 0.71 | -15% |
| 10 | 9.62 | 51.45 | 435% | 0.82 | 0.68 | -17% |
| 11 | 10.41 | 52.08 | 400% | 0.79 | 0.66 | -16% |

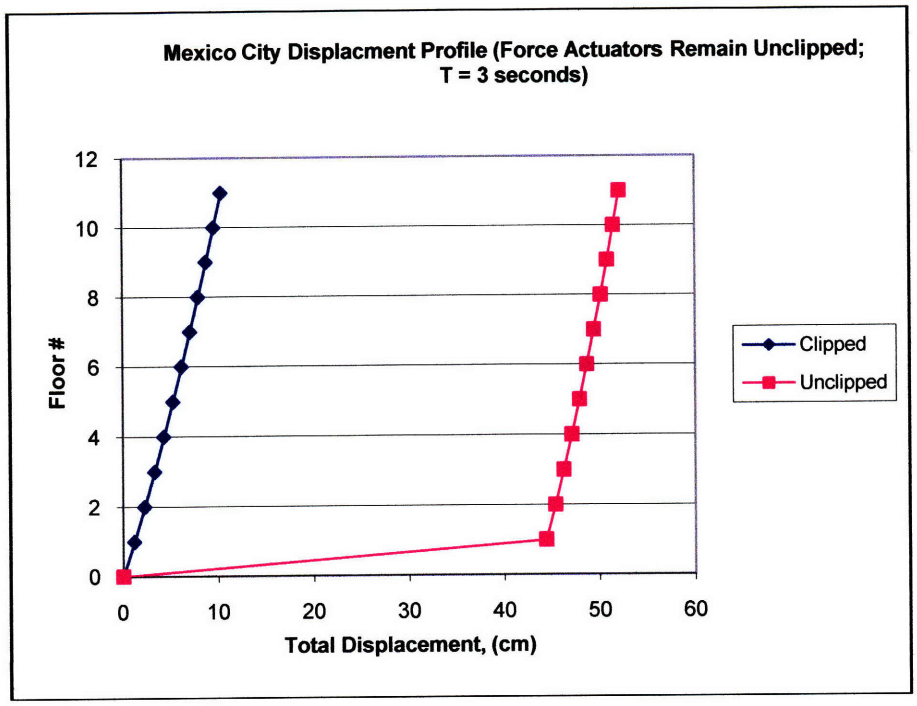


**Figure 33: Mexico City Response Displacement Profiles for T = 3 seconds**

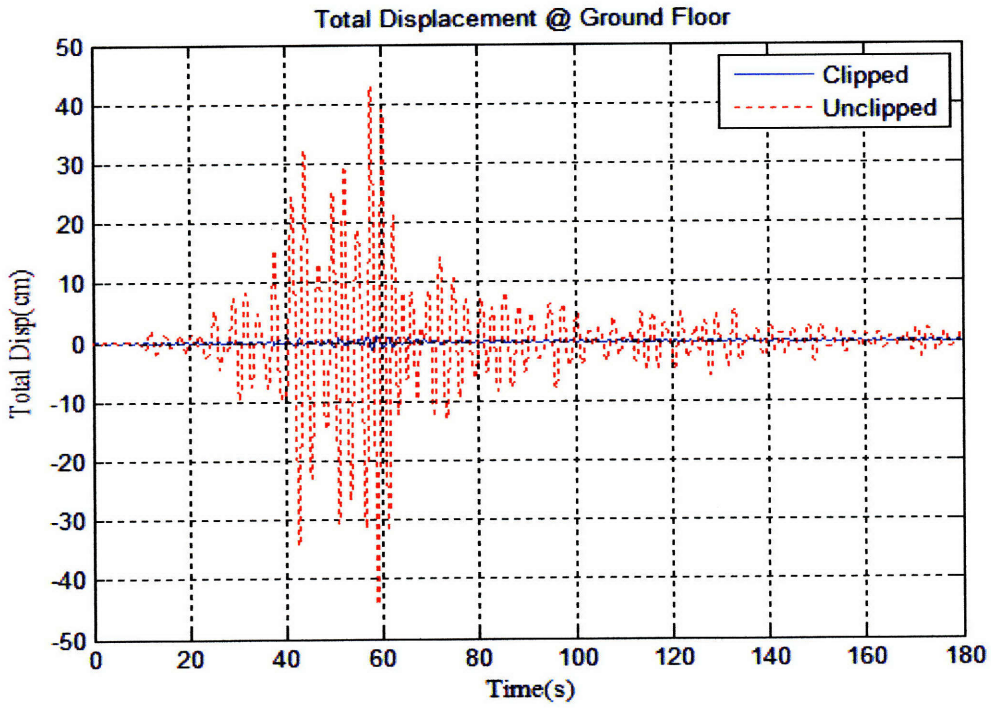


**Figure 34: Total Displacement at Floor 1 due to Mexico City earthquake with T = 3s: Force actuators remain unclipped**

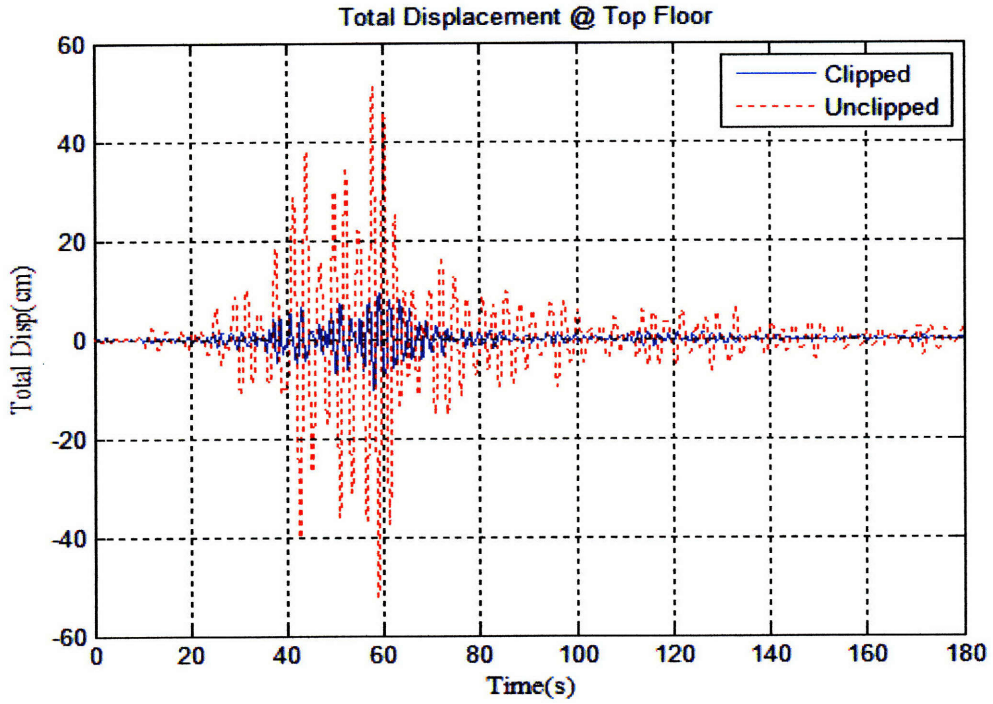


**Figure 35: Total Displacement at Floor 11 due to Mexico City earthquake with T = 3s: Force actuators remain unclipped**

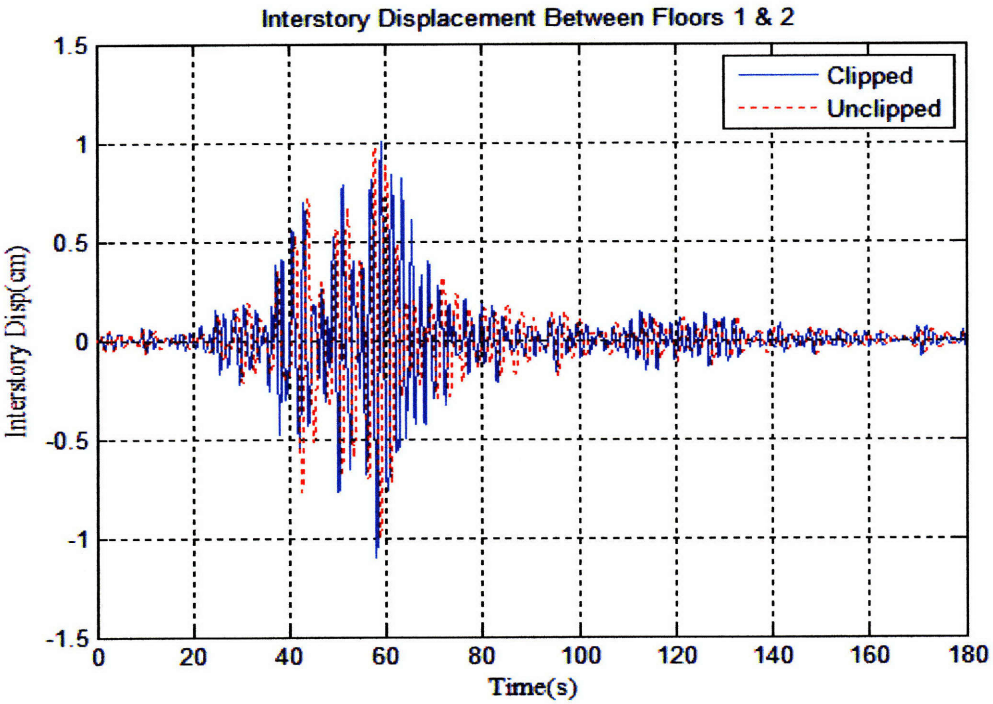


**Figure 36: Interstory Drift between Floors 1 & 2 due to Mexico City earthquake with T = 3s: Force actuators remain unclipped**

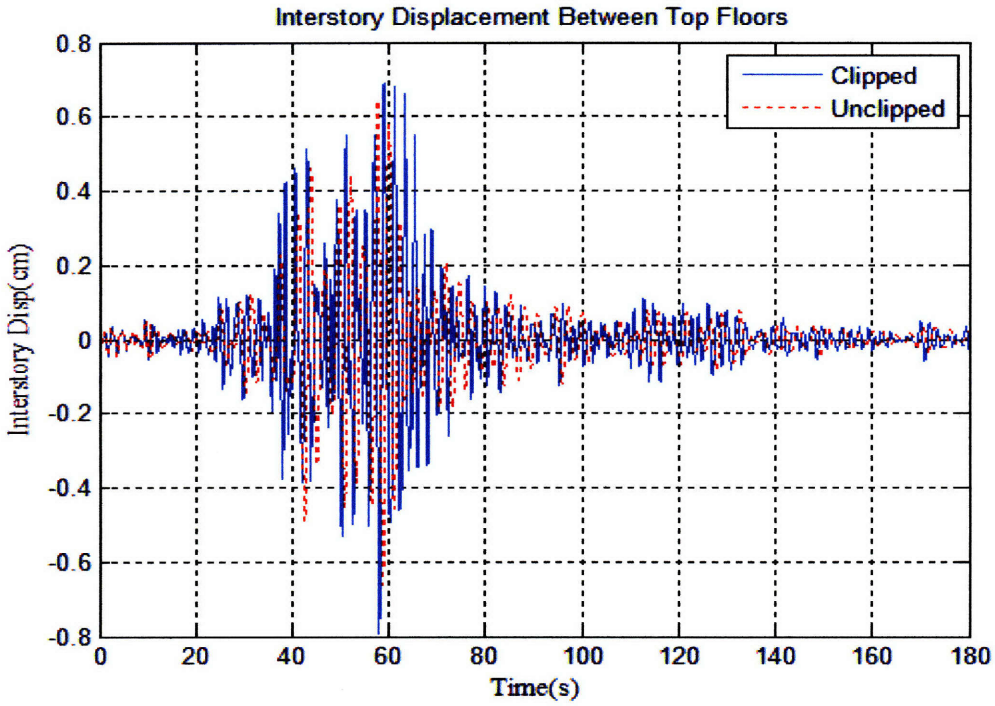


**Figure 37: Interstory Drift between Floors 10 & 11 due to Mexico City earthquake with T = 3s: Force actuators remain unclipped**

### 7.1.5 Mexico City Earthquake with 6 Second Fundamental Period

To improve the results the unclipped fundamental period was increased from 3 seconds to 5 seconds resulting in a new unclipped stiffness of MN/m and a period of seconds. The results from this analysis are similar to those of the other earthquakes studied. Table 9 lists the maximum response summary and Figure 38 illustrates the displacement profile for the structural response. The total displacement was reduced for all floors and the drift was reduced to show the nearly vertical rigid body motion for the structure. Appendix E contains all of the analysis results for the Mexico City earthquake for a period of 6 seconds.

**Table 9: Mexico City Maximum Response Summary for T = 6 seconds**

| Floor | Total Disp (cm) | | | Interstory Drift (cm) | | |
|---|---|---|---|---|---|---|
| | Clipped | Unclipped | Change | Clipped | Unclipped | Change |
| 0 | 0 | 0 | | 0 | 0 | |
| 1 | 1.17 | 24.13 | 1962% | 1.17 | 24.13 | |
| 2 | 2.27 | 24.28 | 970% | 1.1 | 0.25 | -77% |
| 3 | 3.32 | 24.41 | 635% | 1.05 | 0.23 | -78% |
| 4 | 4.32 | 24.55 | 468% | 1 | 0.22 | -78% |
| 5 | 5.28 | 24.68 | 367% | 0.96 | 0.21 | -78% |
| 6 | 6.2 | 24.81 | 300% | 0.93 | 0.2 | -78% |
| 7 | 7.1 | 24.92 | 251% | 0.89 | 0.19 | -79% |
| 8 | 7.96 | 25.04 | 215% | 0.87 | 0.19 | -78% |
| 9 | 8.8 | 25.15 | 186% | 0.84 | 0.18 | -79% |
| 10 | 9.62 | 25.25 | 162% | 0.82 | 0.18 | -78% |
| 11 | 10.41 | 25.35 | 144% | 0.79 | 0.17 | -78% |

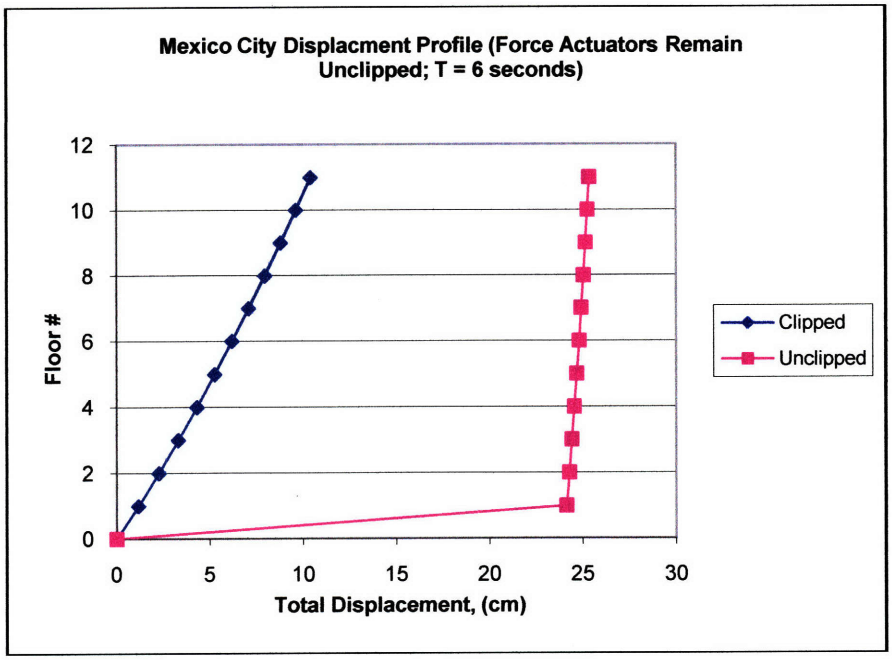


**Figure 38: Mexico City Response Displacement Profiles for T = 6 seconds**

## 7.2 Earthquake Response: Force Actuators Continuously Unclip and Clip

A second clipping scheme was modeled where a low threshold on the earthquake ground acceleration was set at 0.005g. Once this threshold was reached, the force actuators would then re-clip the stiffness back to the original value. Throughout the earthquake time history the actuators were allowed to continuously clip and unclip when the two thresholds were reached, and the corresponding stiffness was used to compute the response for that time interval. Figure 39 illustrates when each threshold was reached and when the system was clipped or unclipped. A value of 1 means clipped and 0 means unclipped.

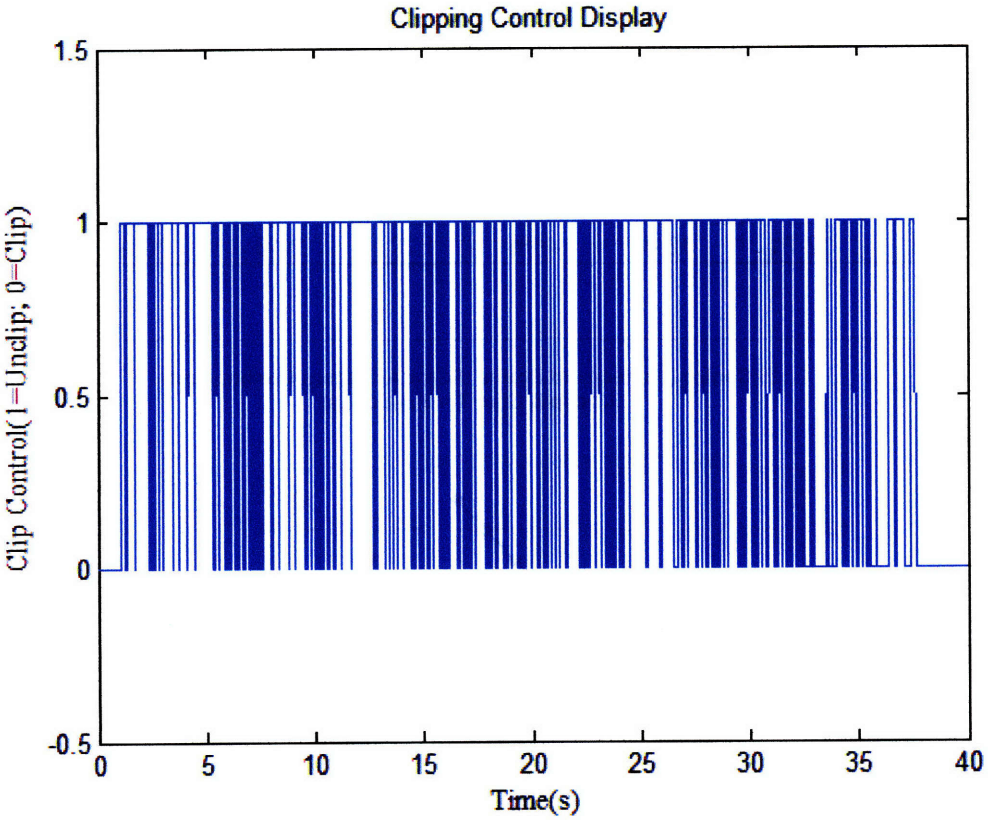


**Figure 39: Control Scheme for El Centro earthquake with force actuators continuously clipping & unclipping**

The results for the El Centro earthquake are shown below and are not as favorable as when the system remains unclipped. Table 10 lists the maximum response summary and Figure 40 illustrates the displacement profile for the structural response. Similar results were obtained for the Mexico City, Kobe and Pacoima earthquakes. Appendix E, F and G contain the results for these responses.

**Table 10: El Centro Maximum Response Summary**

| Floor | Total Disp (cm) | | | Interstory Drift (cm) | | |
|---|---|---|---|---|---|---|
| | Clipped | Unclipped | Change | Clipped | Unclipped | Change |
| 0 | 0 | 0 | | 0 | 0 | |
| 1 | 1.3 | 10.59 | 715% | 1.3 | 10.59 | |
| 2 | 2.43 | 10.8 | 344% | 1.22 | 3.52 | 189% |
| 3 | 3.61 | 11.18 | 210% | 1.22 | 2.85 | 134% |
| 4 | 4.81 | 11.6 | 141% | 1.22 | 2.42 | 98% |
| 5 | 6 | 12.36 | 106% | 1.23 | 2.21 | 80% |
| 6 | 7.17 | 13.04 | 82% | 1.23 | 1.92 | 56% |
| 7 | 8.33 | 13.83 | 66% | 1.23 | 1.77 | 44% |
| 8 | 9.47 | 14.79 | 56% | 1.23 | 1.68 | 37% |
| 9 | 10.58 | 15.77 | 49% | 1.24 | 1.66 | 34% |
| 10 | 11.65 | 16.88 | 45% | 1.25 | 1.76 | 41% |
| 11 | 12.71 | 18.4 | 45% | 1.27 | 2.16 | 70% |

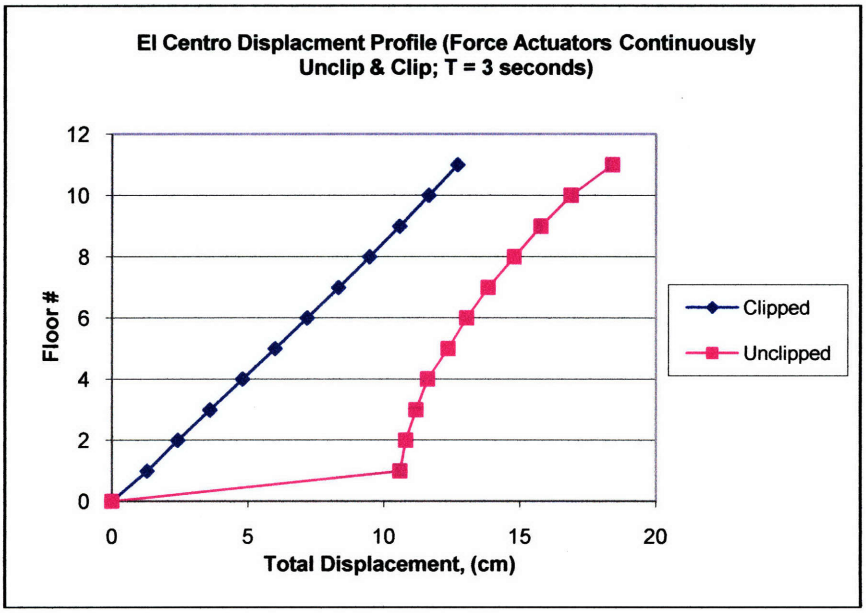


**Figure 40: El Centro Response Displacement Profile**

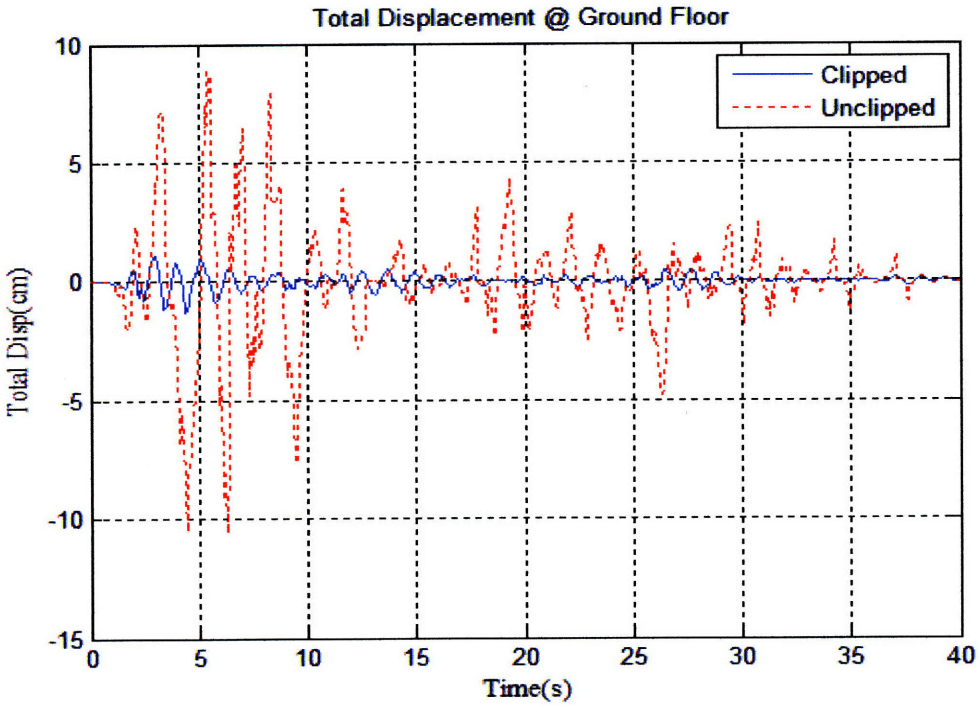


**Figure 41: Total Displacement at Floor 1 due to El Centro earthquake: Continuous Unclipping/Clipping**

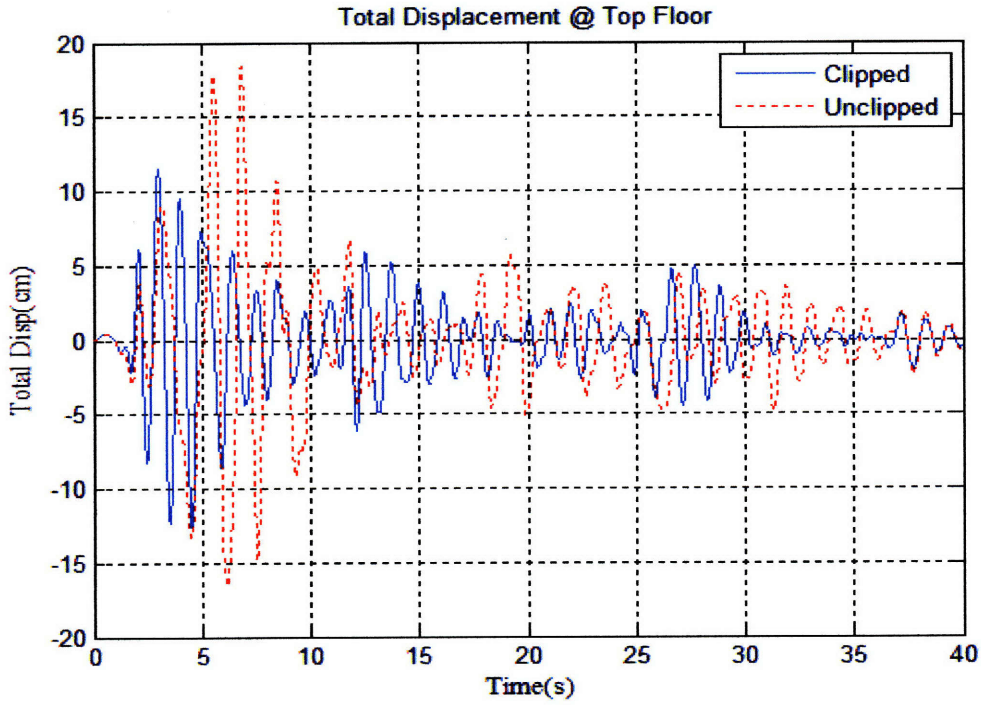


**Figure 42: Total Displacement at Floor 11 due to El Centro earthquake: Continuous Unclipping/Clipping**

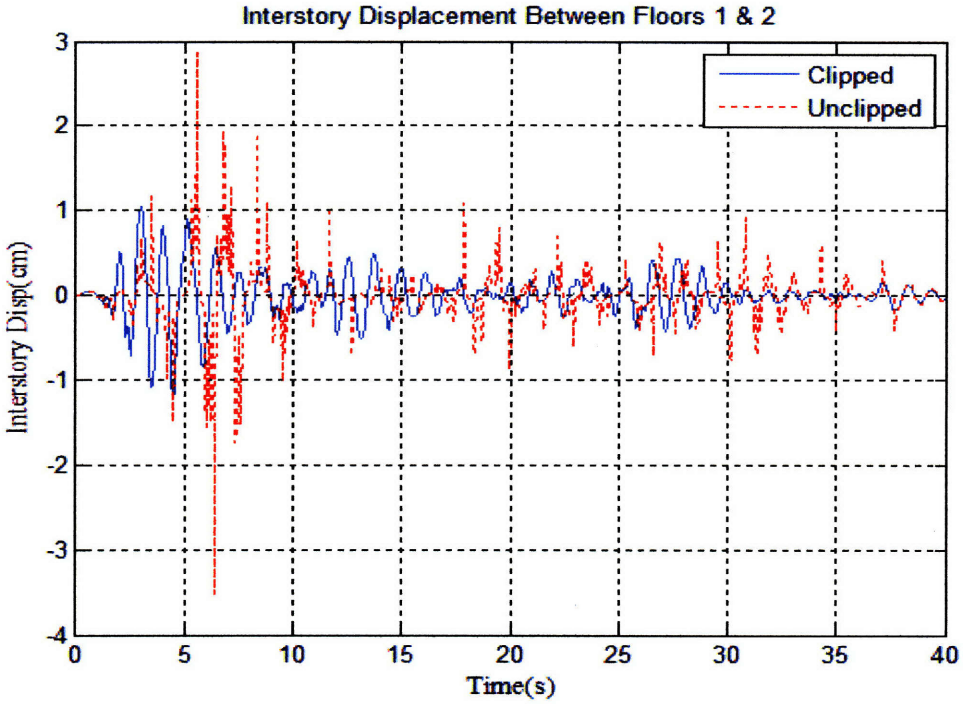


**Figure 43: Interstory drift between Floors 1 & 2 due to El Centro earthquake: Continuous unclipping/clipping**

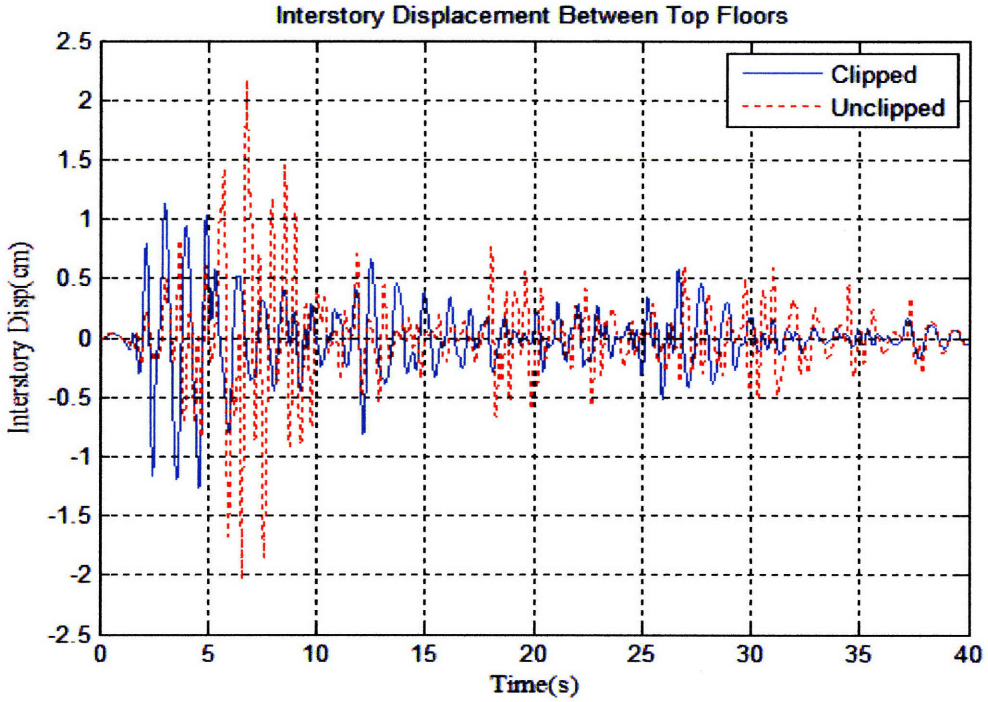


**Figure 44: Interstory drift between Floors 10 & 11 due to El Centro earthquake: Continuous unclipping/clipping**

## 8.0 CONCLUSION AND RECOMMENDATIONS

Based on the analysis results it has been shown that using force actuators or some other device to immediately unclip and remove the base floor stiffness of an isolated structure is beneficial to the overall structural behavior. The structure does respond in a very similar fashion to a base isolated structure. Various combinations of devices and systems can be used to achieve these results. Ultimately the interstory drift was reduced and would lead to improved structural performance during seismic events and reduced repair costs as hypothesized.

The analysis with continuous stiffness variation during the seismic event was only briefly investigated. This type of system could be refined by varying the threshold limits and time intervals for which the stiffness would be reduced. The goal would be to reduce the potential whip action that may occur once the inertia forces are moving the structure.

The overall results are consistent with other research and analyses that have been conducted in the past. It is recommended that additional research and design analysis be conducted on the use of magnetic force actuators in combination with VSS and base isolation systems. Some areas to investigate include the design of the physical device and the application scheme, varying the unclipping threshold to evaluate the affect on the response, and progressive stiffness reduction would reduce the stiffness more gradually rather than instantaneously.

## 9.0 REFERENCES


1. Agrawal, A. K., and J. N. Yang. 2000. A semi-active hybrid isolation system for buildings subject to near-field earthquakes. Structures.

2. Aiken, I., P. Clark, K. Kazuhiko, E. Ko, and I. Kumuar. 1999. Design procedures for buildings incorporating hysteretic damping devices. Proceedings, 68th Annual Convention, Structural Engineers Association of California (October 1999).

3. Bovis. 2001, http://www.bovislendlease.com/llweb/bll/main.nsf/images/pdf_country_us_la_cityhall.pdf/$file/pdf_country_us_la_cityhall.pdf

4. Celikbas, Ayse. 1999. Economics of damage controlled seismic design. S.M., Massachusetts Institute of Technology, Dept. of Civil and Environmental Engineering.

5. Connor, J. J. 2003. Introduction to structural motion control. 1st ed. Upper Saddle River, New Jersey 07458: Prentice Hall, Pearson Education, Inc.

6. Connor, J. J., A. Wada, M. Iwata, and Y. H. Huang. 1997. Damage-controlled structures. I: Preliminary design methodology for seismically active regions. Journal of Structural Engineering 123, (4) (April 1997): 423-31.

7. Huang, S., M. Skokan, and S. Islam. 2006. Essential facility benefits from new base isolation technology. Structures 2006.

8. Iwata, M. 1994. Damage level control design. 109, (1352): 42-4.

9. Kelly. 1998, http://nisee.berkeley.edu/lessons/kelly.html

10. Kelly, J. M., G. Leitmann, and A. G. Soldatos. 1987. Robust control of base-isolated structures under earthquake excitation. Journal of Otimization Theory and Applications 53, (2) (May 1987): 159-80.

11. Keten, S. 2006. A Performance Based Approach for Seismic Design with Hysteretic Dampers. MEng, Massachusetts Institute of Technology, Department of Civil and Environmental Engineering

12. Los Angeles City Department of Public Works, Bureau of Engineering. http://www.lacityhall.org/

13. Naeim, F., and J. M. Kelly. 1999. Design of seismic isolated structures.

14. Nagarajaiah, S., and S. Xiaohong. 2001. Base-isolated FCC building: Impact response in northridge earthquake. Journal of Structural Engineering 127, (9) (September 2001): 1063-75.

15. Nagarajaiah, S., and S. Xiaohong. 2000. Response of base-isolated USC hospital building in northridge earthquake. Journal of Structural Engineering 126, (10) (October 2000): 1177-86.

16. Ng, Charles W. W., and L. M. Zhang. 2001. Three-dimensional analysis of performance of laterally loaded sleeved piles in sloping ground. Journal of Geotechnical and Geoenvironmental Engineering 127, (6) (June 2001): 499-509.

17. Roberts, J. E. 2005. Caltrans structural control for bridges in high-seismic zones. Earthquake Engineering & Structural Dynamics 34, (January 2005): 449-70.

18. Thai, K. B., Jabbari, F., Bobrow, J. E. 1997. Structural Control via Semi-Active and Hybrid Control. Proceedings on the 1997 American Control Conference, June 1997

19. Wikipedia.org. http://en.wikipedia.org/wiki/LA_City_Hall

20. Yang, J. N., Li, Z., Wu, J. C. 1994. Control of Seismic-Excited Buildings using Active Variable Stiffness Systems. Proceedings of the American Control Conference, Baltimore, MD, June 1994: 1083-1088

21. Yang, J. N., Kim, J. H., Agrawal, A. K. 1999a. A Semi-Active Stiffness Damper for Vibration Control of Civil Engineering Structures. Proceedings of the 17th International Modal Analysis Conference: 437-443

22. Yang, J. N., Kim, J. H., Agrawal, A. K. 1999b. Seismic Response Control using a Semi-Active Stiffness Damper. Proceedings of the International Workshop on Base Isolation, Energy Dissipation and Control of Structures, Guangzhou, China, May 1999

23. Yang, J. N., Kim, J. H., Agrawal, A. K. 1999c. A Resetting Semi-Active Stiffness Damper for Seismic Response Control. Submitted to the ASCE for publication in the Journal of Structural Engineering

24. Zhao, B., X. Lu, M. Wu, and Z. Mei. 2000. Sliding mode control of buildings with base-isolation hybrid protective systems. Earthquake Engineering & Structural Dynamics 29, : 315-26.

# 10.0 APPENDICES

## Appendix A – MATLAB Code: Earthquake Response

```
%ASSUMED BUILDING DESIGN PARAMETERS
n=11;                   %Number of stories
h=4;                    %Story height, (m)
H=h*n;                  %Building height, (m)
L=50;                   %Building length, (m)
W=50;                   %Building width, (m)
d=0.1;                  %Thickness of concrete floor,(m)
concrete=2400;          %Unit weight of concrete,(kg/m3)
steel=40;               %Weight of steel per m2 of building, (kg/m2)
equipment=100;          %Weight of equipment, (kg/m2)
T1=0.1*n;               %Building fundamental period, (s)
w1=2*pi/T1;             %Building design fundamental frequency, (rad/s)
damping=0.1;            %Design damping coefficient

%CALCULATED BUILDING DESIGN PROPERTIES
m=L*W*d*concrete+L*W*(steel+equipment)  %Mass per floor, (kg)
y=1/n;
b=1:n;
phi=y.*transpose(b);                    %Fundamental mode linear
M=eye(n)*m;                             %Mass matrix, (kg)
P=M*phi;
Y1=ones(1,n)*y;
Y2=ones(1,n-1)*y;
S=diag(Y1)-diag(Y2,1);
k_prime=inv(S)*P;
k=w1^2.*k_prime         %Stiffness distribution, (N/m)
alpha=2*damping/w1;     %Stiffness proportional damping
c=alpha.*k;
c(1,1)=0.1*alpha*k(1,1) %Damping distribution, (Ns/m)
for i=1:n-1             %Build full stiffness matrix (N/m)
   K(i,i)=k(i)+k(i+1);  %Sets diagonals
   K(i+1,i)=-k(i+1);    %Sets values below diagonal
   K(i,i+1)=-k(i+1);    %Sets values above diagonal
   K(n,n)=k(n);         %Sets value for K(n,n)
   C(i,i)=c(i)+c(i+1);
   C(i+1,i)=-c(i+1);
   C(i,i+1)=-c(i+1);
   C(n,n)=c(n);
end
w=sqrt(eig(inv(M)*K))   %Calculates modal frequencies, clipped building
T=(2*pi)./w             %Calculates modal periods, clipped building

%EARTHQUAKE LOAD DATA
g=9.81;                 %gravity (m/s2)
load ImpVal2.txt        %Loads El Centro EQ data; dt = 0.01s for 40s
load Mexcit2.txt        %Loads Mexico City EQ data; dt = 0.02s for 180s
load Kobe.txt           %Loads Kobe EQ data; 0.01 for 40s
load Pacoima1.txt       %Loads Pacoima EQ data; 0.01 for 40s
ag_elcentro=ImpVal2(:,2); %Extracts all data from row 2
ag_mexico=Mexcit2(:,2);
ag_kobe=Kobe(:,2);
```

```
ag_pacoima=Pacoima1(:,2);
dt=0.01;                    %time steps (match specific earthquake)
duration=40;
steps=duration/dt;      %total steps = (EQ time of interest)/dt
p_ag=ag_elcentro*g;     %Stores earthquake acceleration data in a vector

%STATE SPACE FORMULATION
A=[zeros(n),eye(n);-K/M,-C/M]; %18X18 matrix, 0's top left, I top
                               right, -K/M bot left, -C/M bot right
Bg=[zeros(n,1);ones(n,1)];     %Vector w/0's in rows 1 through n,
                               1's inrows n+1 through 2*n
Xeqclip=zeros(2*n,steps);      %Initialization of variables (Required
%because solving for X & Xdot starting   from i+1;Creates matrix of
zero's with 18(28*n) rows and # of steps columns
Xequnclip=zeros(2*n,steps);

%CLIPPED RESPONSE TO EARTHQUAKE
for j=1:steps
  Xeqclip(:,j+1)=expm(A*dt)*Xeqclip(:,j)+inv(A)*(expm(A*dt)-
eye(2*n))*(Bg.*p_ag(j));                          %Connor 2003 eqn 8.271
   Xdoteqclip(:,j+1)=A*Xeqclip(:,j)+Bg.*p_ag(j); %Connor 2003 eqn 8.218
   time(j)=dt*j;
end

%UNCLIPPED RESPONSE TO EARTHQUAKE
Tp1=3;
wp1=2*pi/Tp1;
kp1=wp1^2*m*n;
Kunc=K;
Kunc(1,1)=kp1-Kunc(1,2);
Kp=K;                                             %starts clipped
Ap=A;
control=0;

for j=1:steps
   if (abs(p_ag(j)))>.01*g && (control==0) %if clipped & above
                                           threshold, unclip
       Kp=Kunc;
       control=1;
       Ap=[zeros(n),eye(n);-Kp/M,-C/M];
   end
   if (abs(p_ag(j)))<0.005*g && (control==1) %if unclipped & below
                                             threshold, clip
       Kp=K;
       control=0;
       Ap=[zeros(n),eye(n);-Kp/M,-C/M];
   end
   Xequnclip(:,j+1)=expm(Ap*dt)*Xequnclip(:,j)+inv(Ap)*(expm(Ap*dt)-
eye(2*n))*(Bg.*p_ag(j));
   Xdotequnclip(:,j+1)=Ap*Xequnclip(:,j)+Bg.*p_ag(j);
   ctrl_store(j)=control;
end

wp=sqrt(eig(inv(M)*Kp)) %Calculates modal frequencies, unclipped bldg
Tp=(2*pi)./wp           %Calculates modal periods, unclipped building
```

```
for j=1:steps
   for a=2:n
       inter_clip(a,j)=Xeqclip(a,j)-Xeqclip(a-1,j);
       inter_unclip(a,j)=Xequnclip(a,j)-Xequnclip(a-1,j);
   end
   inter_clip(1,j)=Xeqclip(1,j);
   inter_unclip(1,j)=Xequnclip(1,j);
end

%PLOT TOTAL DISPLACEMENT
plot(time(1:steps),Xeqclip(1,1:steps)*100,'b'); hold all;
plot(time(1:steps),Xequnclip(1,1:steps)*100,'r:');
grid on;
legend('Clipped','Unclipped')
ylabel('\fontname{times} Total Disp(cm)', 'FontSize', 10)
xlabel('\fontname{times} Time(s)', 'FontSize', 10)
title('Total Displacement @ Ground Floor')
pause;
close;

plot(time(1:steps),Xeqclip(n,1:steps)*100,'b'); hold all;
plot(time(1:steps),Xequnclip(n,1:steps)*100,'r:');
grid on;
legend('Clipped','Unclipped')
ylabel('\fontname{times} Total Disp(cm)', 'FontSize', 10)
xlabel('\fontname{times} Time(s)', 'FontSize', 10)
title('Total Displacement @ Top Floor')
pause;
close;

%PLOT INTERSTORY DRIFT
plot(time(1:steps),inter_clip(2,1:steps)*100,'b'); hold all;
plot(time(1:steps),inter_unclip(2,1:steps)*100,'r:');
grid on;
legend('Clipped','Unclipped')
ylabel('\fontname{times} Interstory Disp(cm)', 'FontSize', 10)
xlabel('\fontname{times} Time(s)', 'FontSize', 10)
title('Interstory Displacement Between Floors 1 & 2')
pause;
close;

plot(time(1:steps),inter_clip(n,1:steps)*100,'b'); hold all;
plot(time(1:steps),inter_unclip(n,1:steps)*100,'r:');
grid on;
legend('Clipped','Unclipped')
ylabel('\fontname{times} Interstory Disp(cm)', 'FontSize', 10)
xlabel('\fontname{times} Time(s)', 'FontSize', 10)
title('Interstory Displacement Between Top Floors')
pause;
close;
```

## Appendix B – MATLAB Code: Wind Response

```
%ASSUMED BUILDING DESIGN PARAMETERS (SAME AS EARTHQUAKE CODE)

%CALCULATED BUILDING DESIGN PROPERTIES (SAME AS EARTHQUAKE CODE)

%WIND LOAD DATA
sswind=958;                  %Steady state pressure at 100mph (N/m2)
F_sswind=(sswind*L*H)/(n-1) %Steady state force acting at each node,(N)
T_sswind=50;                 %Period steady state wind acts (s)
omega_sswind=2*pi/T_sswind; %Steady syae forcing frequency (rad/s)
gust=479;                    %Gust pressure at 50mph (N/m2)
F_gust=(gust*L*H)/(n-1)      %Gust force acting at each node,(N)
T_gust=5;                    %Period gust acts (s)
omega_gust=2*pi/T_gust;      %Gust forcing frequency (rad/s)
for j=1:steps                %Stores wind data in a vector
   p_wind(j)=F_sswind*sin(omega_sswind*j*dt);
end
for j=10/dt:15/dt
   p_wind(j)=p_wind(j)+F_gust*sin(omega_gust*j*dt);
end

%STATE SPACE FORMULATION (SAME AS EARTHQUAKE CODE)

%CLIPPED RESPONSE TO WIND
for j=1:steps
  time(j)=dt*j;
  Xwindclip(:,j+1)=expm(A*dt)*Xwindclip(:,j)+inv(A)*(expm(A*dt)-
eye(2*n))*(Bp.*p_wind(j));
  Xdotwindclip(:,j+1)=A*Xwindclip(:,j)+Bp.*p_wind(j);
end

%UNCLIPPED RESPONSE TO WIND
Tp1=3;
wp1=2*pi/Tp1;
kp1=wp1^2*m*n;
Kunc=K;
Kunc(1,1)=kp1-Kunc(1,2);
Aunc=[zeros(n),eye(n);-Kunc/M,-C/M]; %Unclipped A matrix

for j=1:steps
Xwindunclip(:,j+1)=expm(Aunc*dt)*Xwindunclip(:,j)+inv(Aunc)*(expm(Aunc*
dt)-eye(2*n))*(Bp.*p_wind(j));
   Xdotwindunclip(:,j+1)=Aunc*Xwindunclip(:,j)+Bp.*p_wind(j);
end

%CALCULATES INTERSTORY DRIFT DUE TO WIND
for j=1:steps
   for a=2:n
       inter_clip(a,j)=Xwindclip(a,j)-Xwindclip(a-1,j);
       inter_unclip(a,j)=Xwindunclip(a,j)-Xwindunclip(a-1,j);
   end
   inter_clip(1,j)=Xwindclip(1,j);
   inter_unclip(1,j)=Xwindunclip(1,j);
end
```

```
%PLOT TOTAL DISPLACEMENT DUE TO WIND
for s=1:n
plot(time(1:steps),Xwindclip(s,1:steps)*100,'b'); hold all;
plot(time(1:steps),Xwindunclip(s,1:steps)*100,'r:');
grid on;
legend('Clipped','Unclipped')
ylabel('\fontname{times} Total Disp(cm)', 'FontSize', 10)
xlabel('\fontname{times} Time(s)', 'FontSize', 10)
title('Total Displacement Due to Wind @ All Floors')
end
pause;
close;

%PLOT INTERSTORY DISPLACEMENT DUE TO WIND
plot(time(1:steps),inter_clip(2,1:steps)*100,'b'); hold all;
plot(time(1:steps),inter_unclip(2,1:steps)*100,'r:');
grid on;
legend('Clipped','Unclipped')
ylabel('\fontname{times} Interstory Disp(cm)', 'FontSize', 10)
xlabel('\fontname{times} Time(s)', 'FontSize', 10)
title('Interstory Displacement Between Ground Floors')
pause;
close;

plot(time(1:steps),inter_clip(n,1:steps)*100,'b'); hold all;
plot(time(1:steps),inter_unclip(n,1:steps)*100,'r:');
grid on;
legend('Clipped','Unclipped')
ylabel('\fontname{times} Interstory Disp(cm)', 'FontSize', 10)
xlabel('\fontname{times} Time(s)', 'FontSize', 10)
title('Interstory Displacement Between Floors 10 & 11')
pause;
close;
```

Appendix C – Photos of isolation bearings

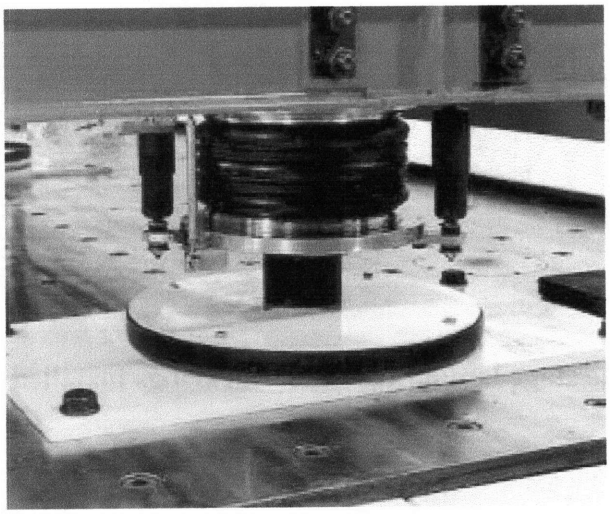

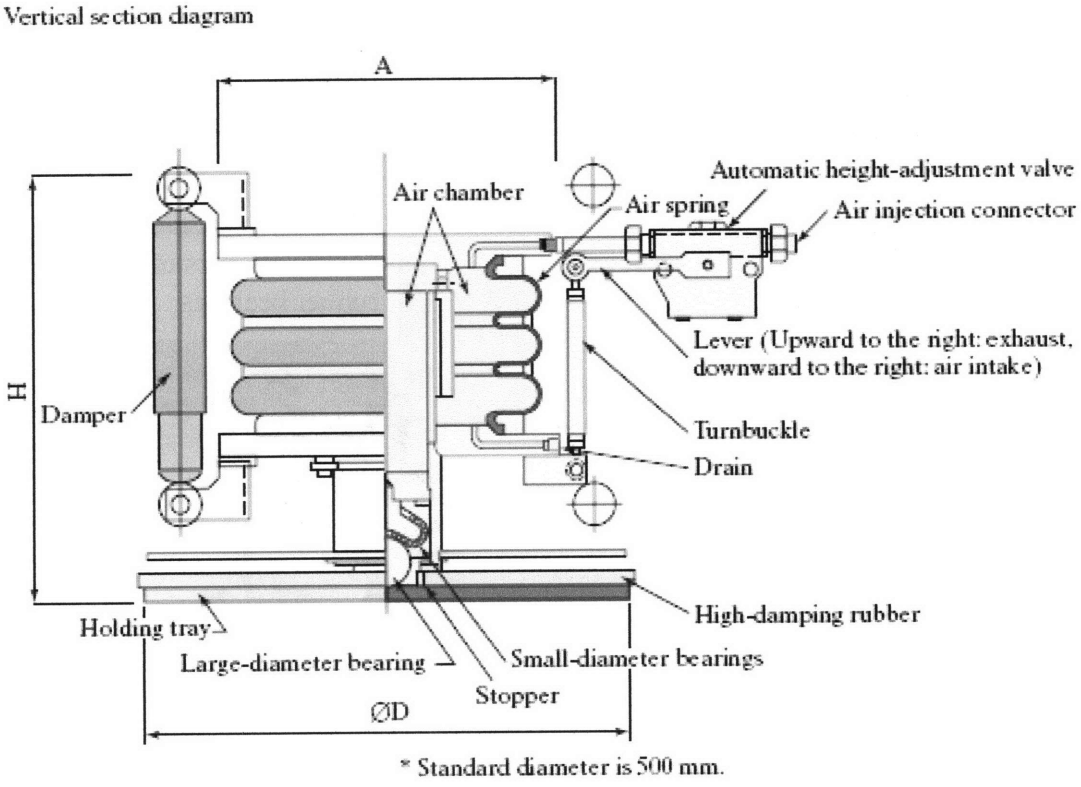


**Figure 45: Air spring damper (Connor, 2003)**

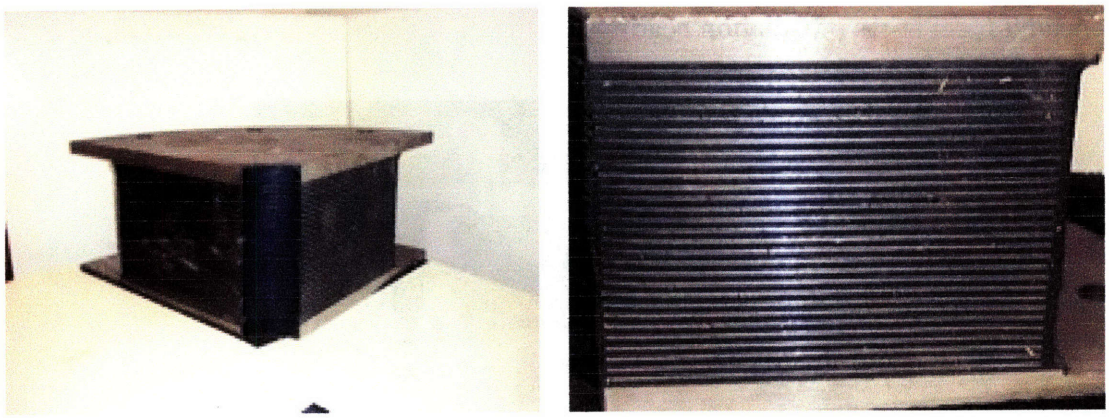

**Figure 46: Single stage laminated rubber bearings installed in LA City Hall**

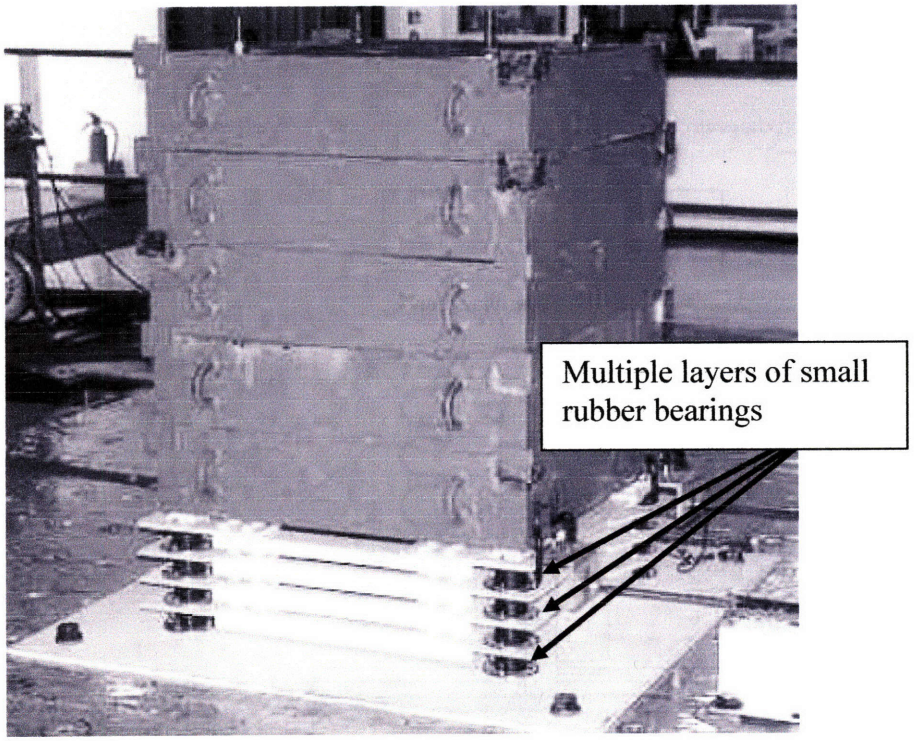


**Figure 47: Multiple Stage laminated rubber bearings (Connor, 2003)**

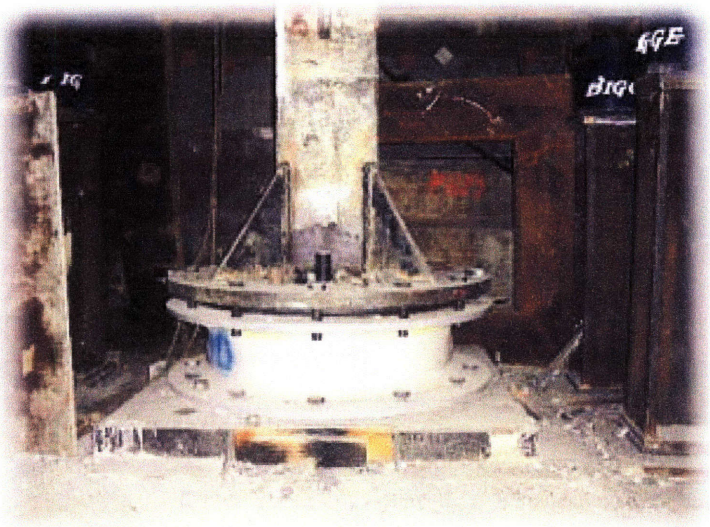

**Figure 48: Rubber bearing installed, LA City Hall (LA DPW)**

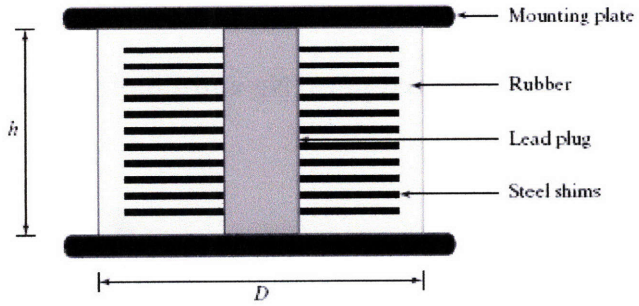


**Figure 49: Typical LRB (Connor, 2003)**

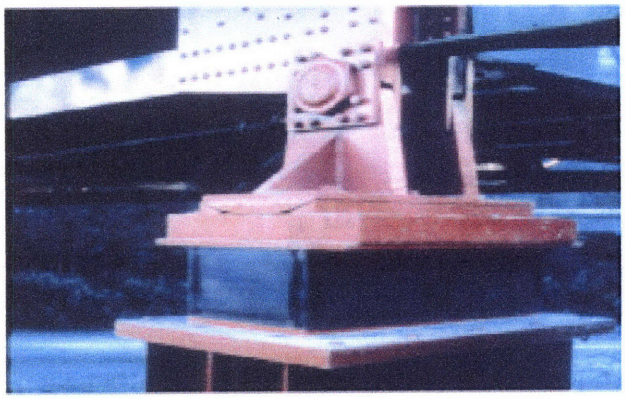

**Figure 50: Rubber-Lead core isolation bearing on California Bridge (Roberts, 2005)**

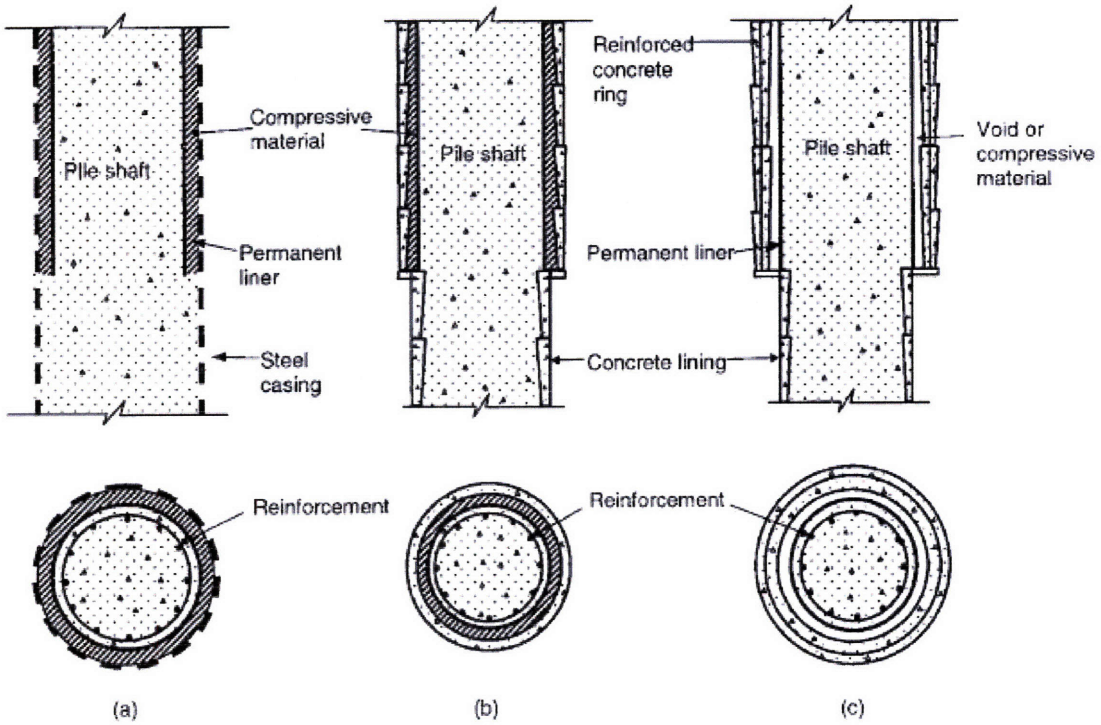


**Figure 51: Sleeved piles (Ng and Zhang, 2001)**

**Figure 52: Inverted pendulum being installed on the Benecia-Martinez Bridge in California (Roberts, 2005)**

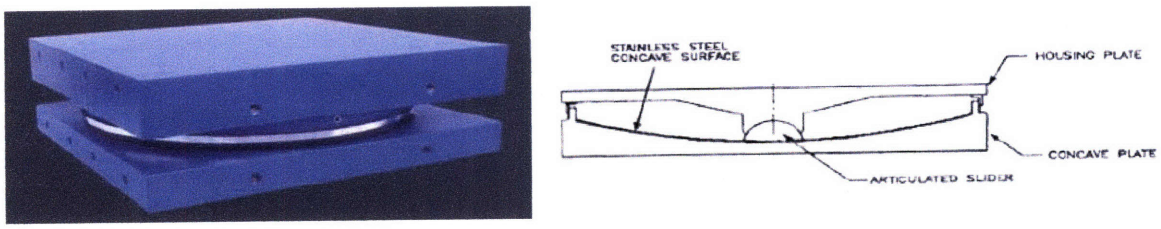


**Figure 53: LA Emergency Operations Center Friction Pendulum Isolator (Huang et al, 2006)**

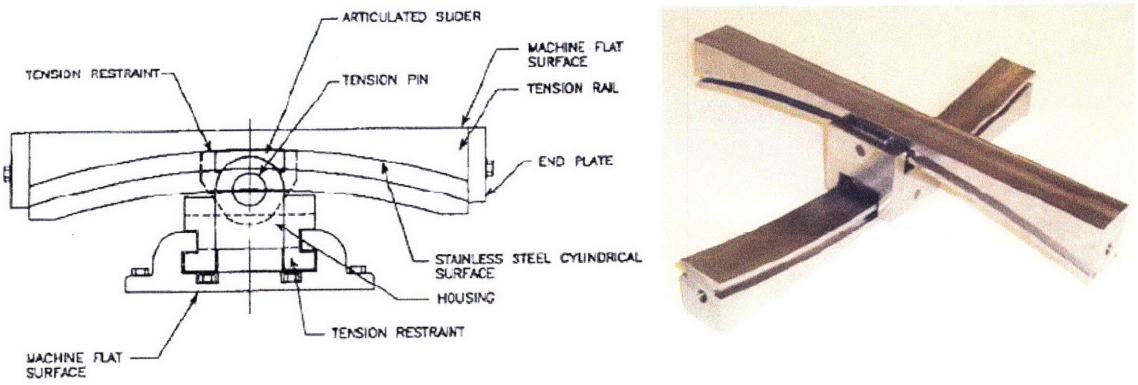


**Figure 54: LA EOC Tension-Restraint Friction Pendulum Isolator (Huang et al, 2006)**

# Appendix D – El Centro Earthquake Response

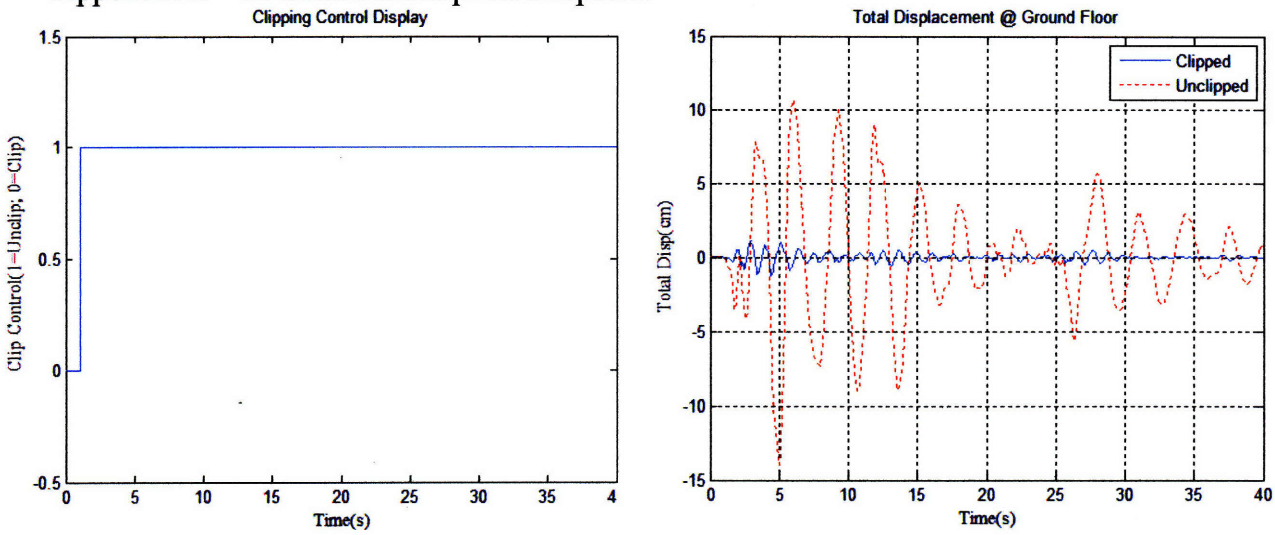


**Figure 55: Total Displacement Floor 1 due to El Centro earthquake: Remain unclipped**

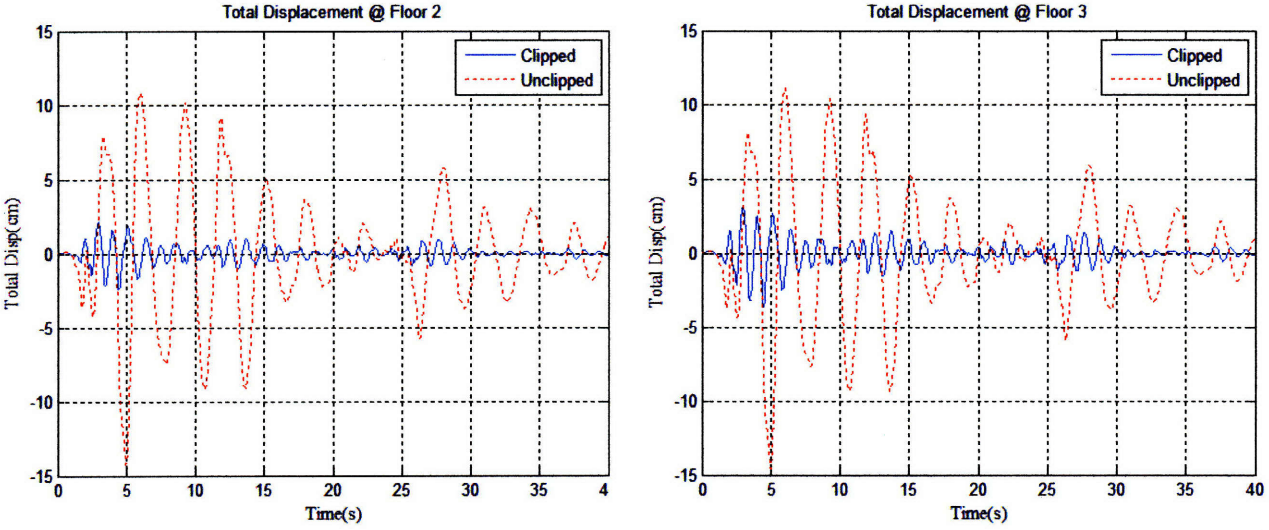


**Figure 56: Total Total Displacement Floors 2 & 3 due to El Centro earthquake: Remain unclipped**

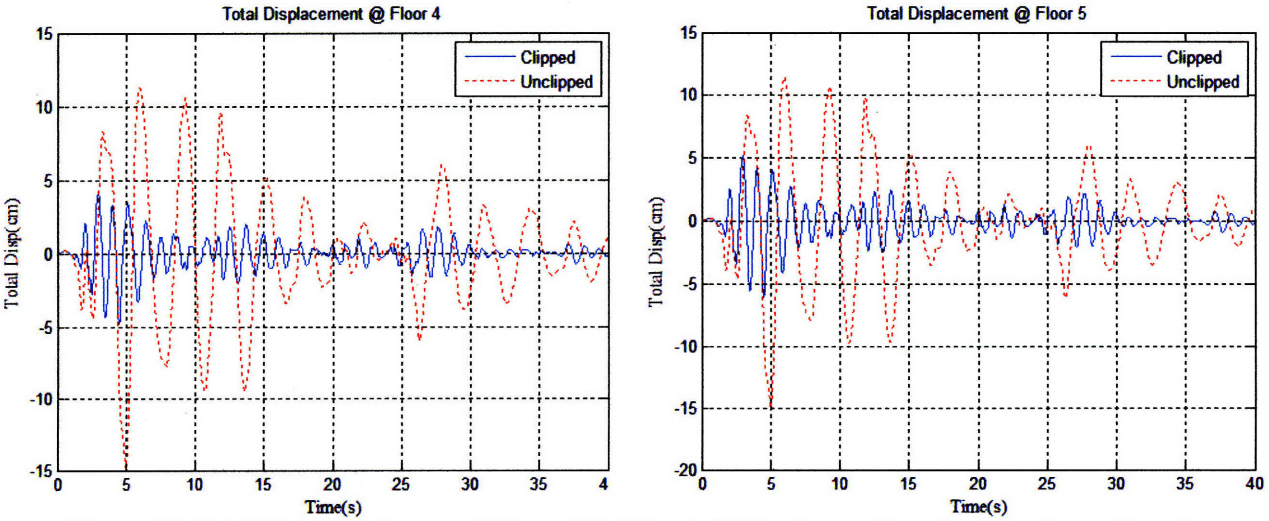


**Figure 57: Total Total Displacement Floors 4 & 5 due to El Centro earthquake: Remain unclipped**

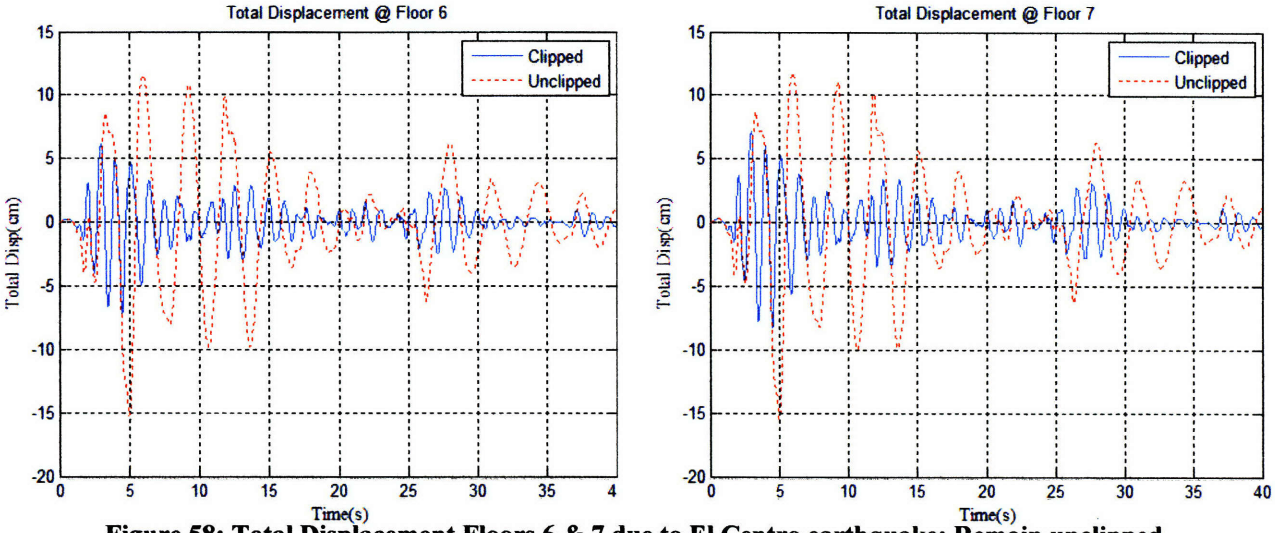


**Figure 58: Total Displacement Floors 6 & 7 due to El Centro earthquake: Remain unclipped**

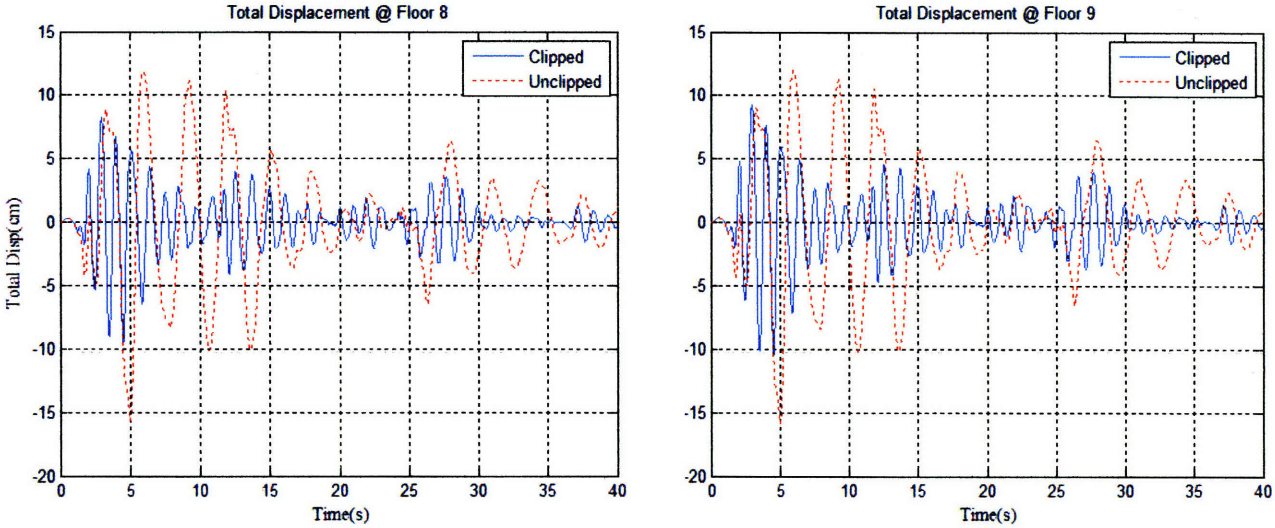


**Figure 59: Total Displacement Floors 8 & 9 due to El Centro earthquake: Remain unclipped**

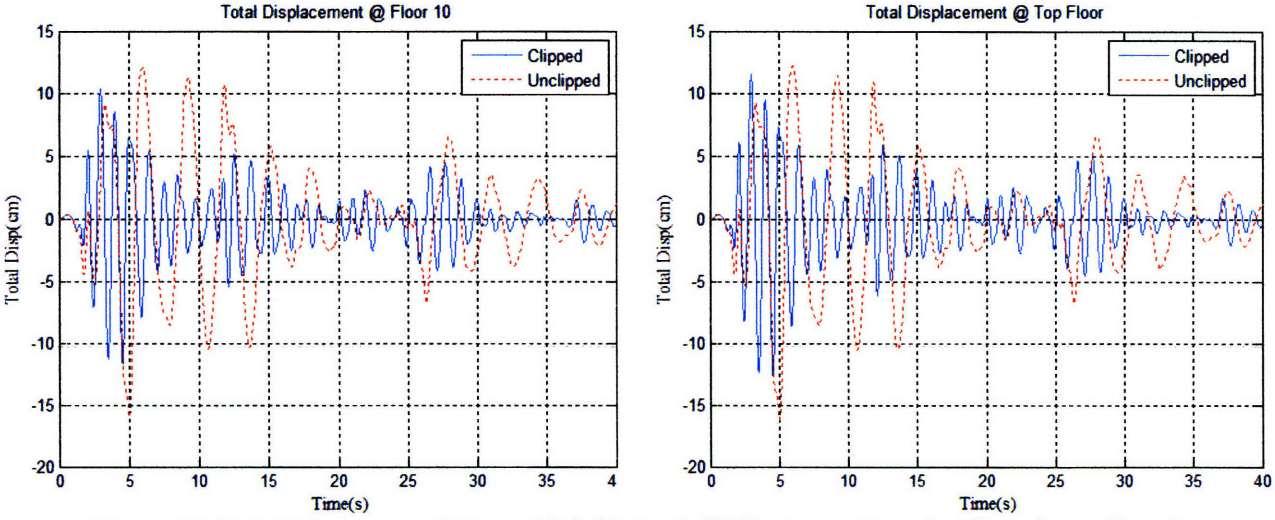


**Figure 60: Total Displacement Floors 10 & 11 due to El Centro earthquake: Remain unclipped**

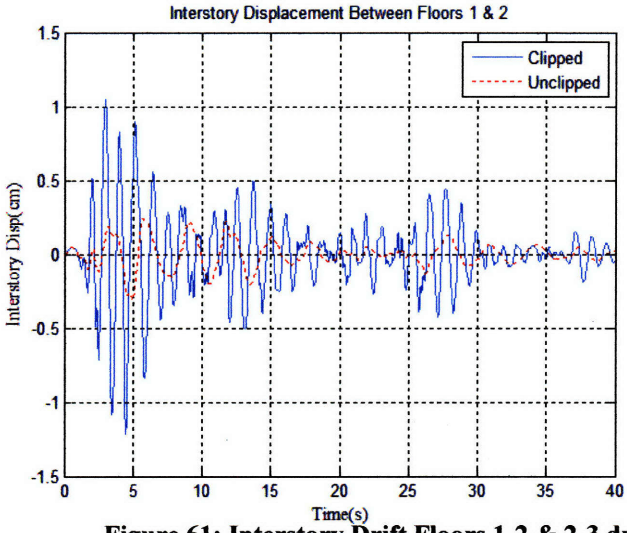


**Figure 61: Interstory Drift Floors 1-2 & 2-3 due to El Centro earthquake: Remain unclipped**

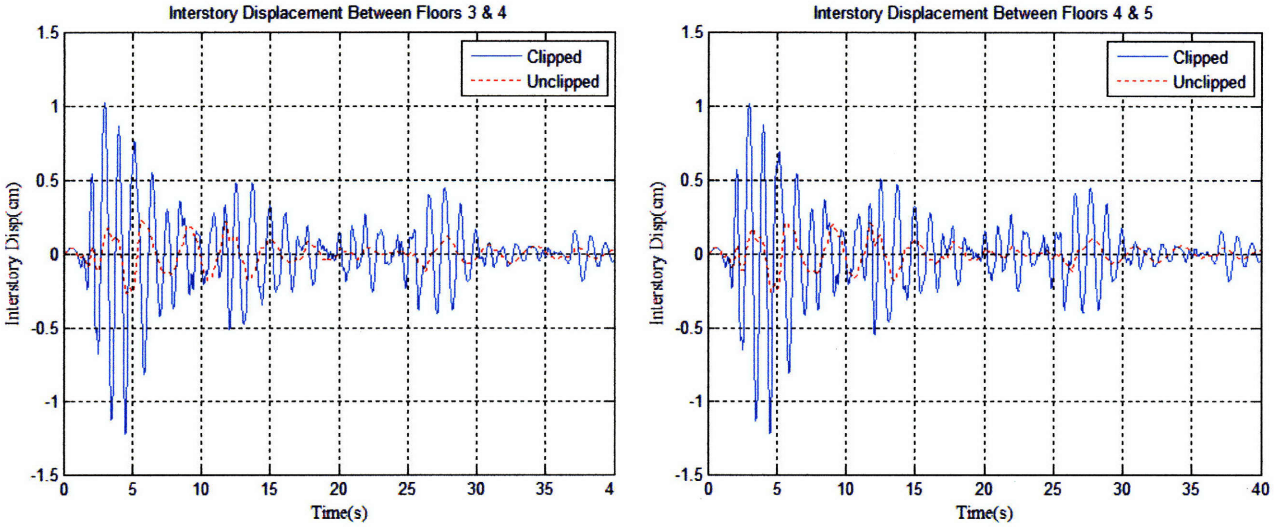


**Figure 62: Interstory Drift Floors 3-4 & 4-5 due to El Centro earthquake: Remain unclipped**

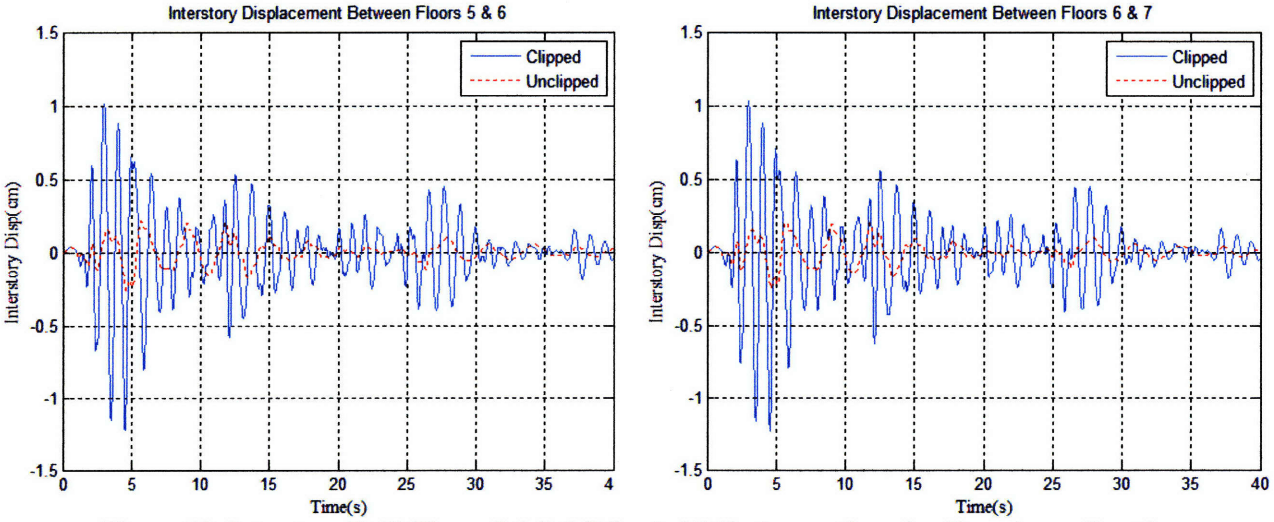


**Figure 63: Interstory Drift Floors 5-6 & 6-7 due to El Centro earthquake: Remain unclipped**

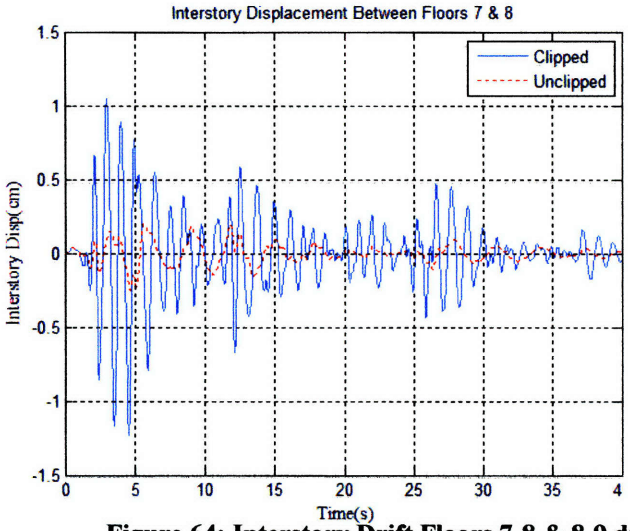


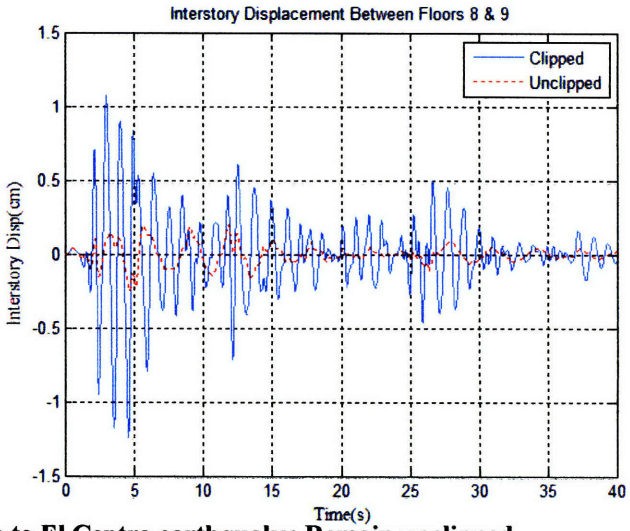


**Figure 64: Interstory Drift Floors 7-8 & 8-9 due to El Centro earthquake: Remain unclipped**

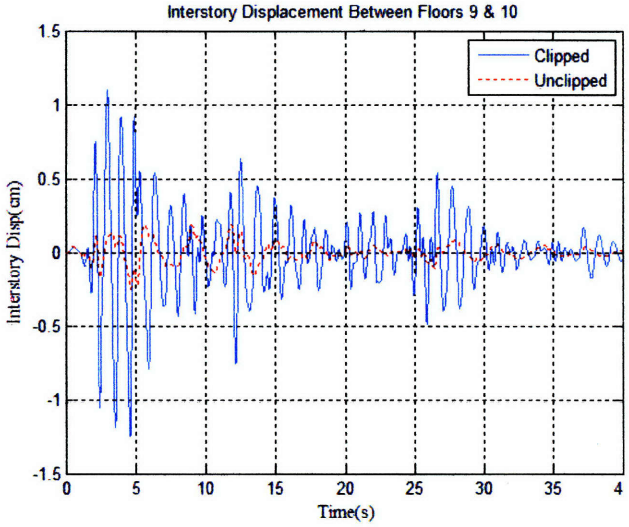


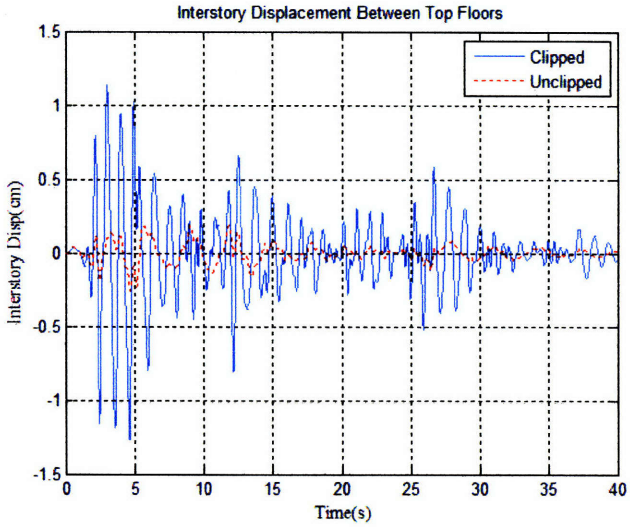


**Figure 65: Drift Floors 9-10 & 10-11 due to El Centro earthquake: Remain unclipped**

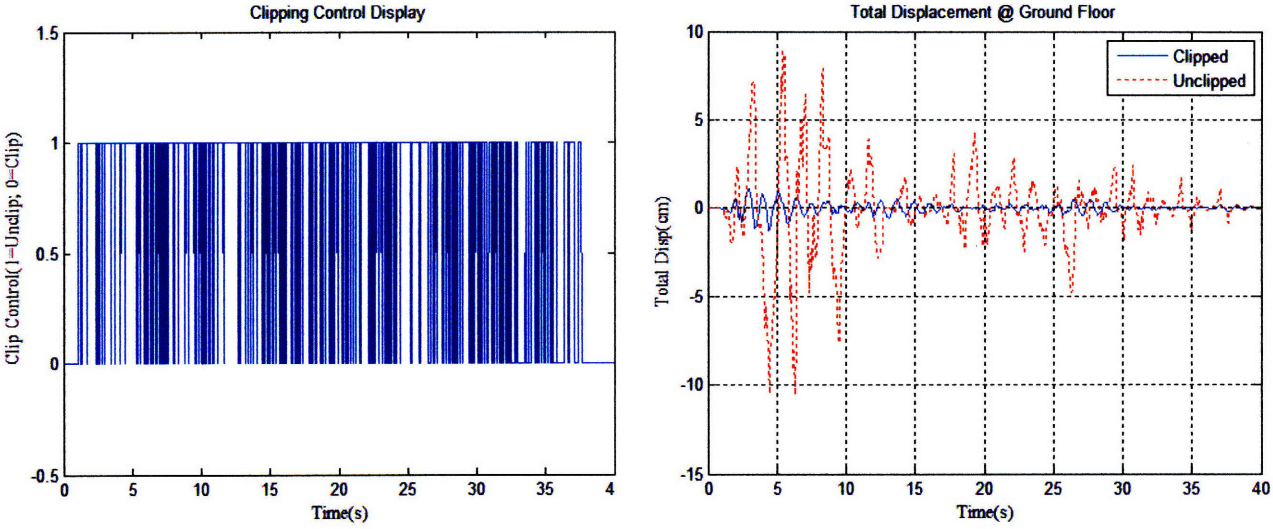


**Figure 66: Total Displacement Floor 1 due to El Centro earthquake: Continuous unclip/clip**

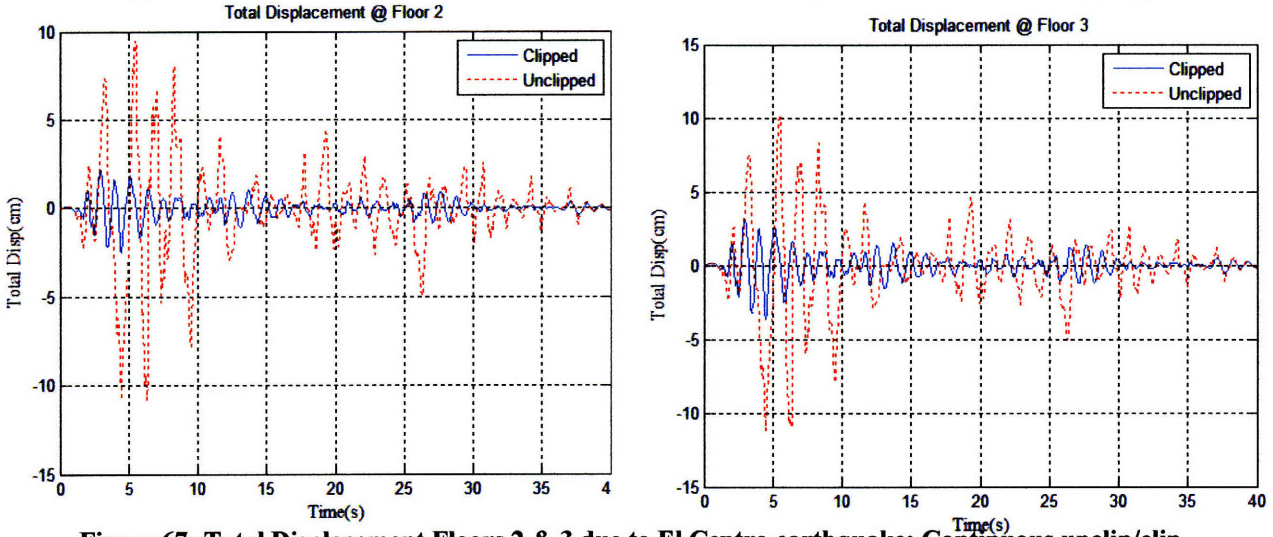


**Figure 67: Total Displacement Floors 2 & 3 due to El Centro earthquake: Continuous unclip/clip**

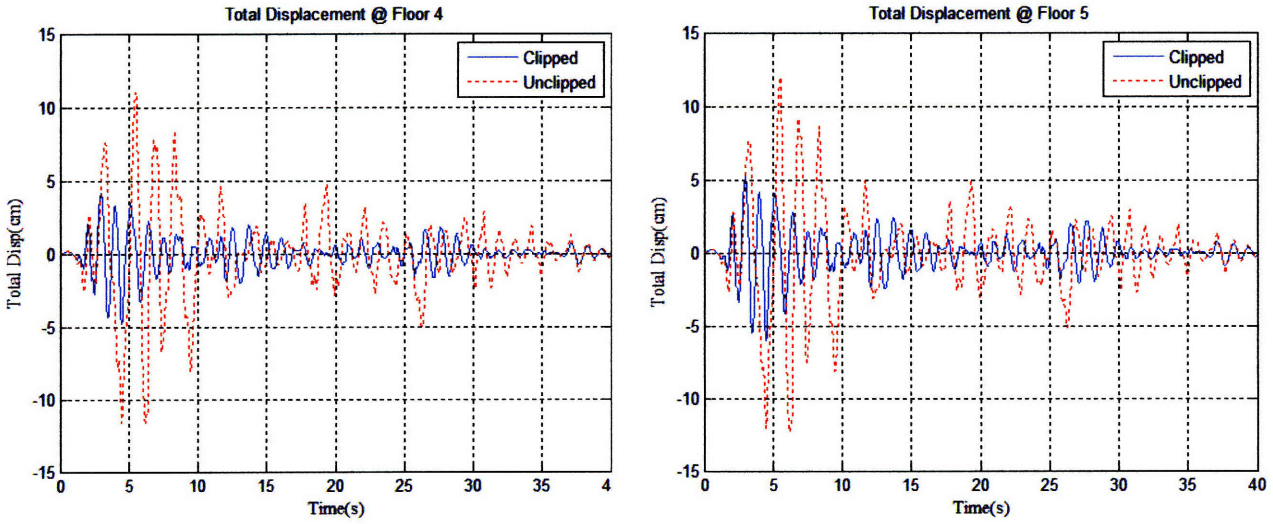


**Figure 68: Total Displacement Floors 4 & 5 due to El Centro earthquake: Continuous unclip/clip**

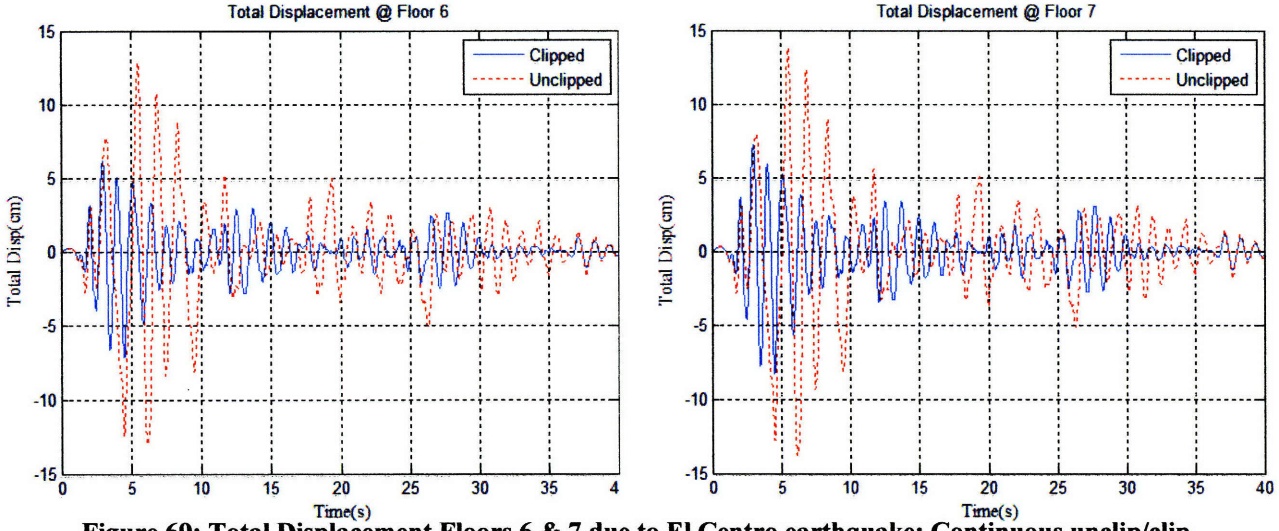


**Figure 69: Total Displacement Floors 6 & 7 due to El Centro earthquake: Continuous unclip/clip**

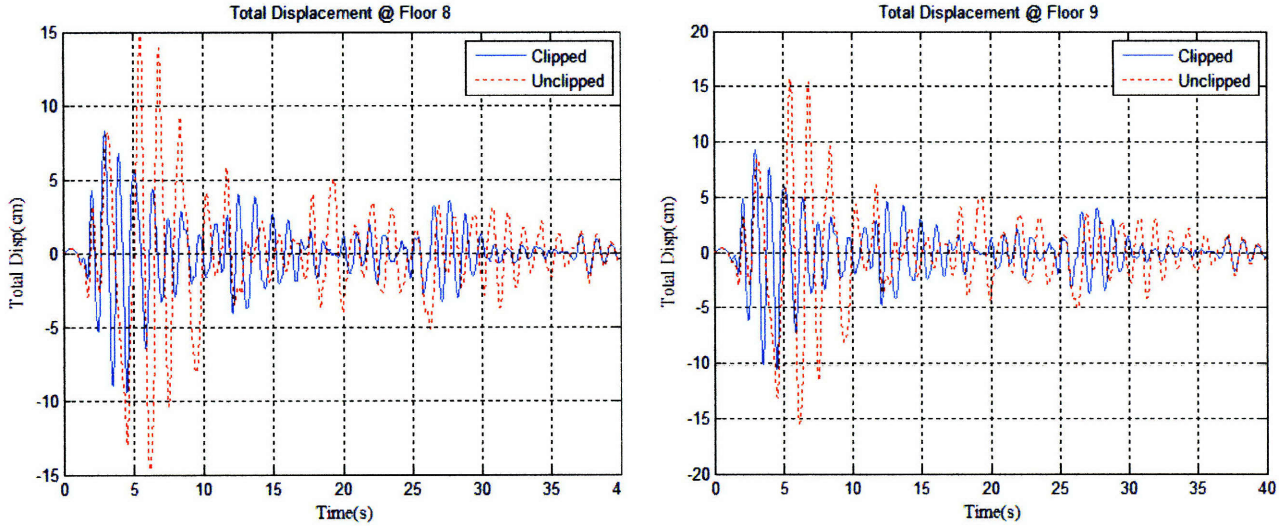


**Figure 70: Total Displacement Floors 8 & 9 due to El Centro earthquake: Continuous unclip/clip**

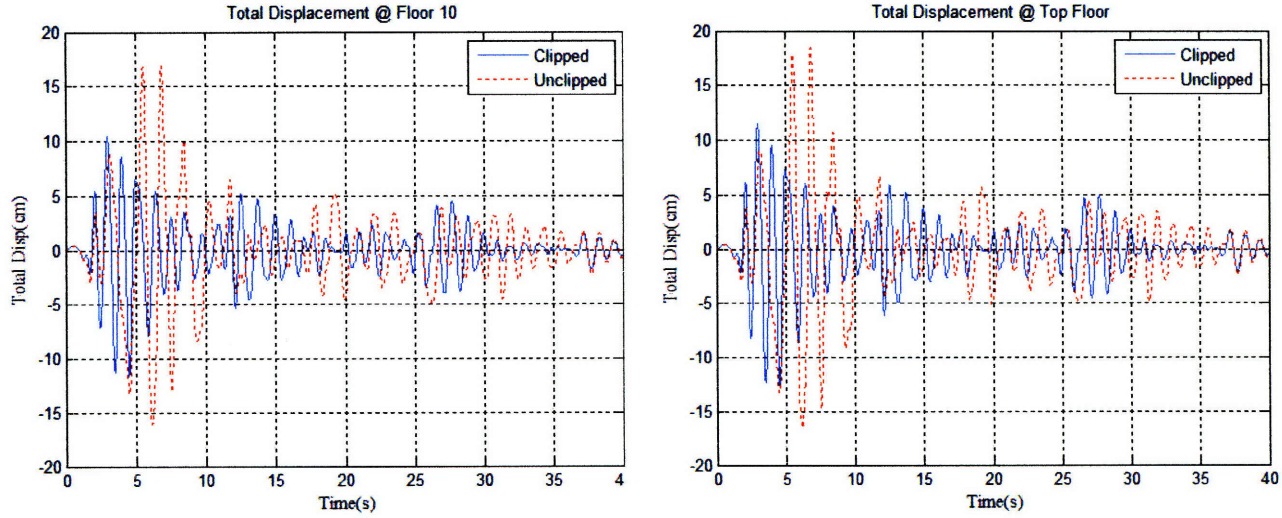


**Figure 71: Total Displacement Floors 10 & 11 due to El Centro earthquake: Continuous unclip/clip**

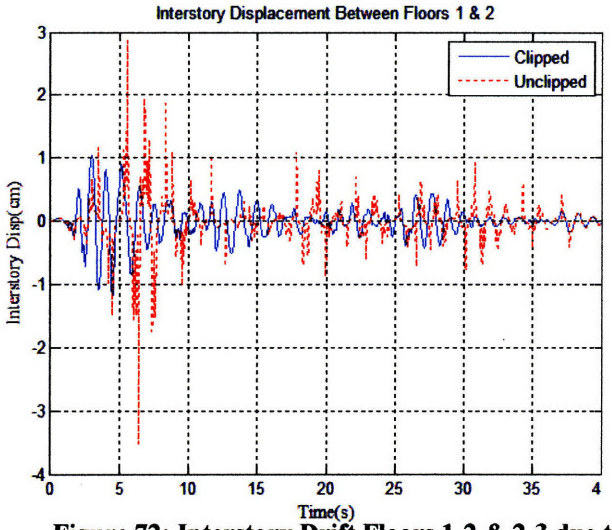


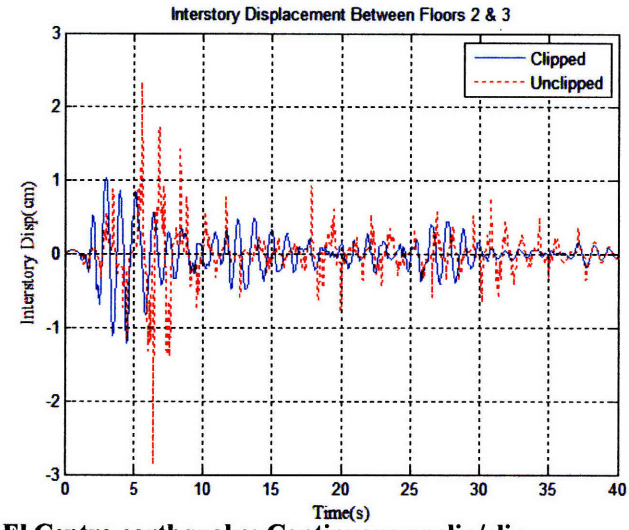


**Figure 72: Interstory Drift Floors 1-2 & 2-3 due to El Centro earthquake: Continuous unclip/clip**

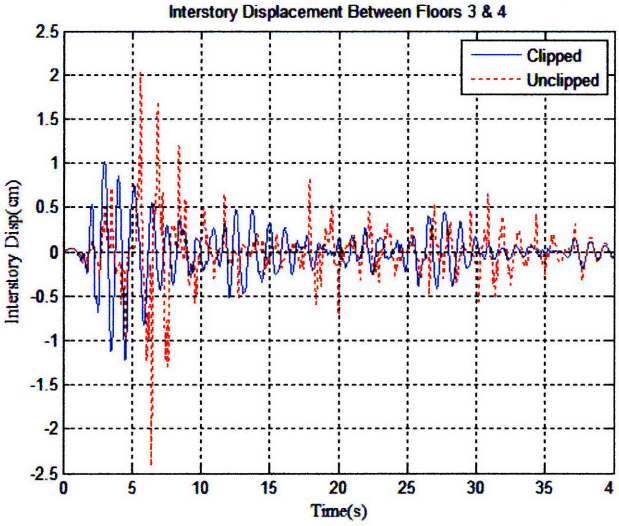


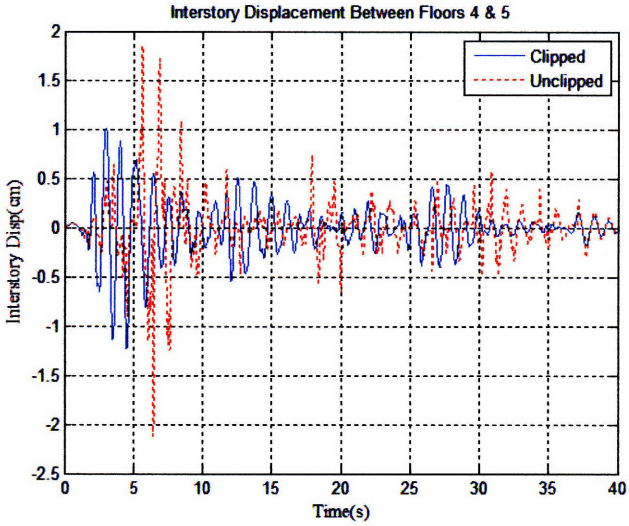


**Figure 73: Interstory Drift Floors 3-4 & 4-5 due to El Centro earthquake: Continuous unclip/clip**

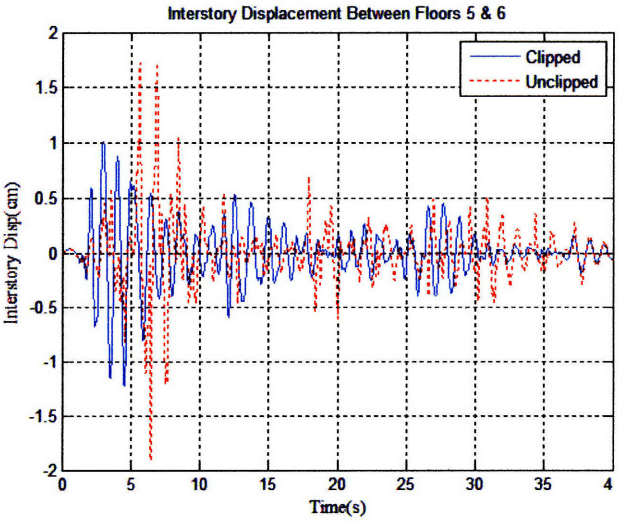


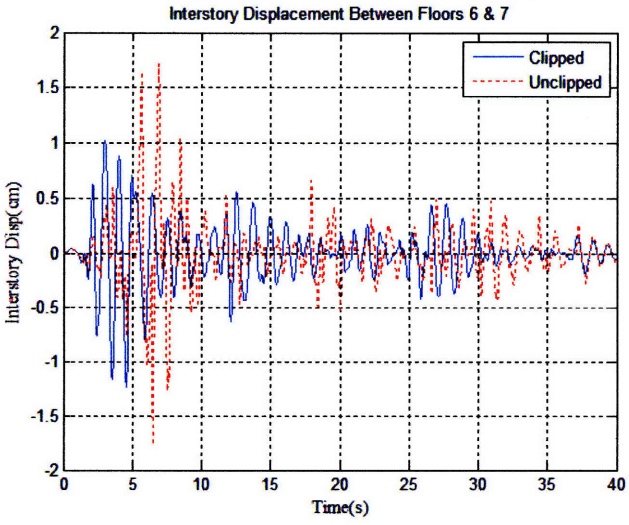


**Figure 74: Interstory Drift Floors 5-6 & 6-7 due to El Centro earthquake: Continuous unclip/clip**

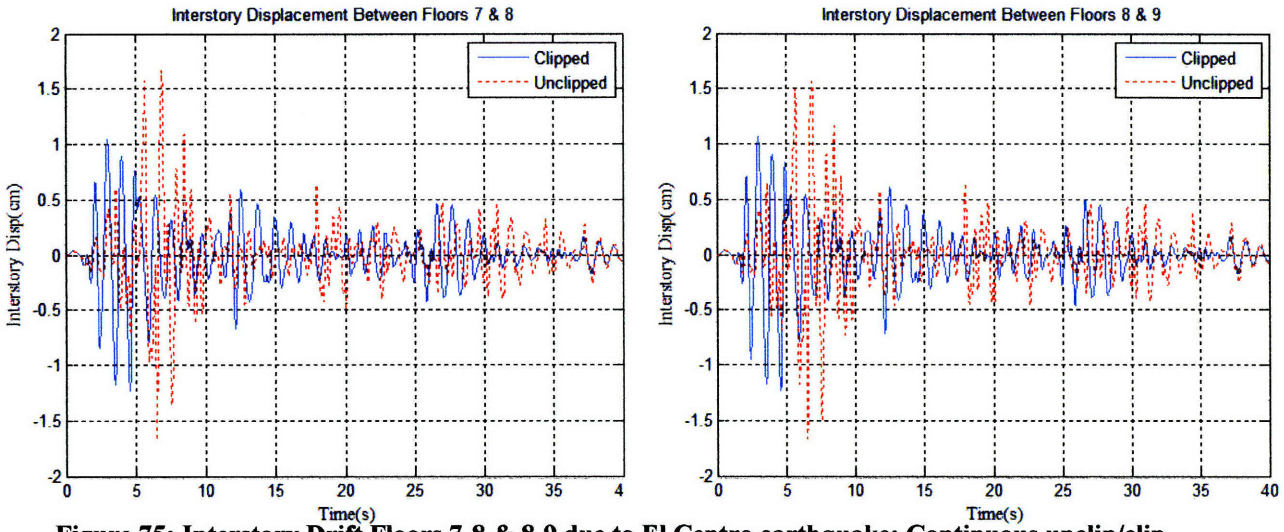


**Figure 75: Interstory Drift Floors 7-8 & 8-9 due to El Centro earthquake: Continuous unclip/clip**

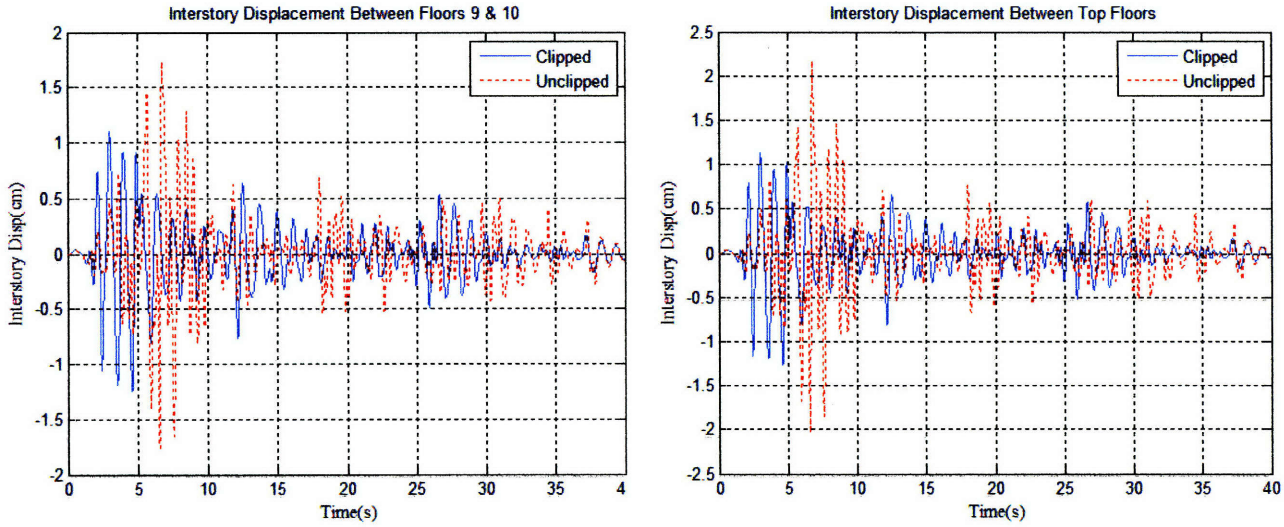


**Figure 76: Interstory Drift Floors 9-10 & 10-11 due to El Centro earthquake: Continuous unclip/clip**

# Appendix E – Mexico City Earthquake Response

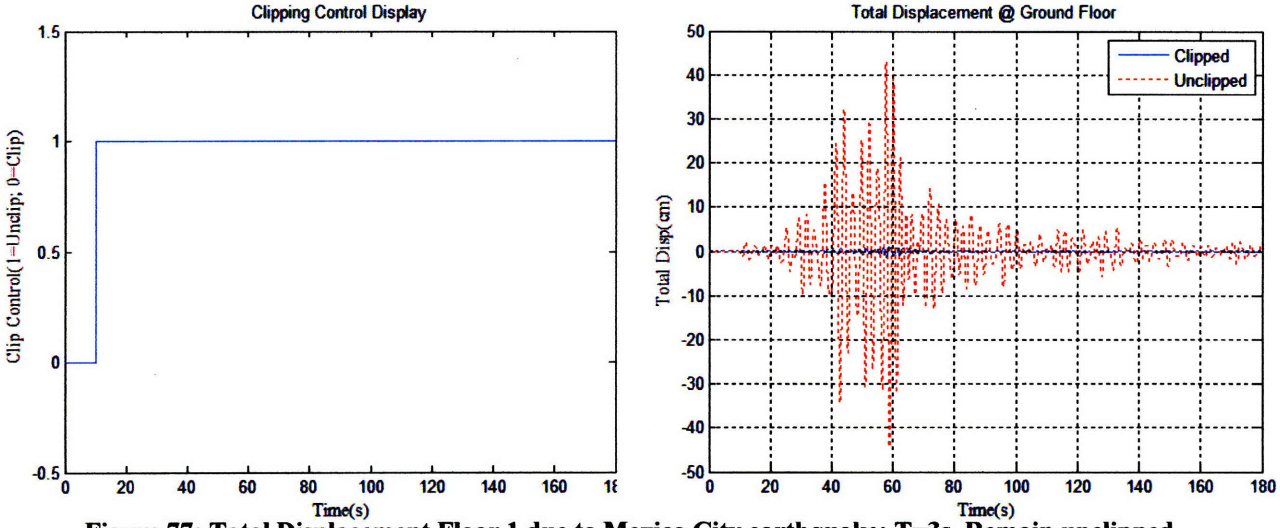


**Figure 77: Total Displacement Floor 1 due to Mexico City earthquake: T=3s, Remain unclipped**

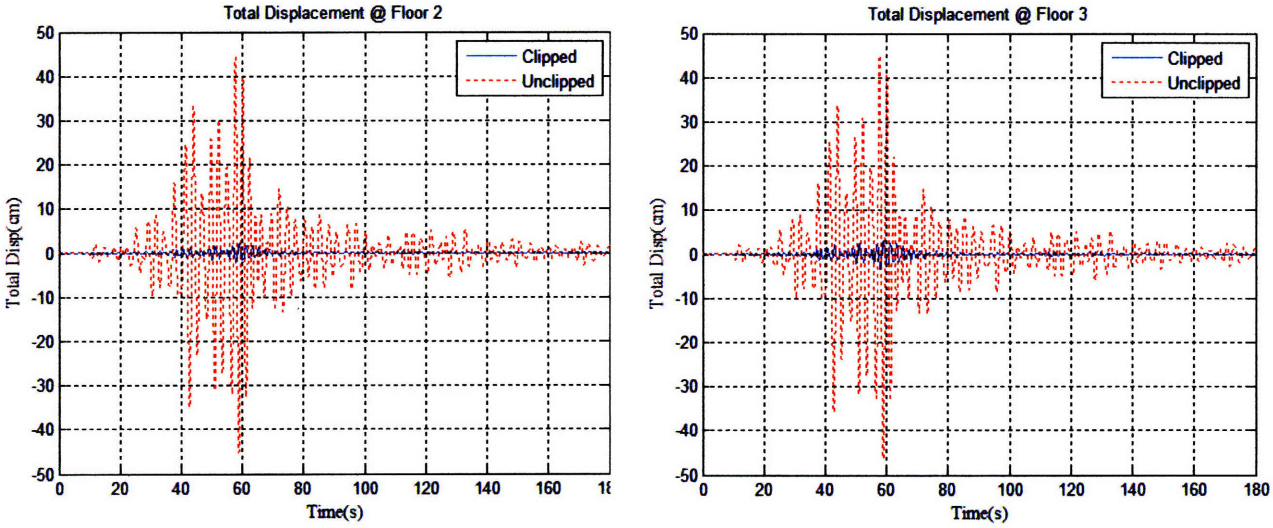


**Figure 78: Total Displacement Floors 2 & 3 due to Mexico City earthquake: T=3s, Remain unclipped**

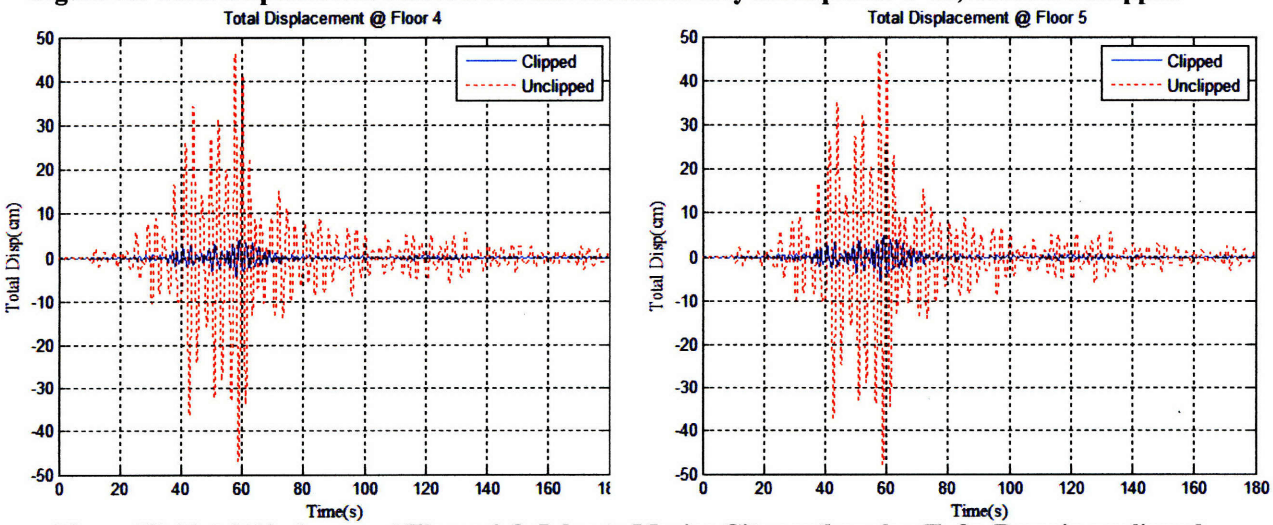


**Figure 79: Total Displacement Floors 4 & 5 due to Mexico City earthquake: T=3s, Remain unclipped**

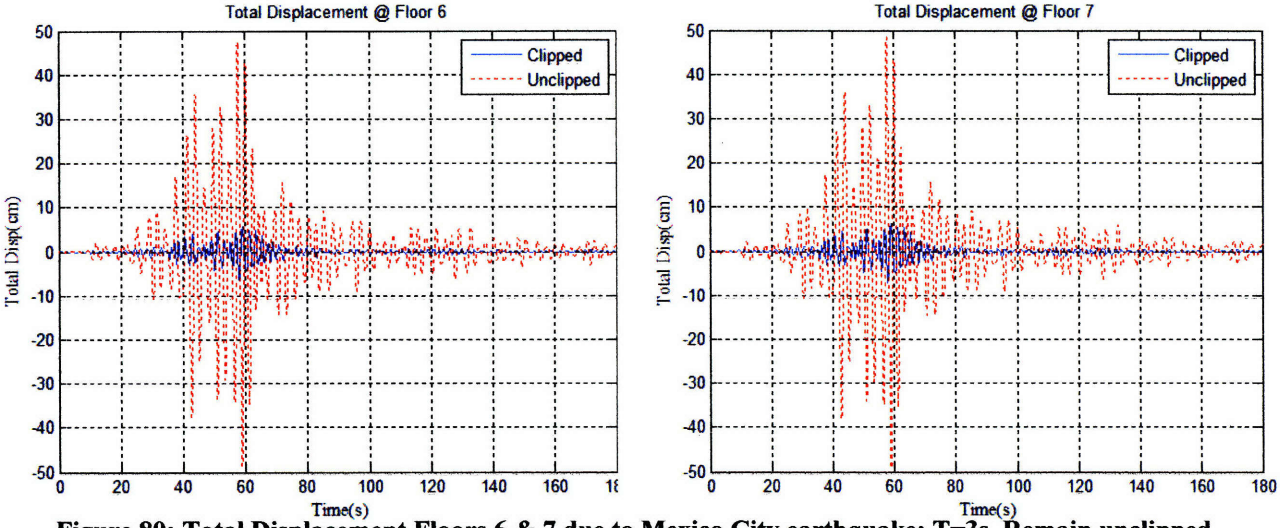


**Figure 80: Total Displacement Floors 6 & 7 due to Mexico City earthquake: T=3s, Remain unclipped**

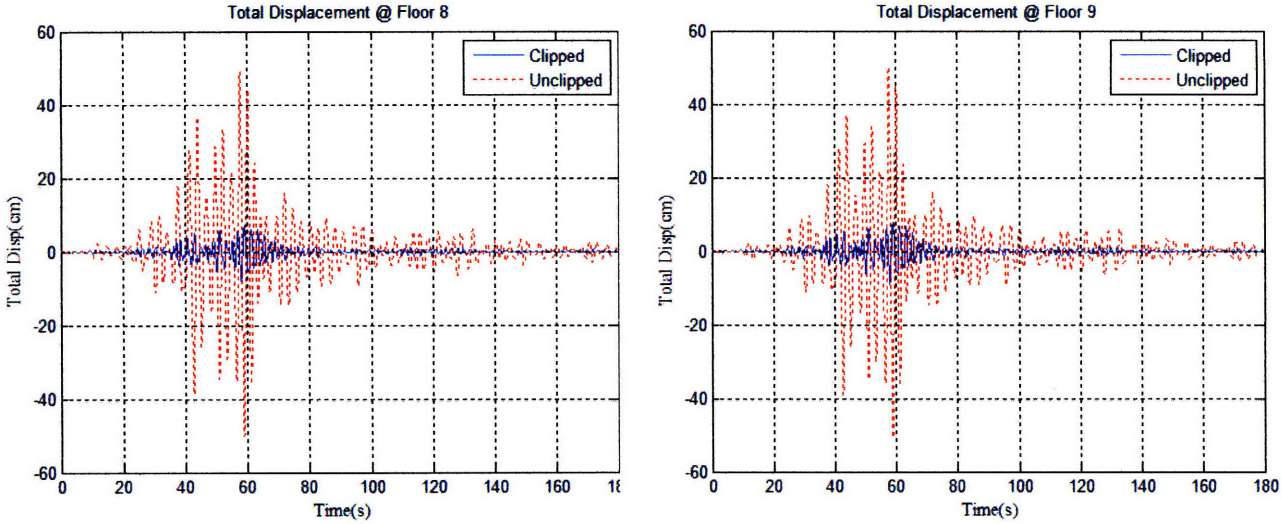


**Figure 81: Total Displacement Floors 8 & 9 due to Mexico City earthquake: T=3s, Remain unclipped**

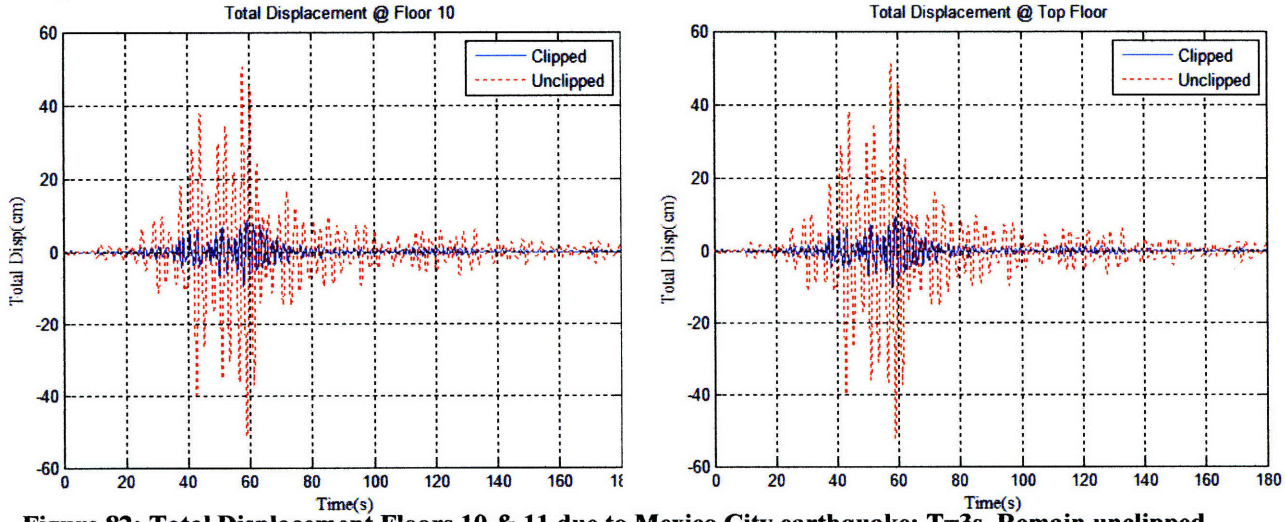


**Figure 82: Total Displacement Floors 10 & 11 due to Mexico City earthquake: T=3s, Remain unclipped**

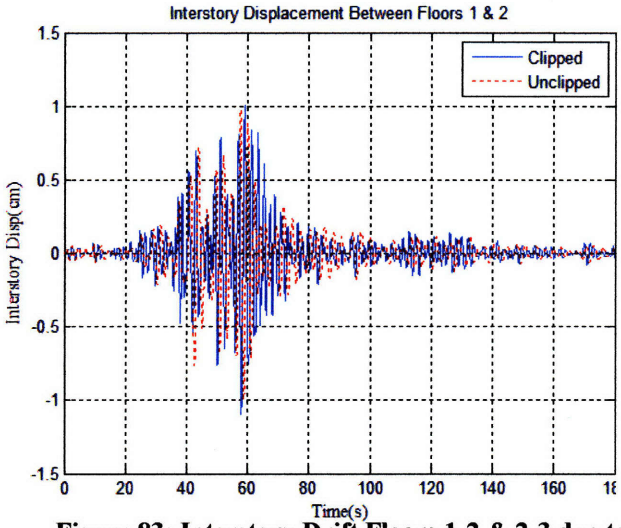


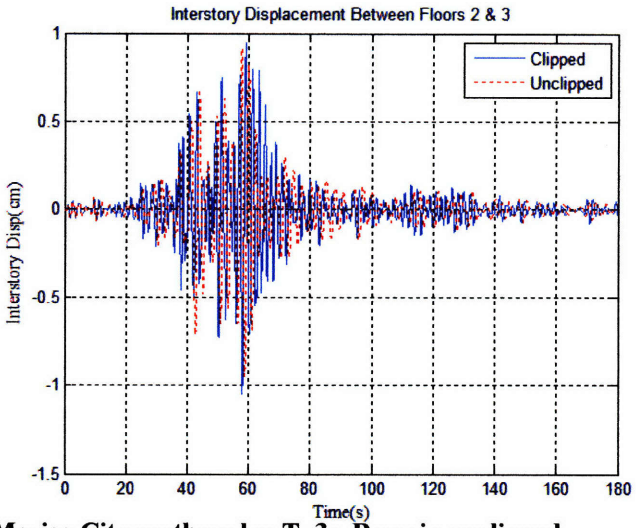


**Figure 83: Interstory Drift Floors 1-2 & 2-3 due to Mexico City earthquake: T=3s, Remain unclipped**

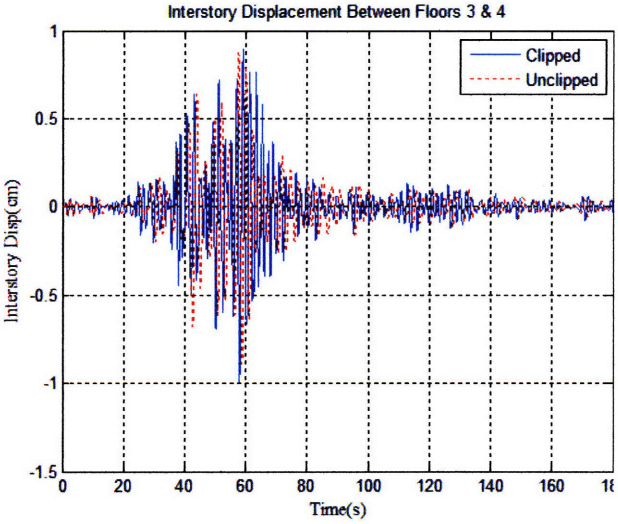


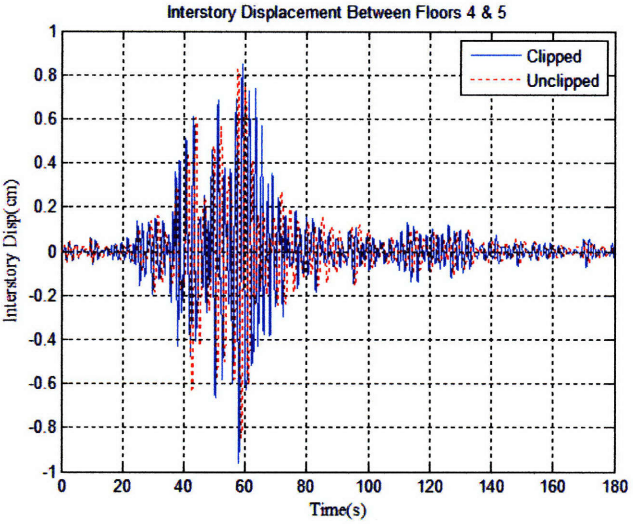


**Figure 84: Interstory Drift Floors 3-4 & 4-5 due to Mexico City earthquake: T=3s, Remain unclipped**

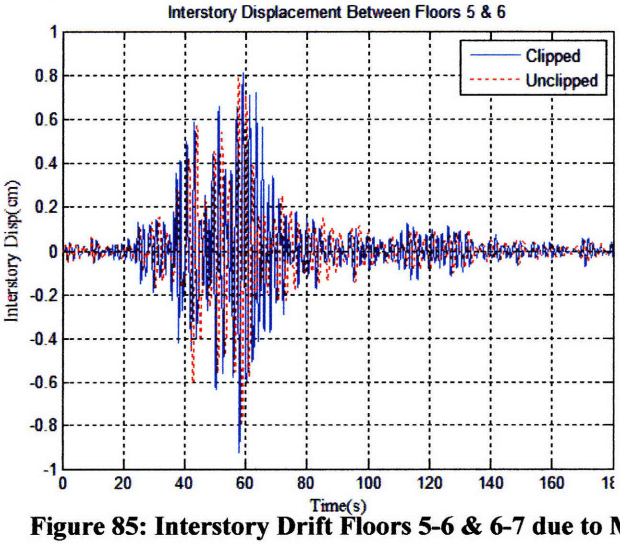


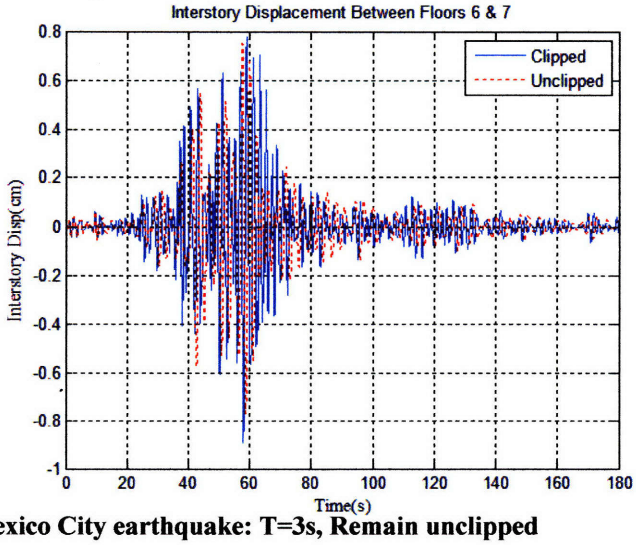


**Figure 85: Interstory Drift Floors 5-6 & 6-7 due to Mexico City earthquake: T=3s, Remain unclipped**

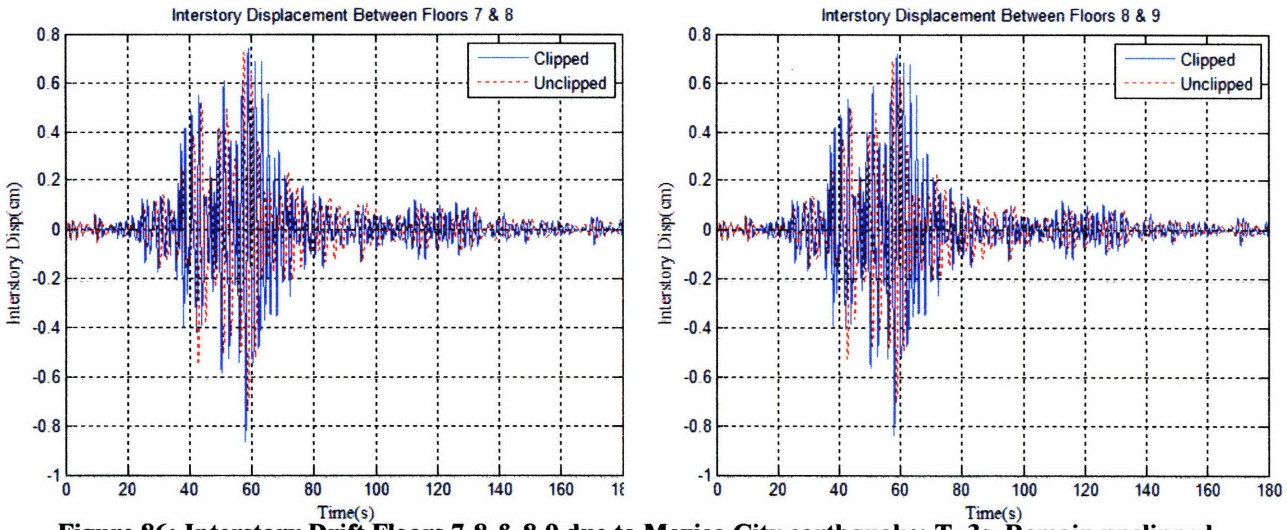


**Figure 86: Interstory Drift Floors 7-8 & 8-9 due to Mexico City earthquake: T=3s, Remain unclipped**

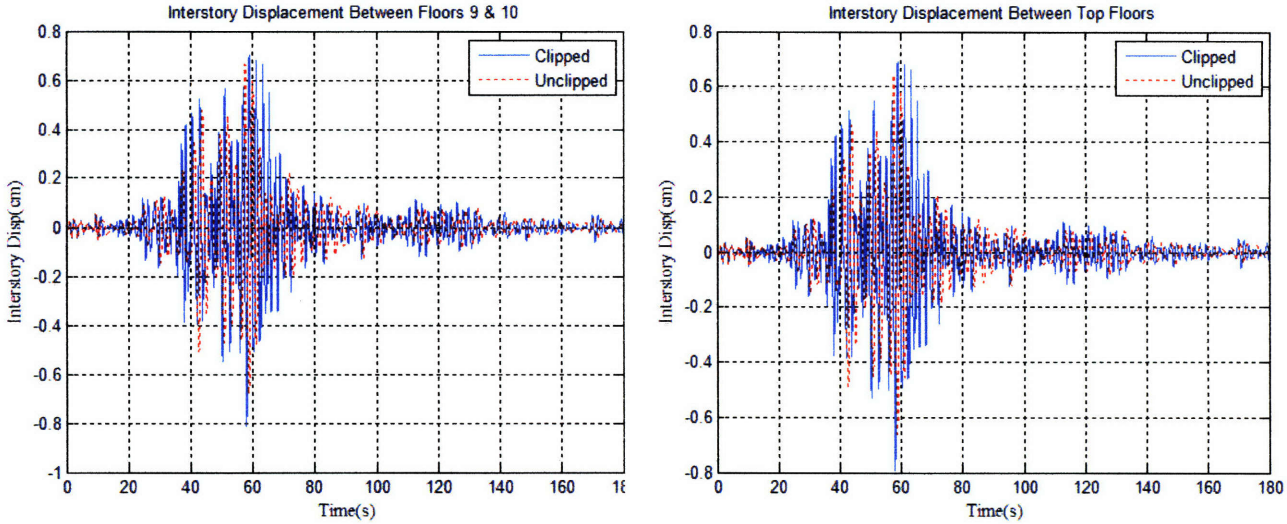


**Figure 87: Interstory Drift Floors 9-10 & 10-11 due to Mexico City earthquake: T=3s, Remain unclipped**

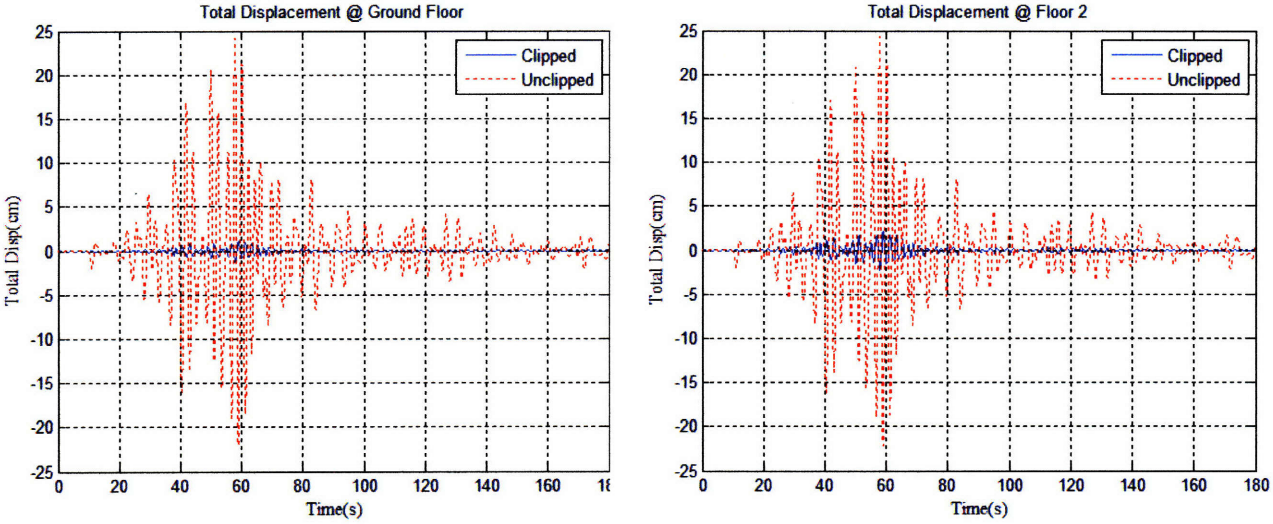


**Figure 88: Total Displacement Floors 1 & 2 due to Mexico City earthquake: T=6s, Remain unclipped**

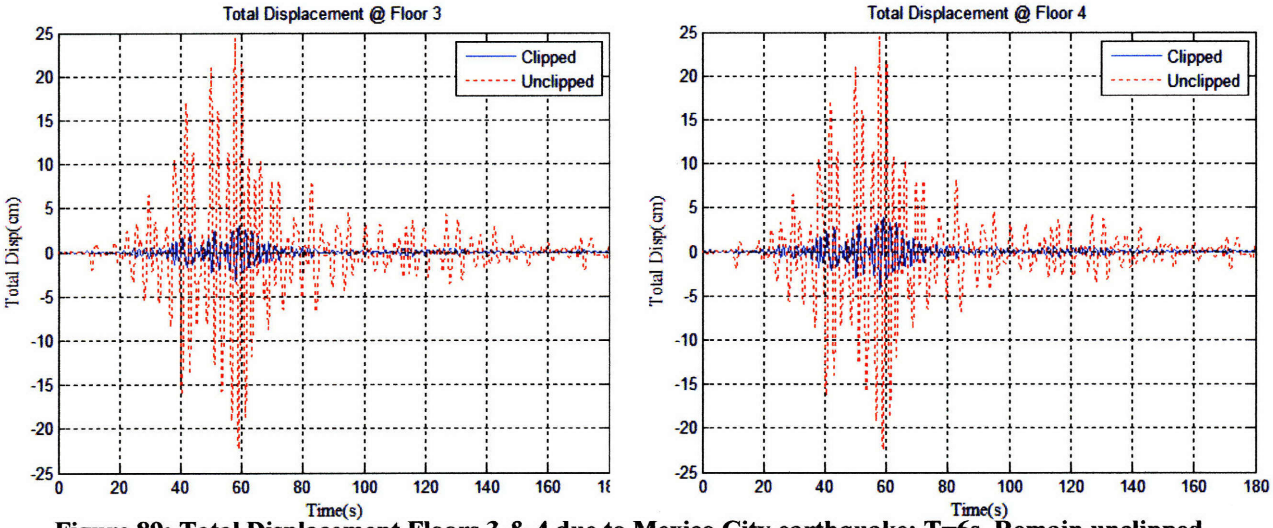


**Figure 89: Total Displacement Floors 3 & 4 due to Mexico City earthquake: T=6s, Remain unclipped**

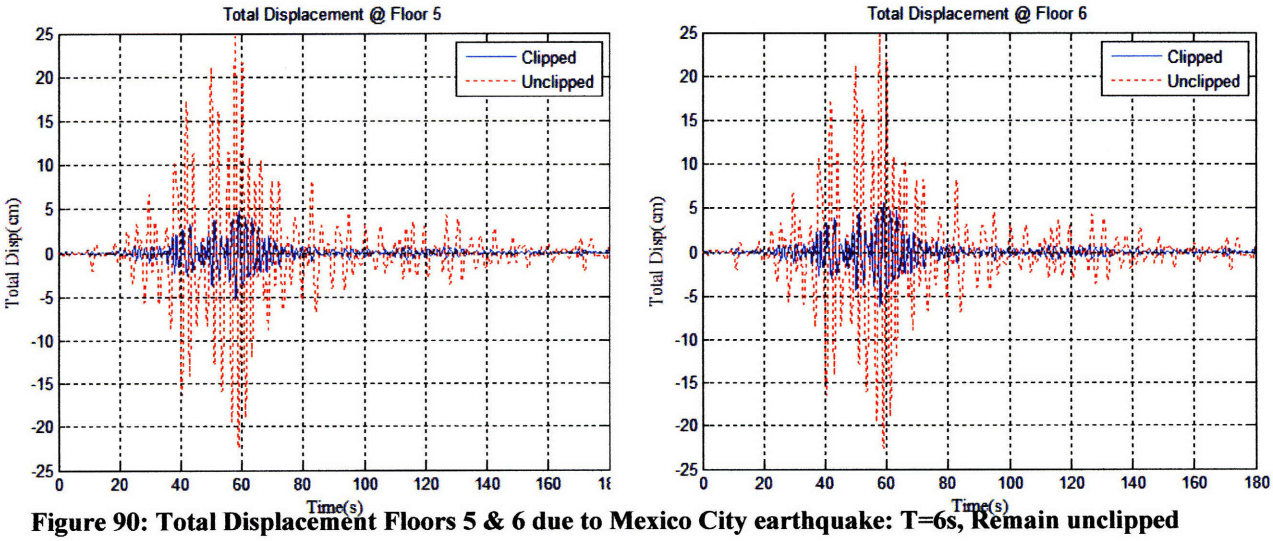


**Figure 90: Total Displacement Floors 5 & 6 due to Mexico City earthquake: T=6s, Remain unclipped**

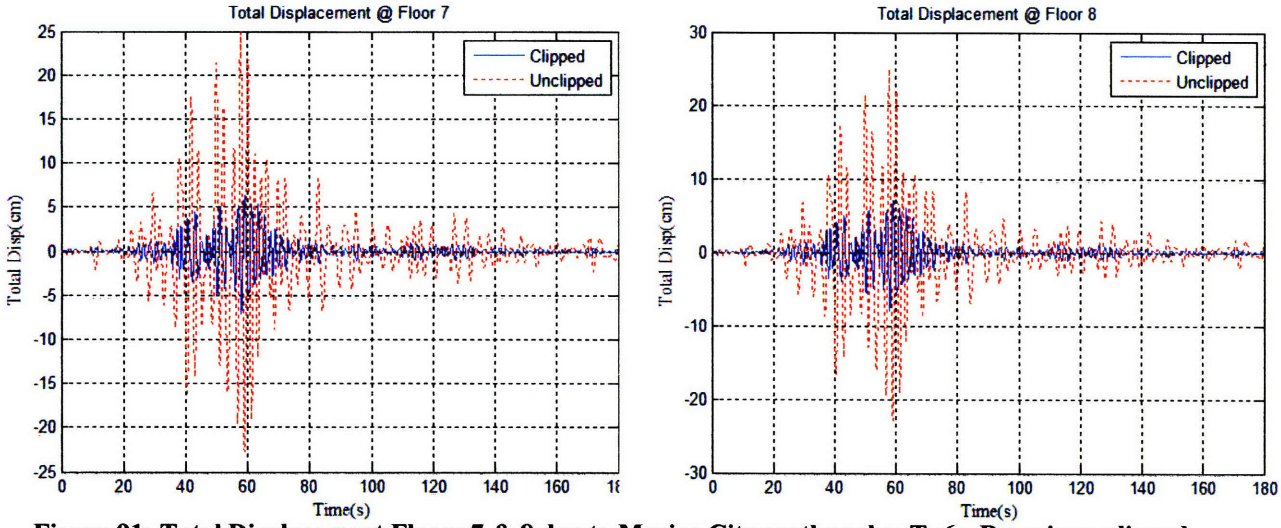


**Figure 91: Total Displacement Floors 7 & 8 due to Mexico City earthquake: T=6s, Remain unclipped**

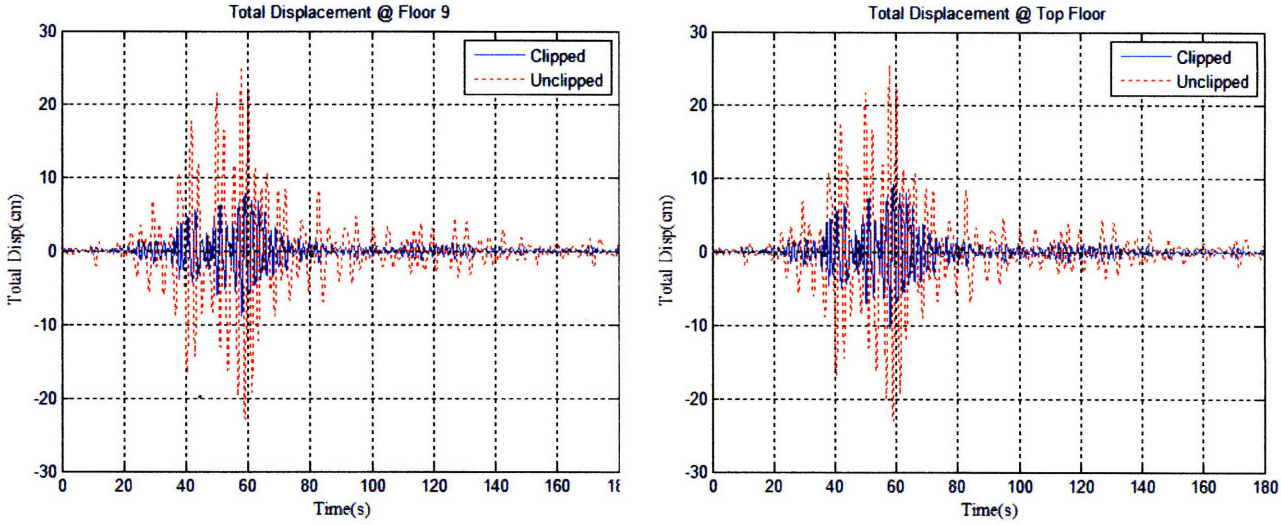


**Figure 92: Total Displ Floors 9 & 10 due to Mexico City earthquake: T=6s, Remain unclipped**

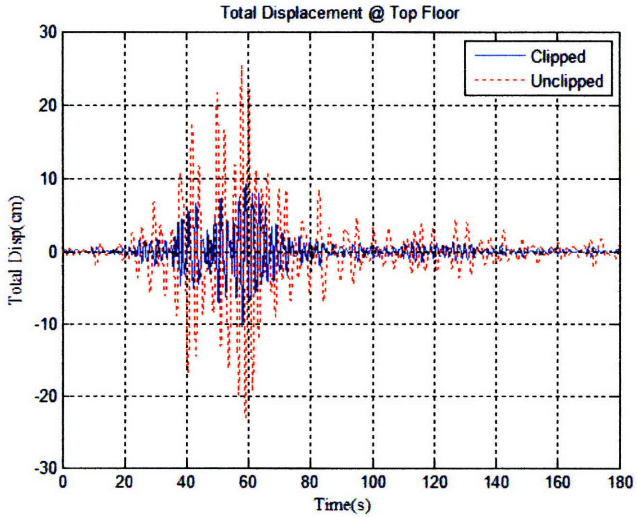


**Figure 93: Total Displacement Floor 11 due to Mexico City earthquake: T=6s, Remain unclipped**

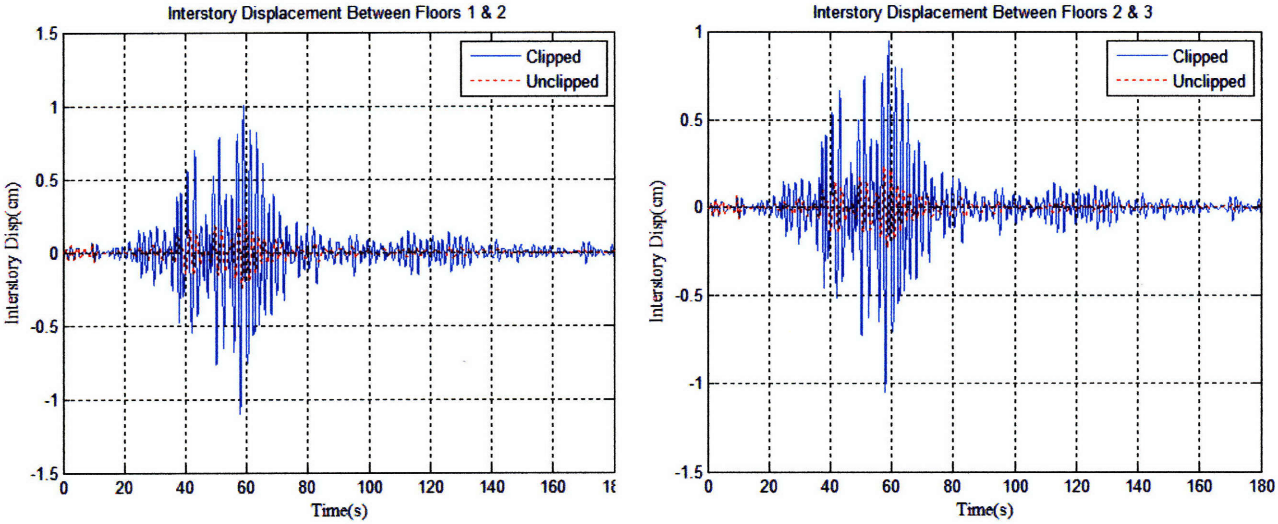


**Figure 94: Interstory Drift Floors 1-2 & 2-3 due to Mexico City earthquake: T=6s, Remain unclipped**

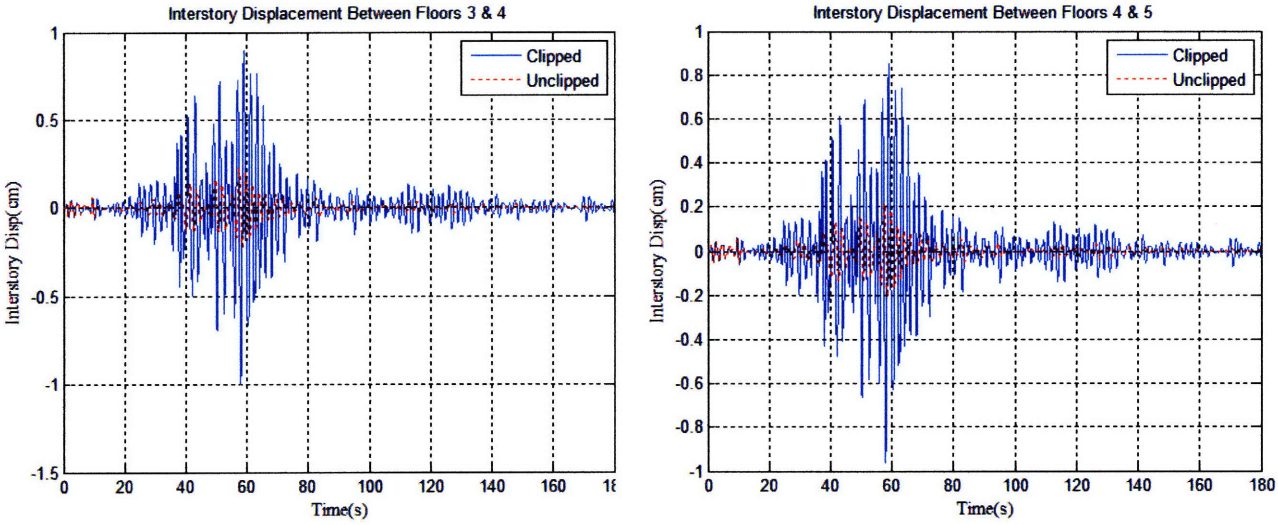


**Figure 95: Interstory Drift Floors 3-4 & 4-5 due to Mexico City earthquake: T=6s, Remain unclipped**

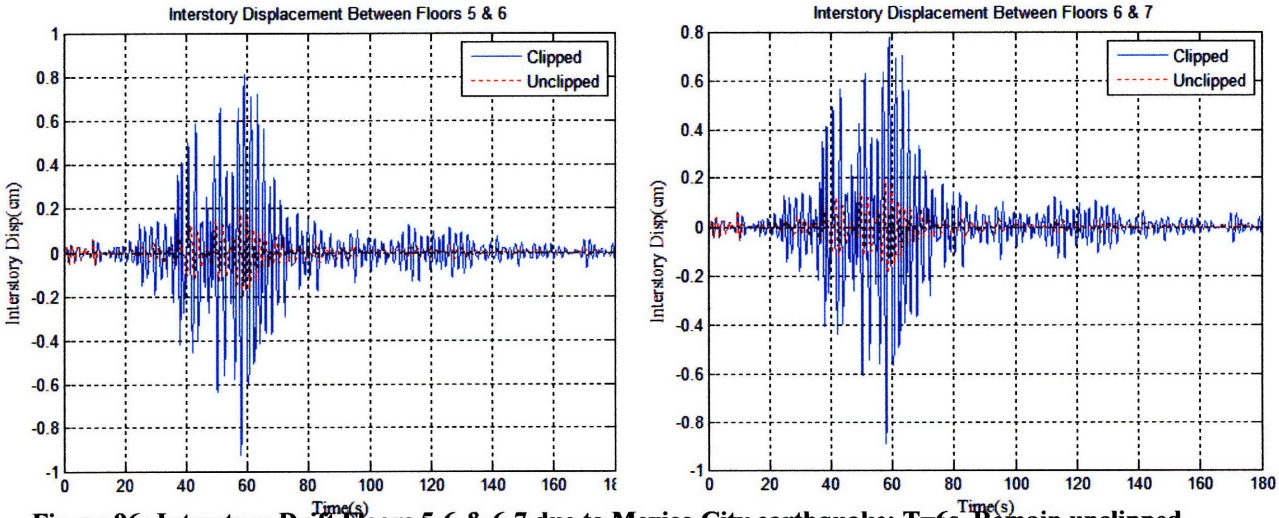


**Figure 96: Interstory Drift Floors 5-6 & 6-7 due to Mexico City earthquake: T=6s, Remain unclipped**

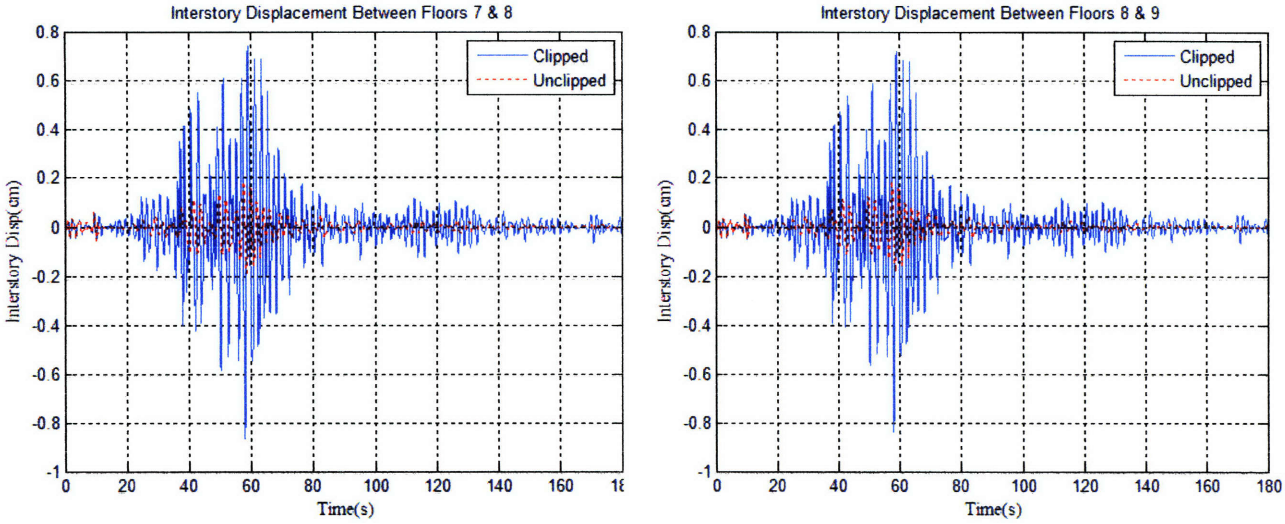


**Figure 97: Interstory Drift Floors 7-8 & 8-9 due to Mexico City earthquake: T=6s, Remain unclipped**

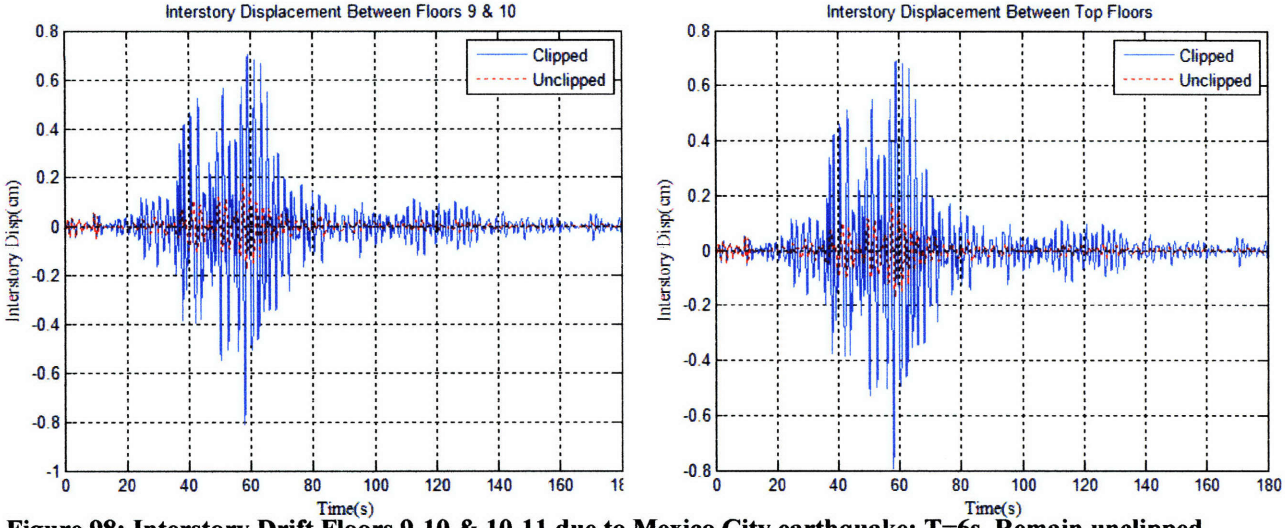


**Figure 98: Interstory Drift Floors 9-10 & 10-11 due to Mexico City earthquake: T=6s, Remain unclipped**

# Appendix F – Kobe Earthquake Response

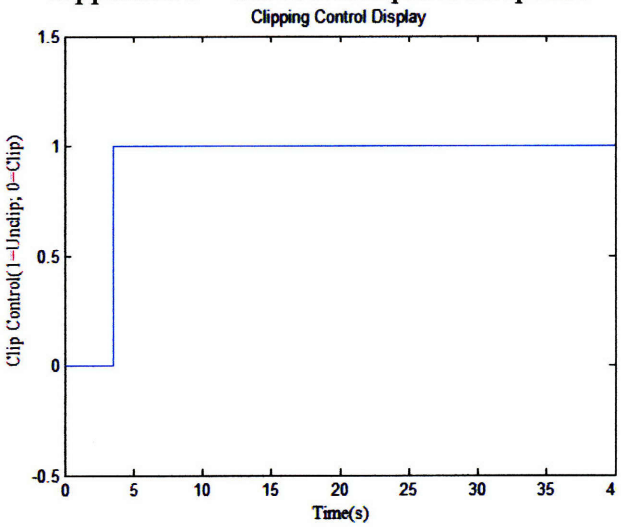


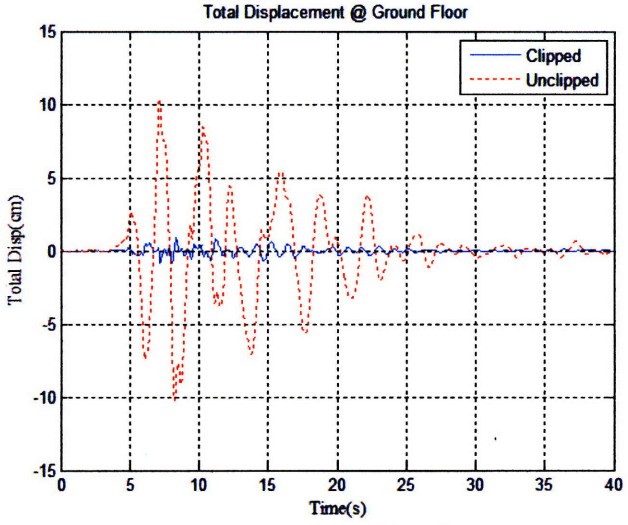


**Figure 99: Total Displacement Floor 1 due to Kobe earthquake: Remain unclipped**

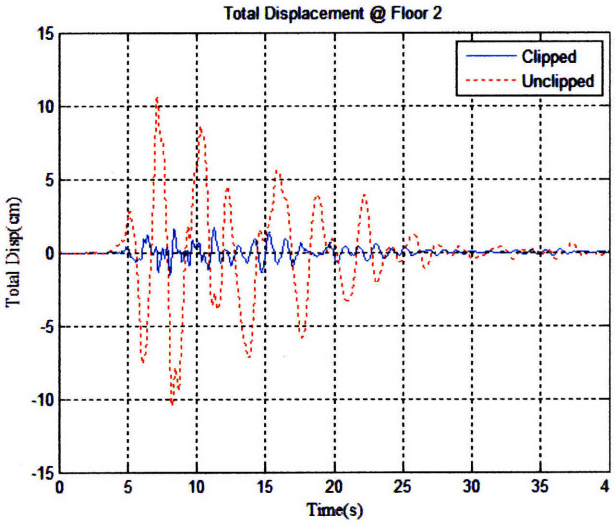


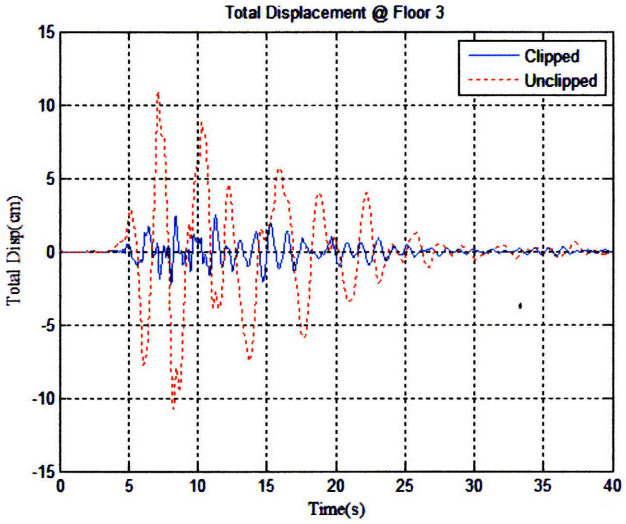


**Figure 100: Total Total Displacement Floors 2 & 3 due to Kobe earthquake: Remain unclipped**

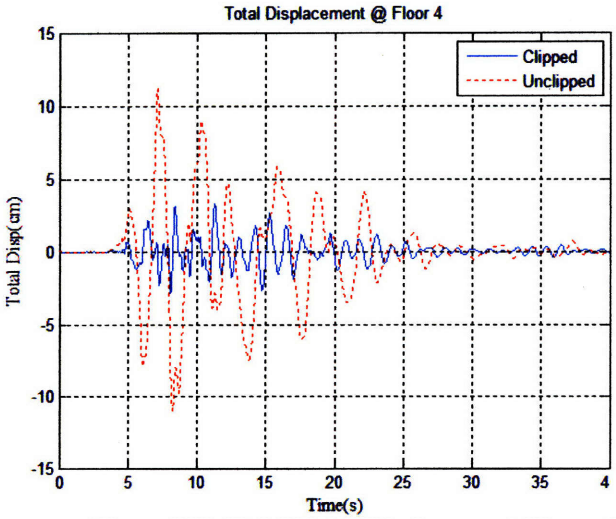


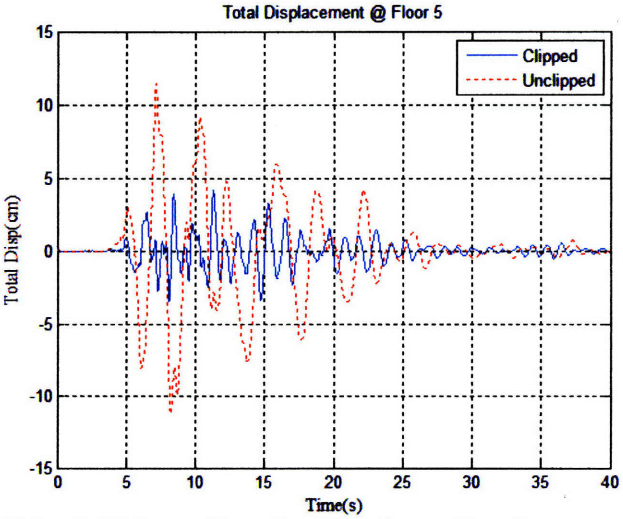


**Figure 101: Total Total Displacement Floors 4 & 5 due to Kobe earthquake: Remain unclipped**

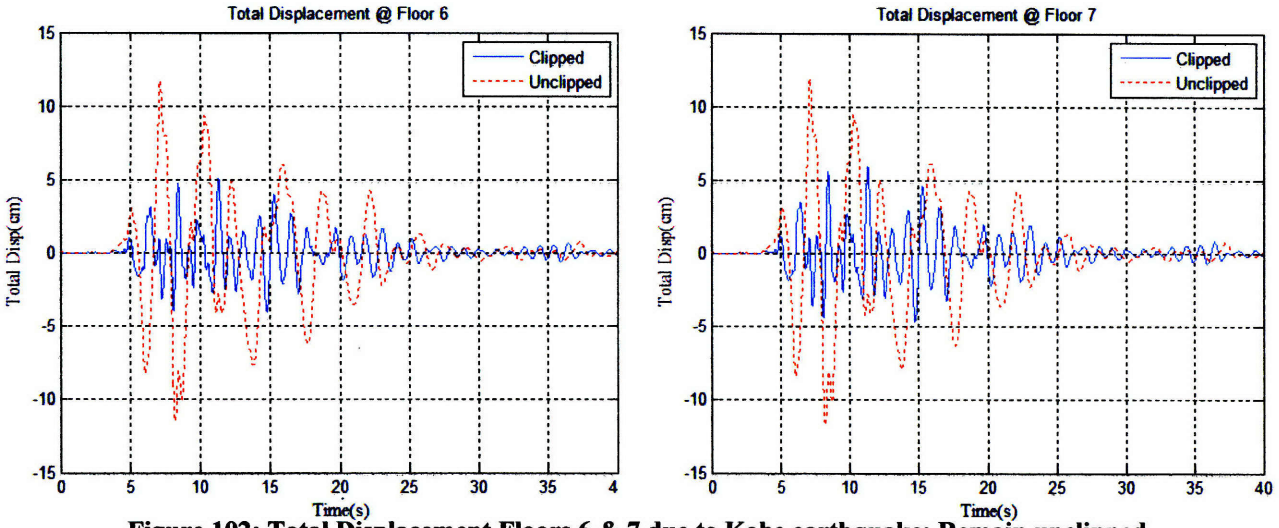


**Figure 102: Total Displacement Floors 6 & 7 due to Kobe earthquake: Remain unclipped**

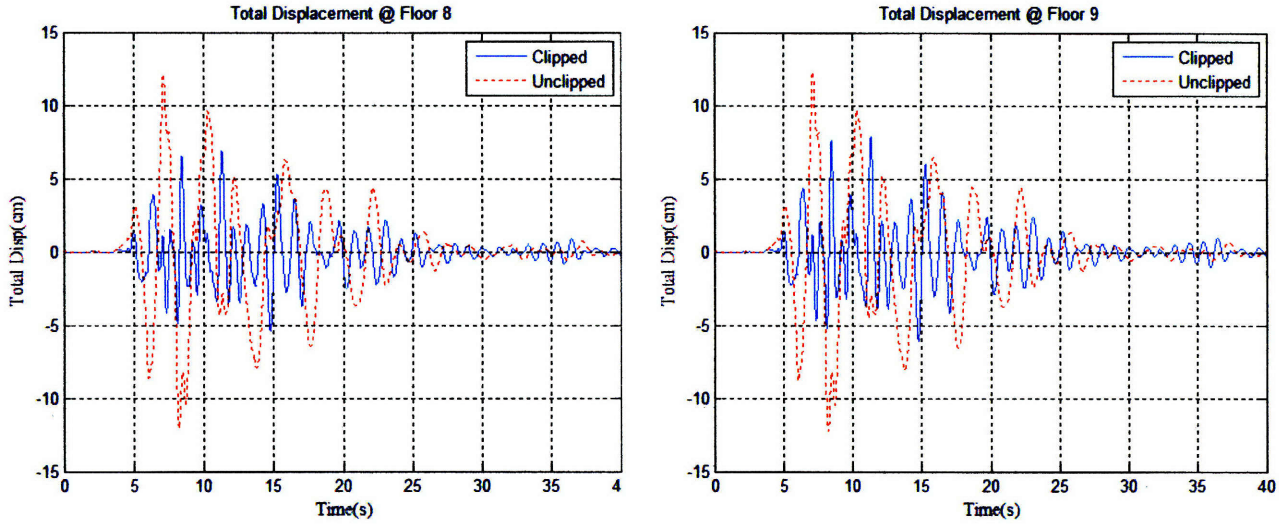


**Figure 103: Total Displacement Floors 8 & 9 due to Kobe earthquake: Remain unclipped**

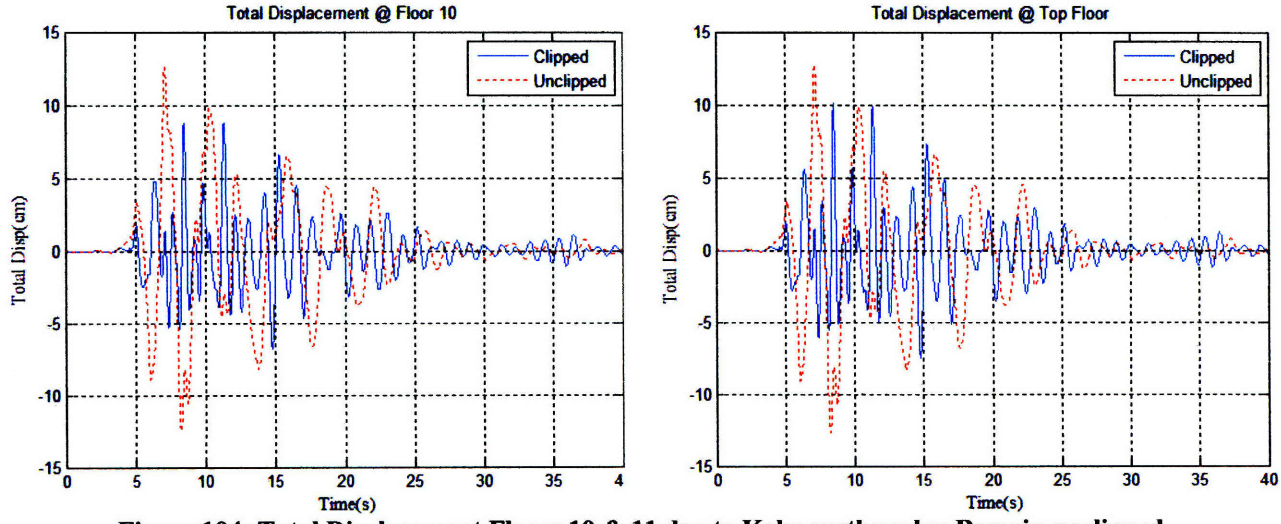


**Figure 104: Total Displacement Floors 10 & 11 due to Kobe earthquake: Remain unclipped**

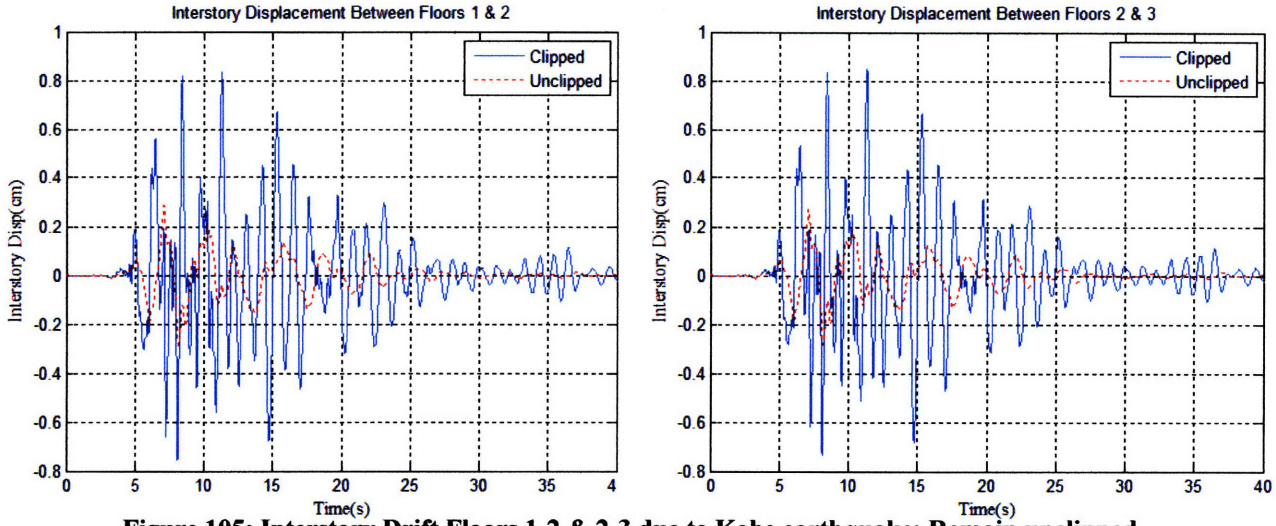


**Figure 105: Interstory Drift Floors 1-2 & 2-3 due to Kobe earthquake: Remain unclipped**

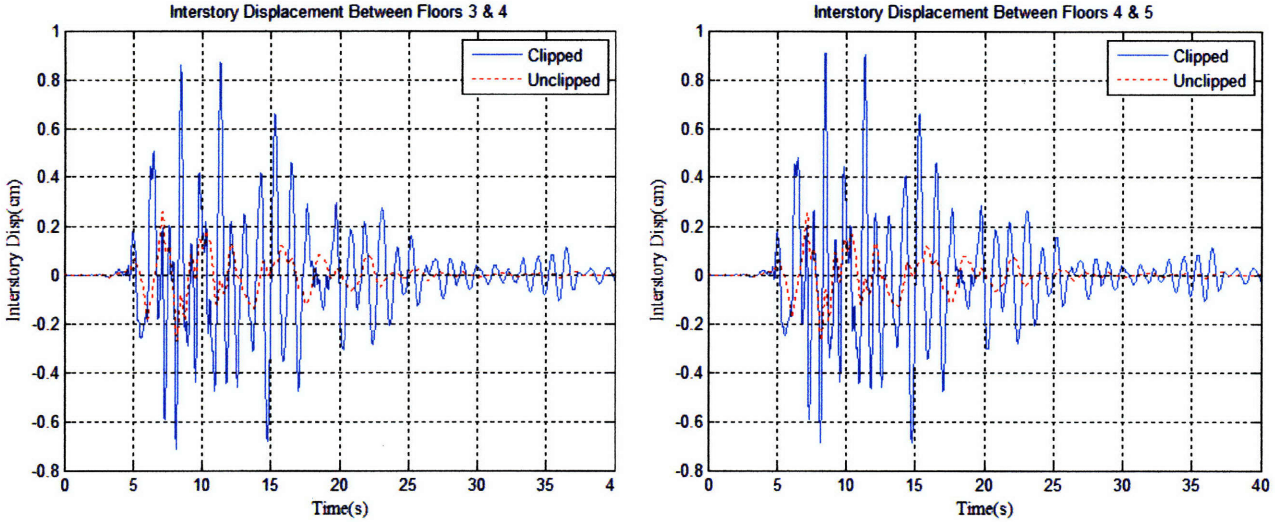


**Figure 106: Interstory Drift Floors 3-4 & 4-5 due to Kobe earthquake: Remain unclipped**

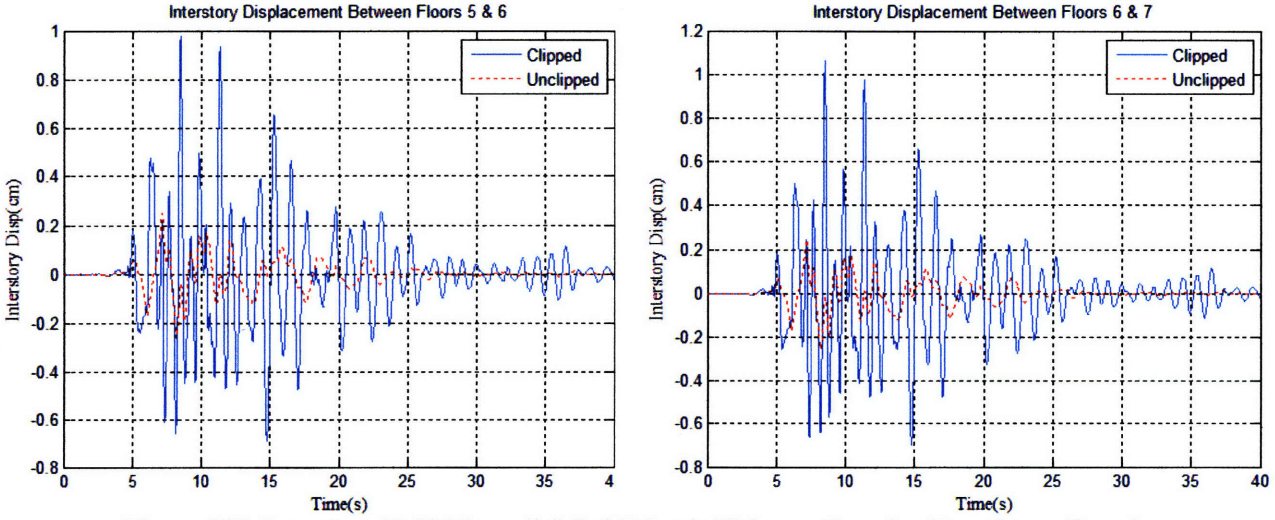


**Figure 107: Interstory Drift Floors 5-6 & 6-7 due to Kobe earthquake: Remain unclipped**

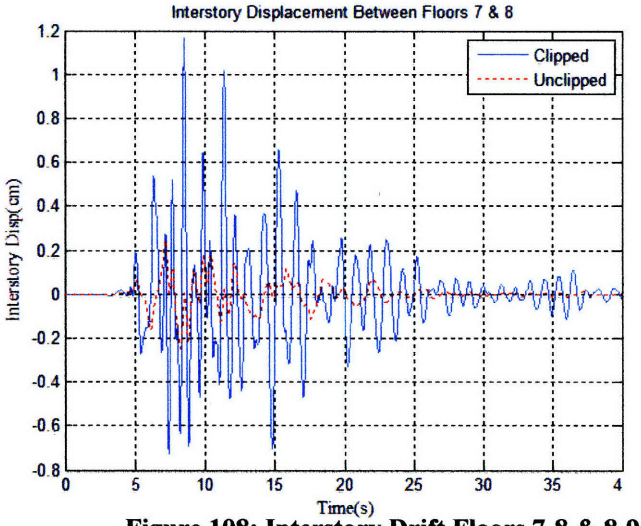


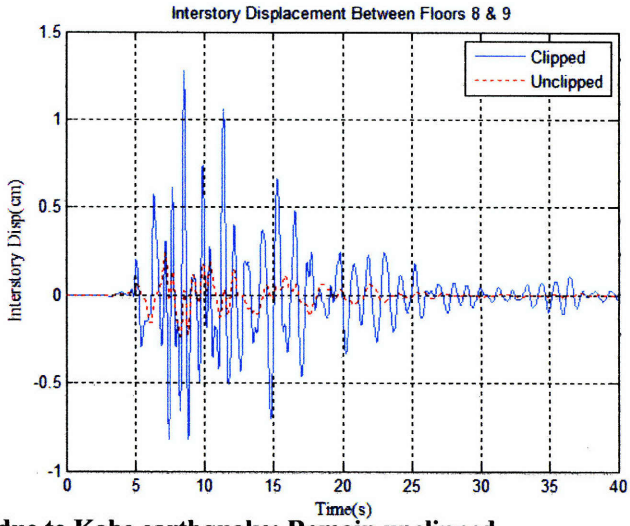


**Figure 108: Interstory Drift Floors 7-8 & 8-9 due to Kobe earthquake: Remain unclipped**

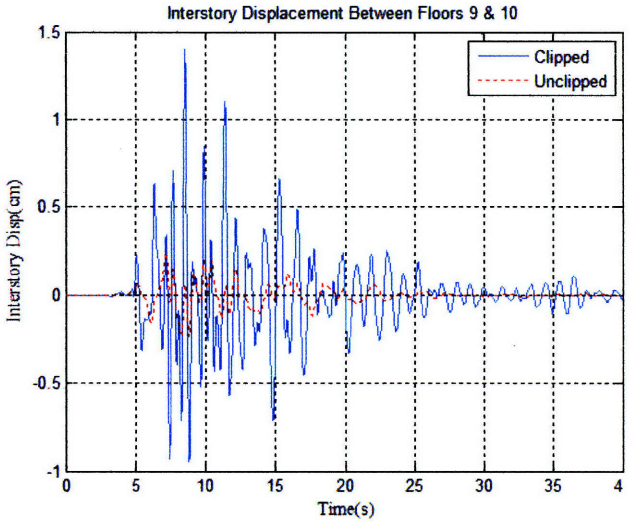


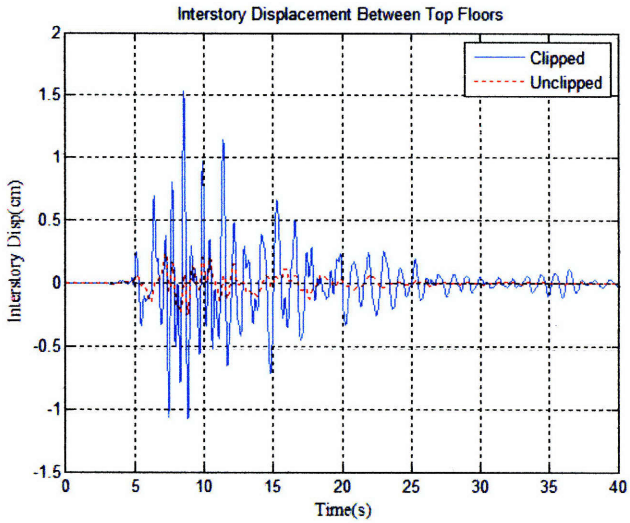


**Figure 109: Interstory Drift Floors 9-10 & 10-11 due to Kobe earthquake: Remain unclipped**

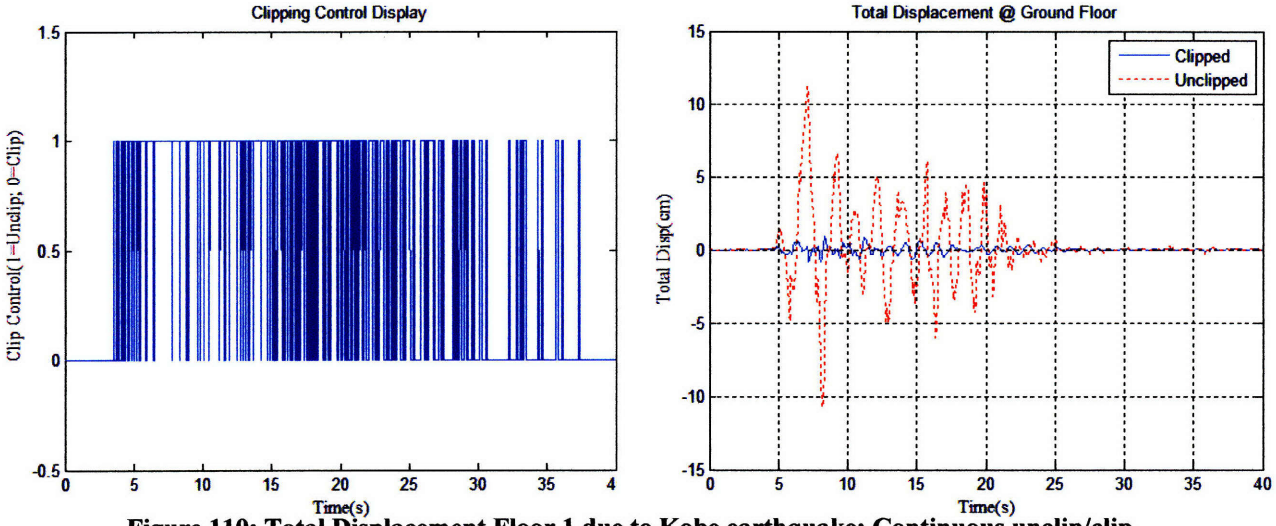


**Figure 110: Total Displacement Floor 1 due to Kobe earthquake: Continuous unclip/clip**

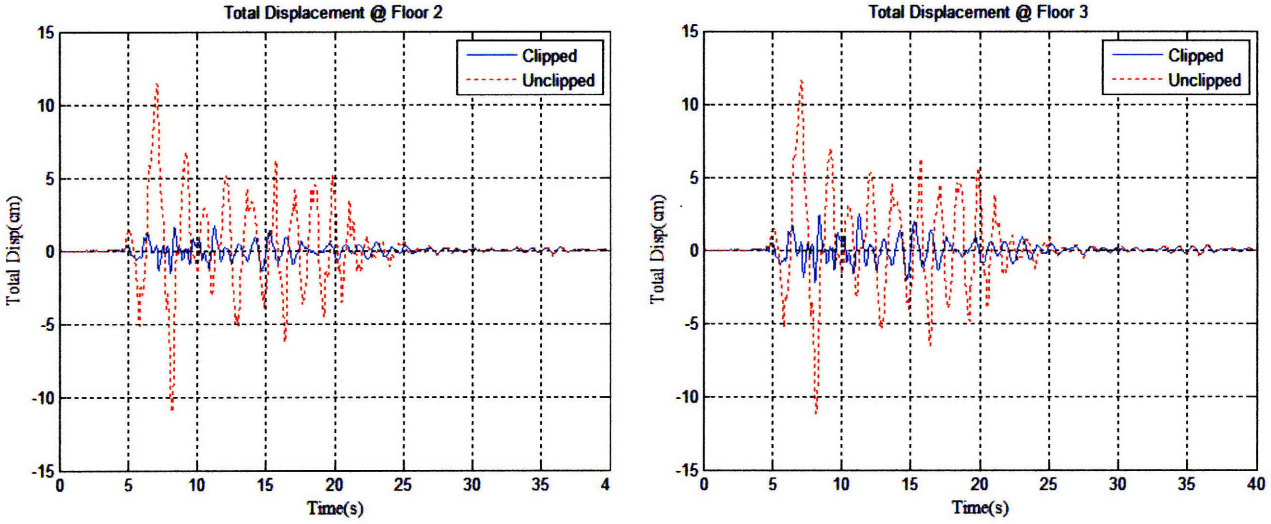


**Figure 111: Total Displacement Floors 2 & 3 due to Kobe earthquake: Continuous unclip/clip**

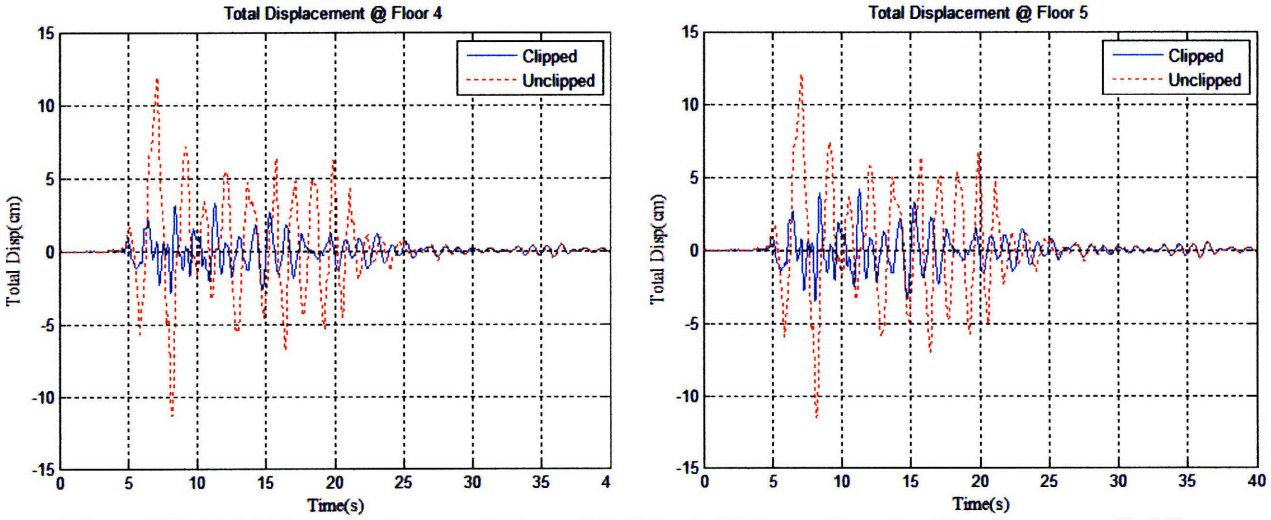


**Figure 112: Total Total Displacement Floors 4 & 5 due to Kobe earthquake: Continuous unclip/clip**

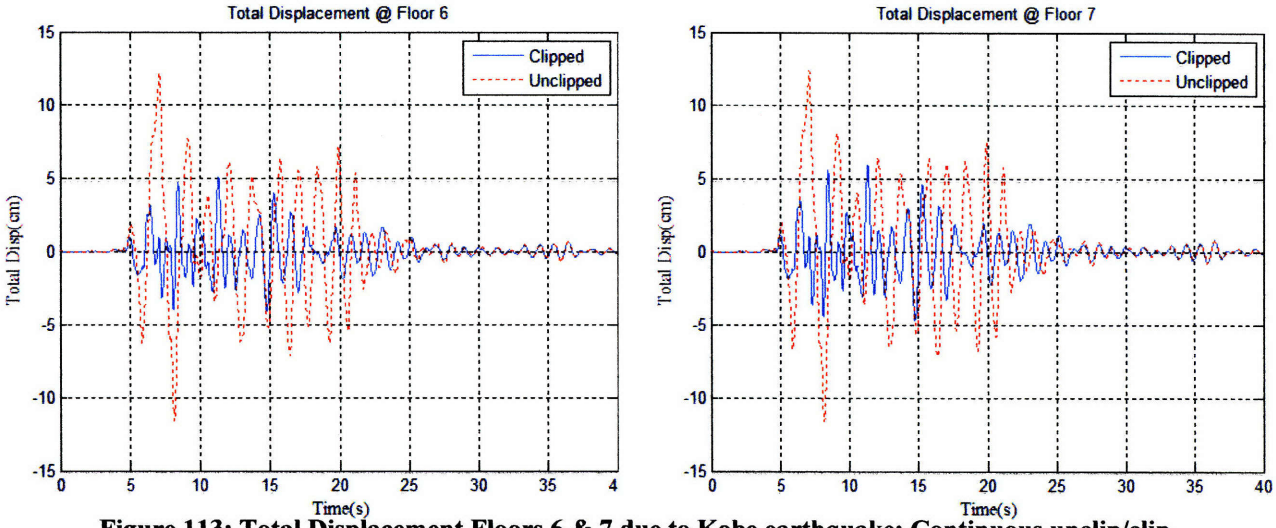


**Figure 113: Total Displacement Floors 6 & 7 due to Kobe earthquake: Continuous unclip/clip**

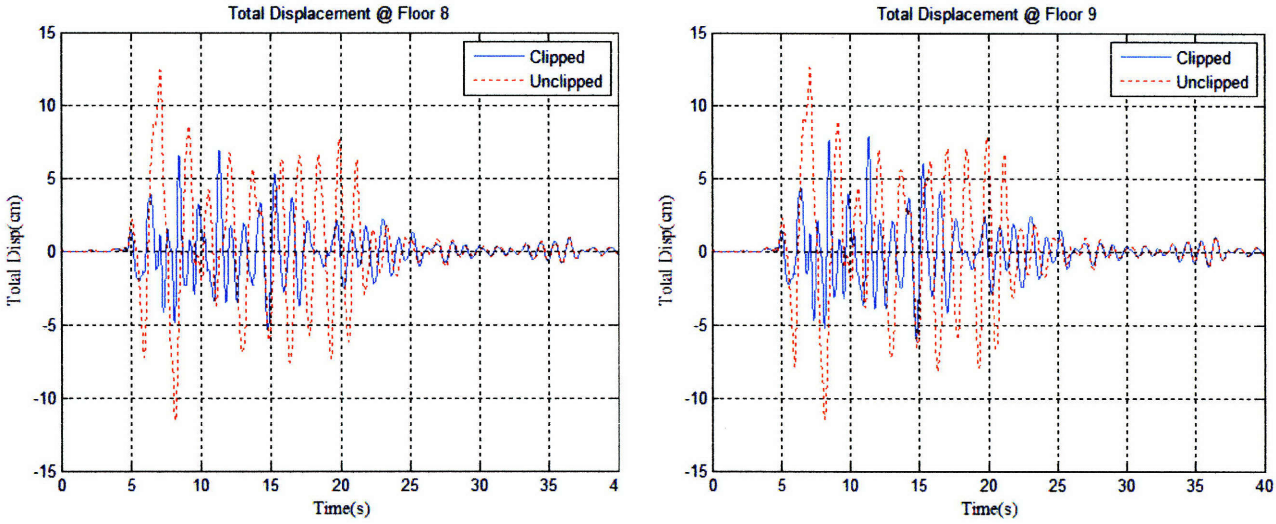


**Figure 114: Total Displacement Floors 8 & 9 due to Kobe earthquake: Continuous unclip/clip**

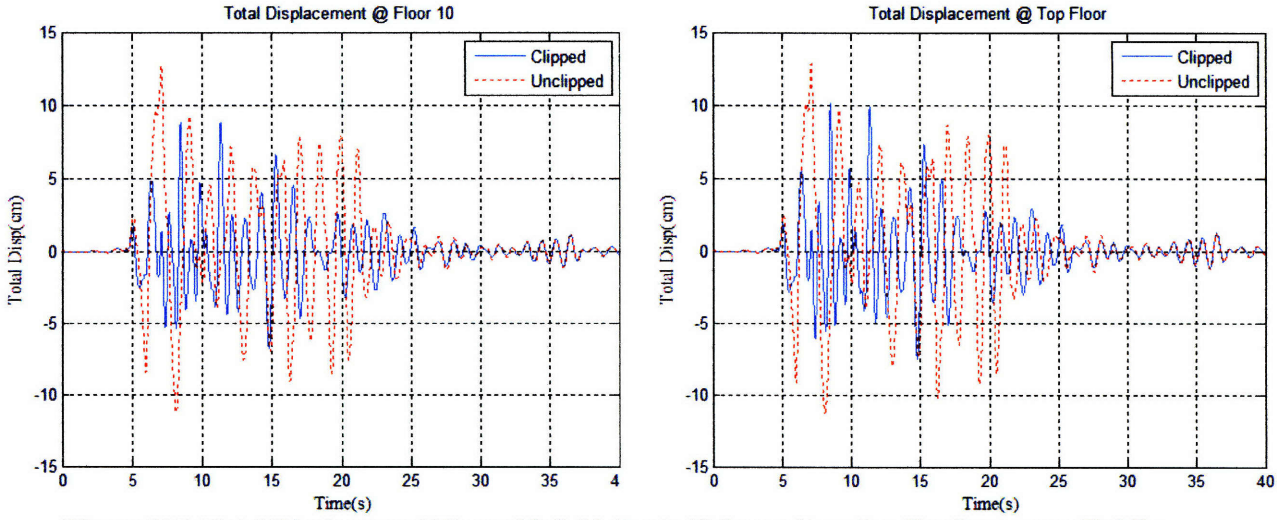


**Figure 115: Total Displacement Floors 10 & 11 due to Kobe earthquake: Continuous unclip/clip**

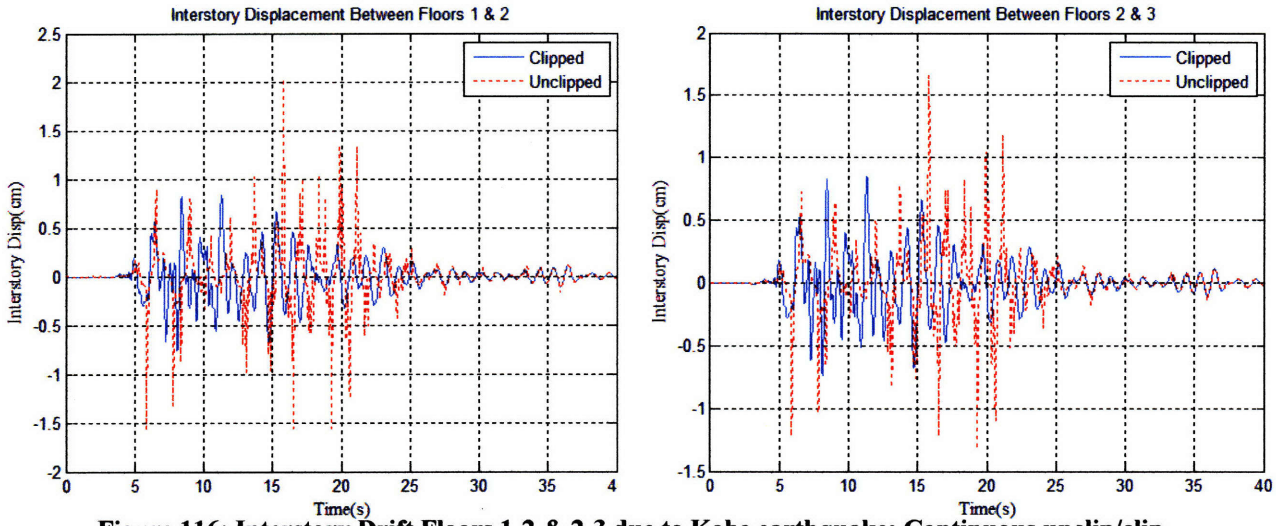


**Figure 116: Interstory Drift Floors 1-2 & 2-3 due to Kobe earthquake: Continuous unclip/clip**

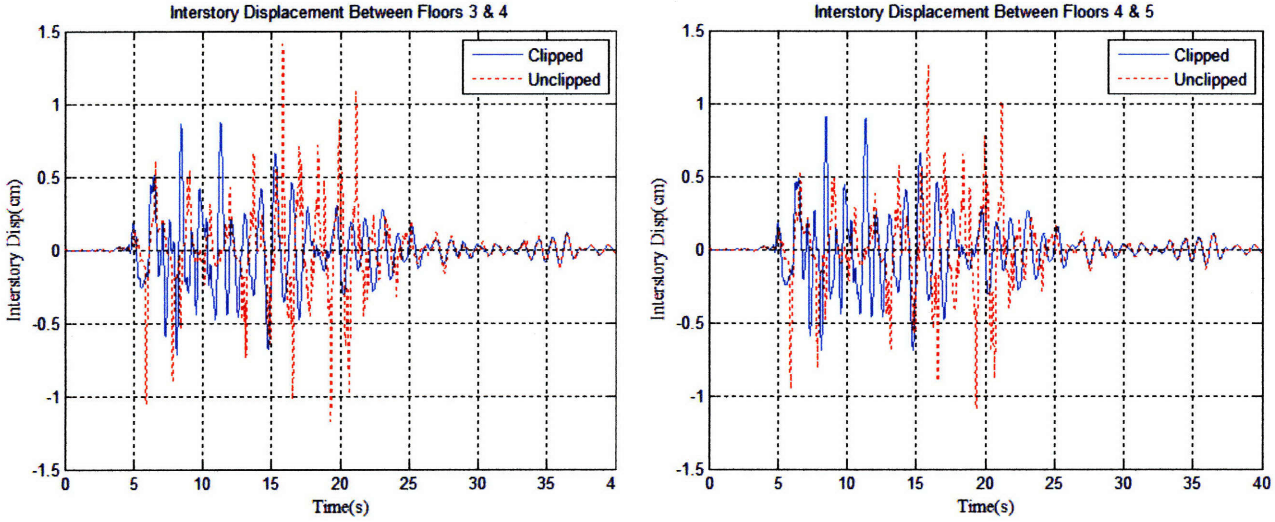


**Figure 117: Interstory Drift Floors 3-4 & 4-5 due to Kobe earthquake: Continuous unclip/clip**

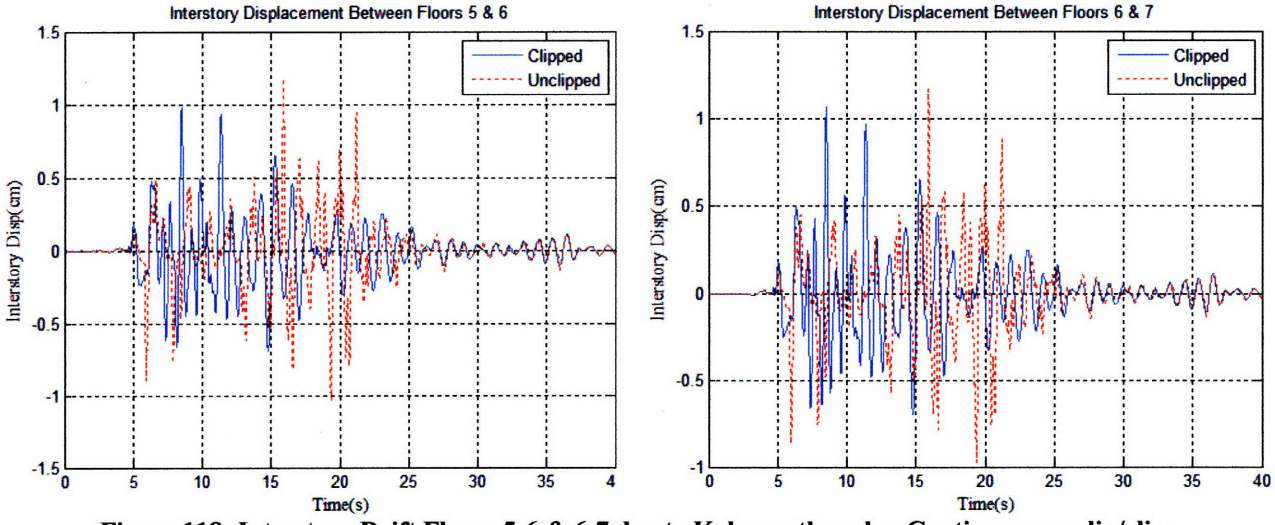


**Figure 118: Interstory Drift Floors 5-6 & 6-7 due to Kobe earthquake: Continuous unclip/clip**

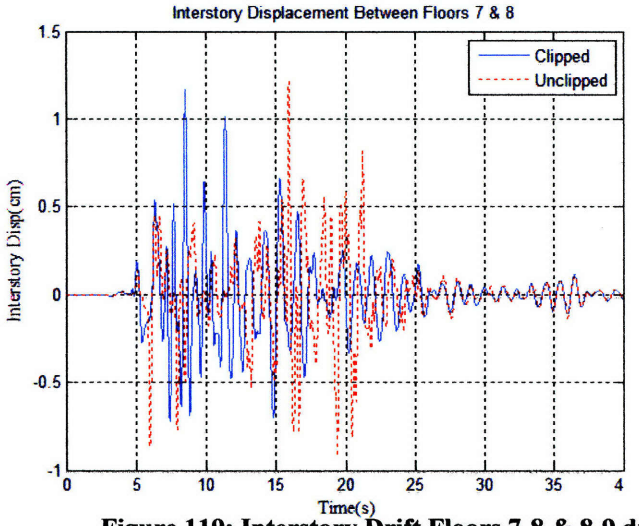


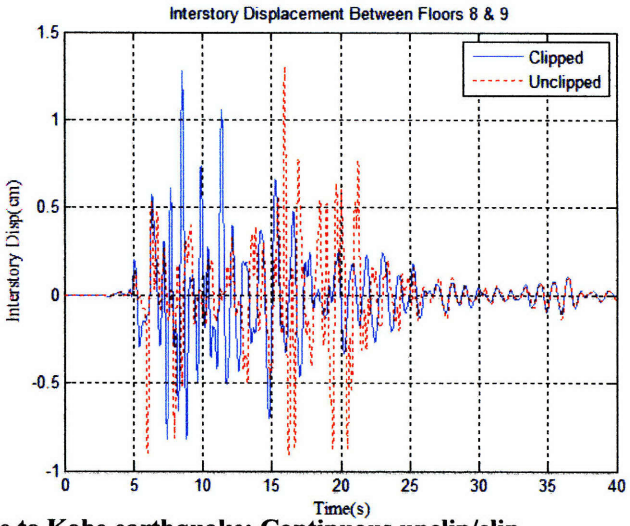


**Figure 119: Interstory Drift Floors 7-8 & 8-9 due to Kobe earthquake: Continuous unclip/clip**

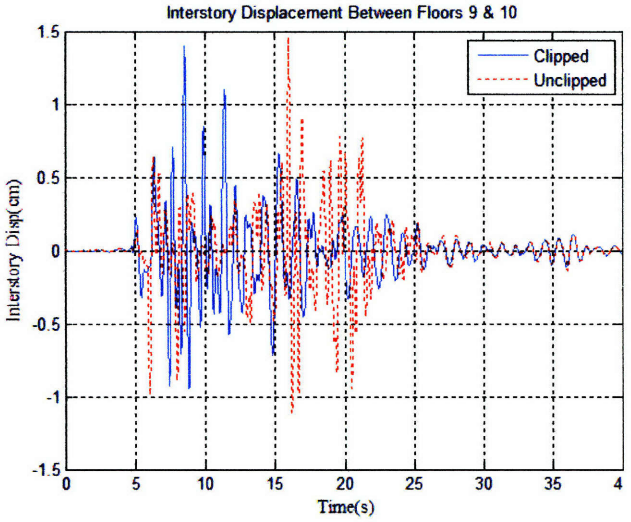


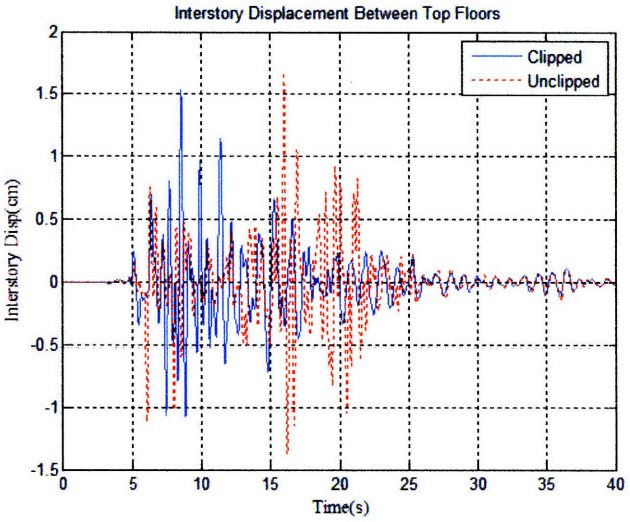


**Figure 120: Interstory Drift Floors 9-10 & 10-11 due to Kobe earthquake: Continuous unclip/clip**

## Appendix G – Pacoima Earthquake Response

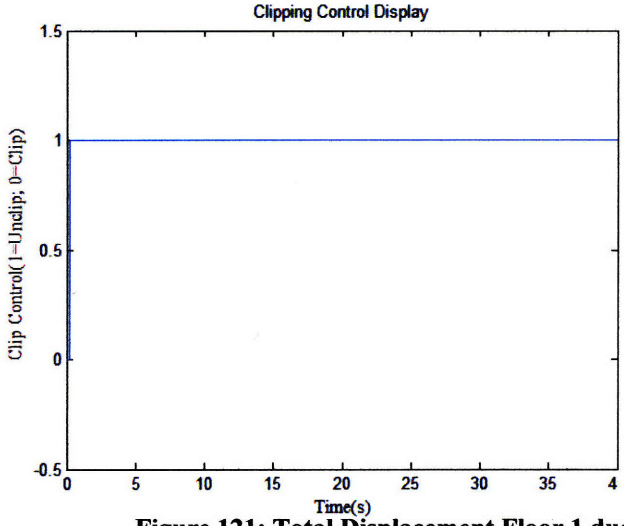


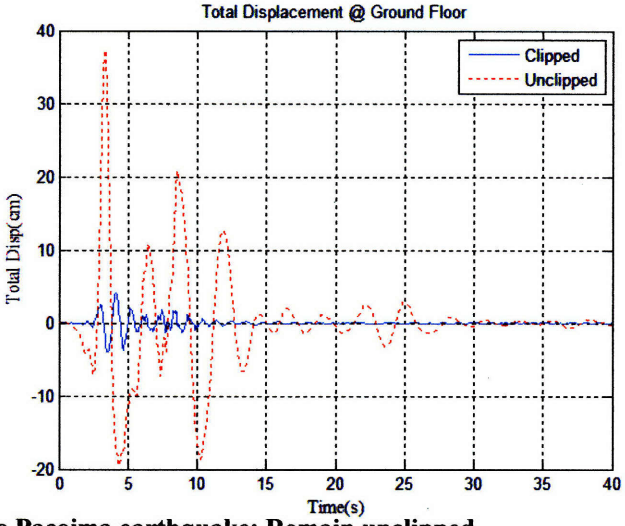


**Figure 121: Total Displacement Floor 1 due to Pacoima earthquake: Remain unclipped**

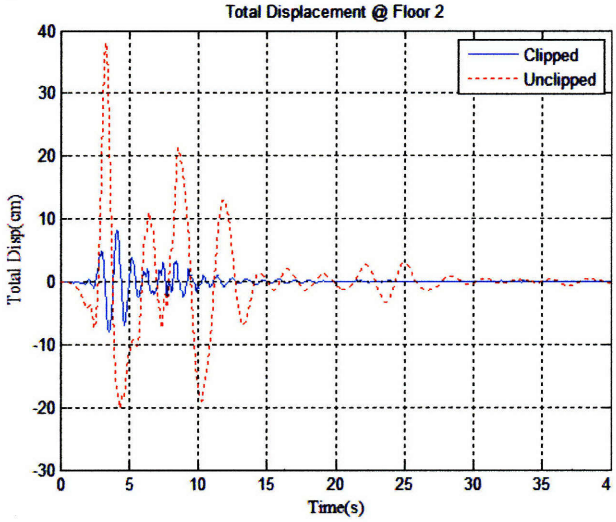


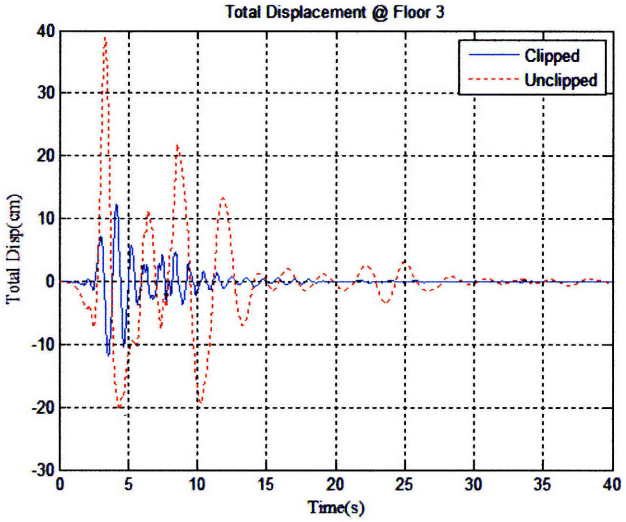


**Figure 122: Total Total Displacement Floors 2 & 3 due to Pacoima earthquake: Remain unclipped**

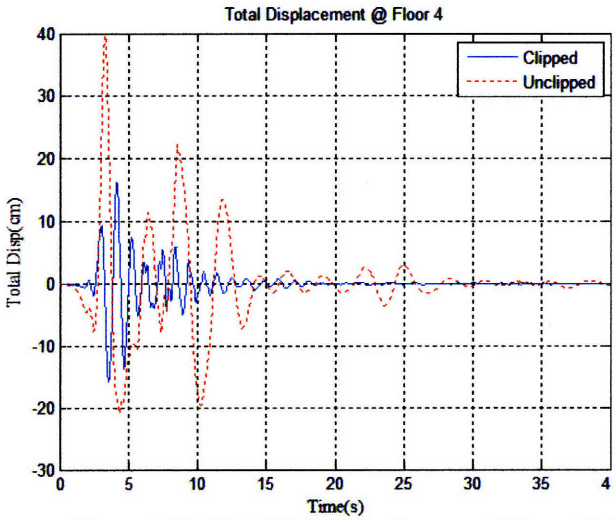


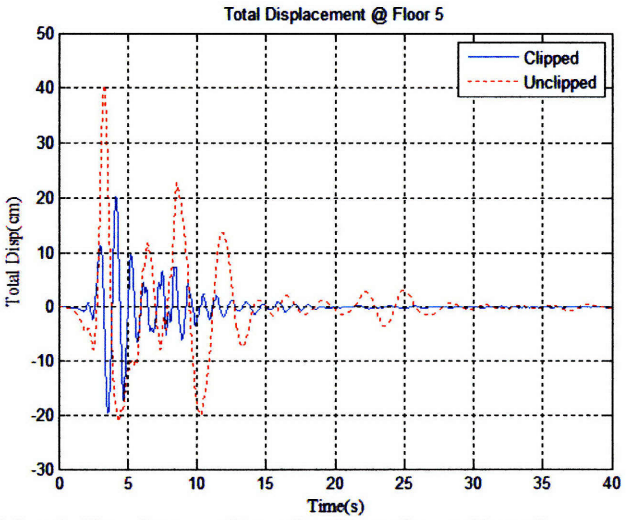


**Figure 123: Total Total Displacement Floors 4 & 5 due to Pacoima earthquake: Remain unclipped**

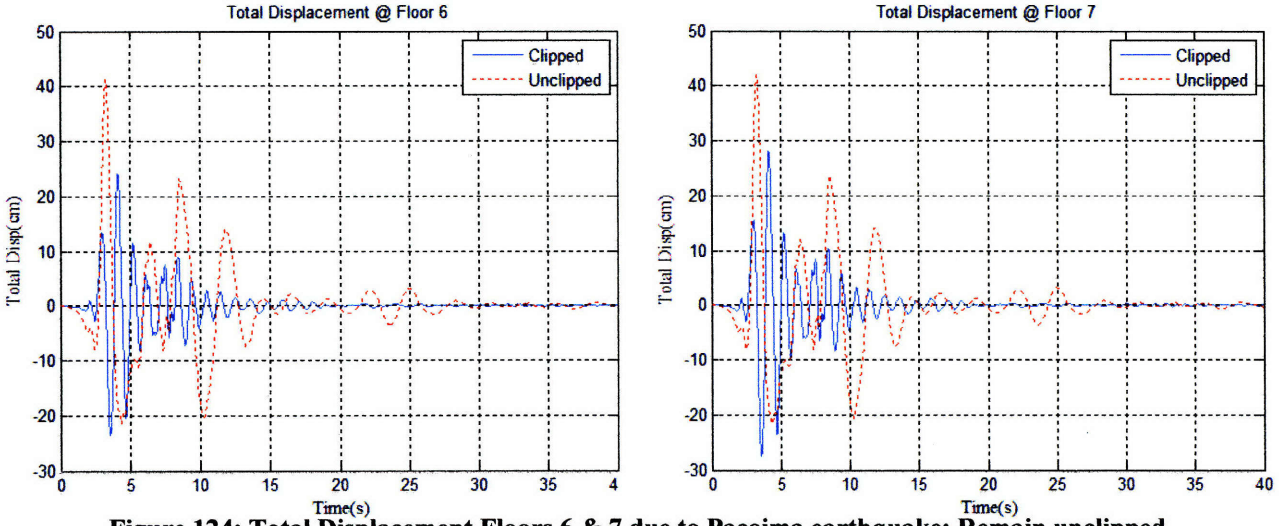


**Figure 124: Total Displacement Floors 6 & 7 due to Pacoima earthquake: Remain unclipped**

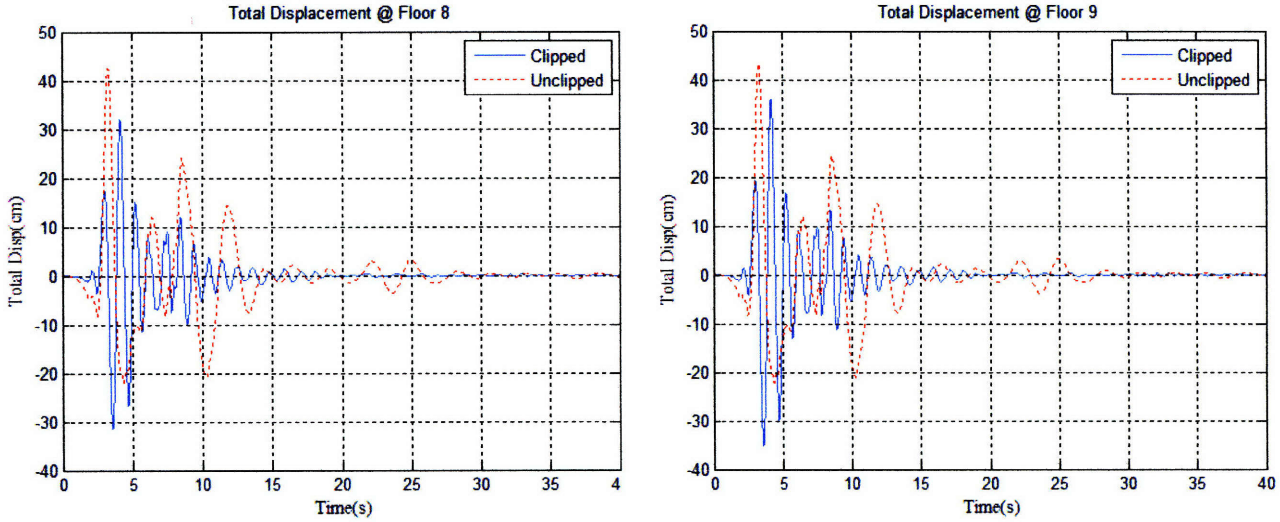


**Figure 125: Total Displacement Floors 8 & 9 due to Pacoima earthquake: Remain unclipped**

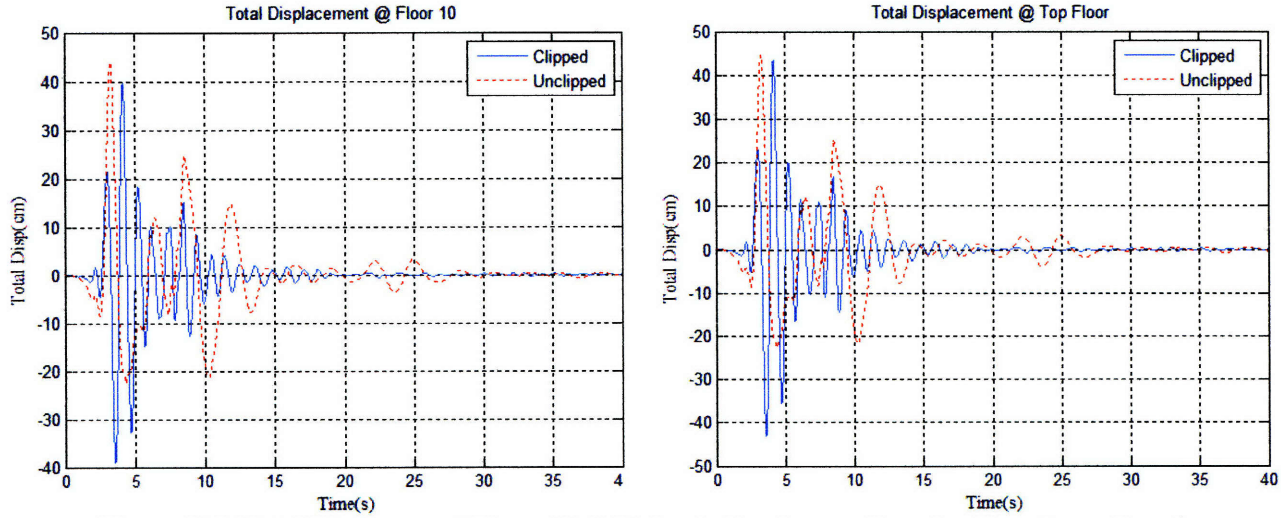


**Figure 126: Total Displacement Floors 10 & 11 due to Pacoima earthquake: Remain unclipped**

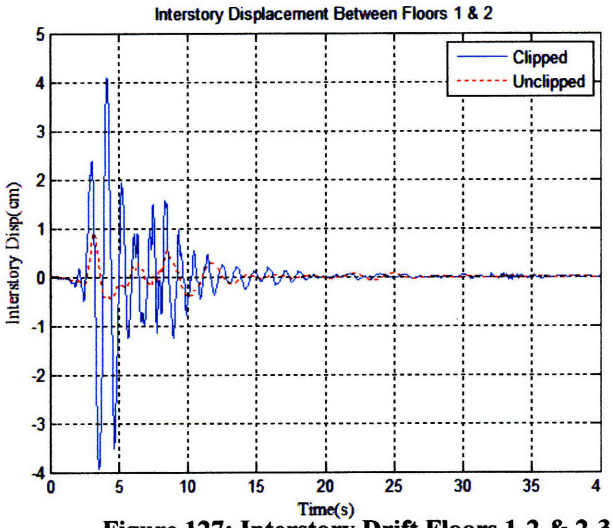


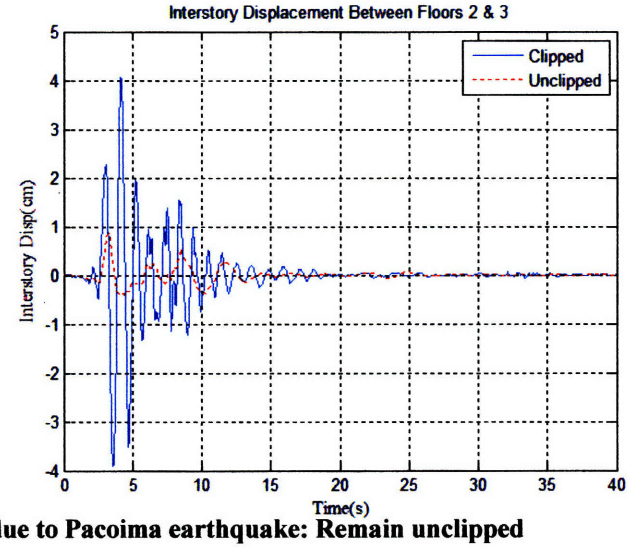


**Figure 127: Interstory Drift Floors 1-2 & 2-3 due to Pacoima earthquake: Remain unclipped**

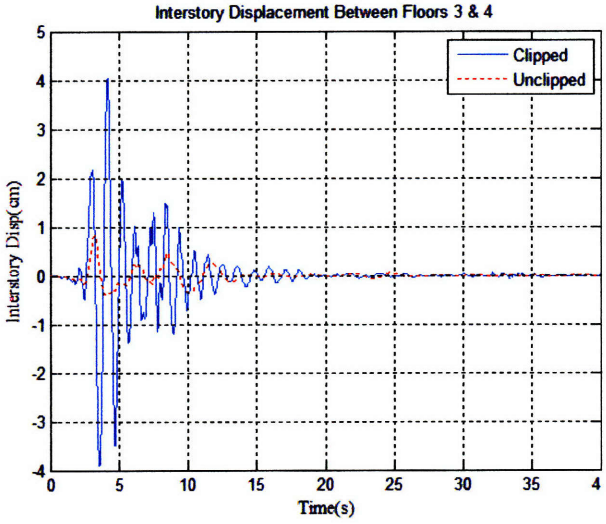


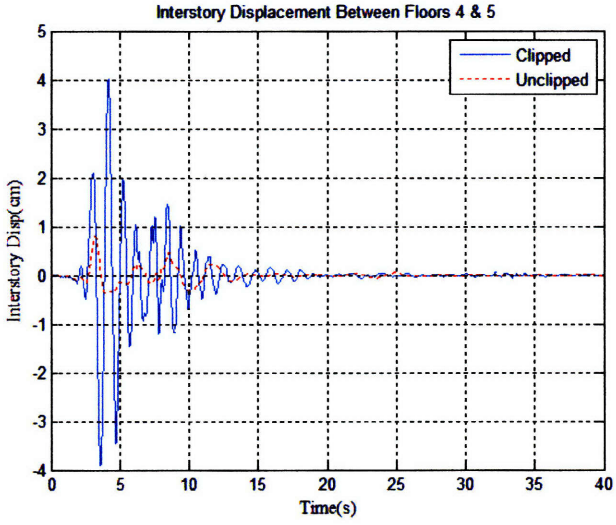


**Figure 128: Interstory Drift Floors 3-4 & 4-5 due to Pacoima earthquake: Remain unclipped**

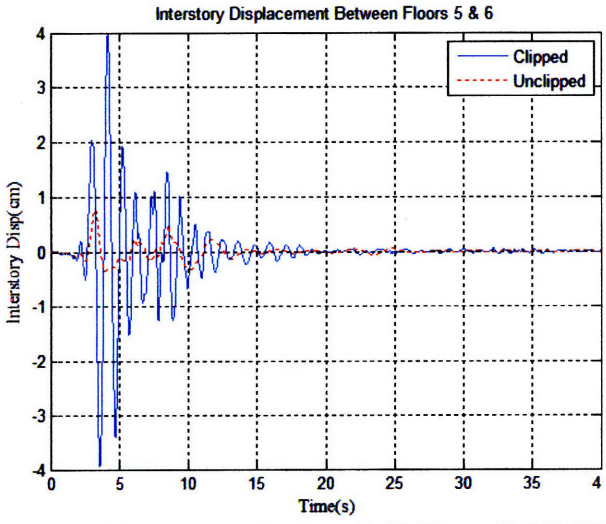


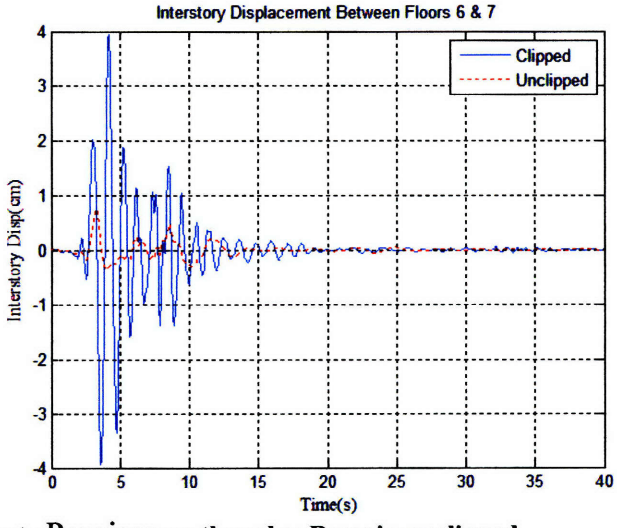


**Figure 129: Interstory Drift Floors 5-6 & 6-7 due to Pacoima earthquake: Remain unclipped**

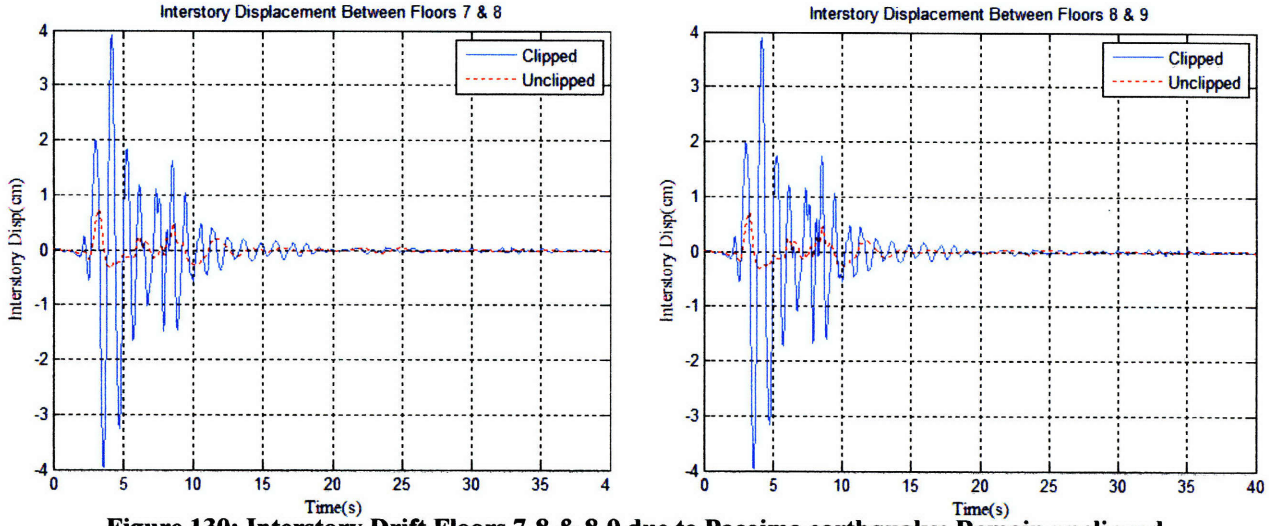


**Figure 130: Interstory Drift Floors 7-8 & 8-9 due to Pacoima earthquake: Remain unclipped**

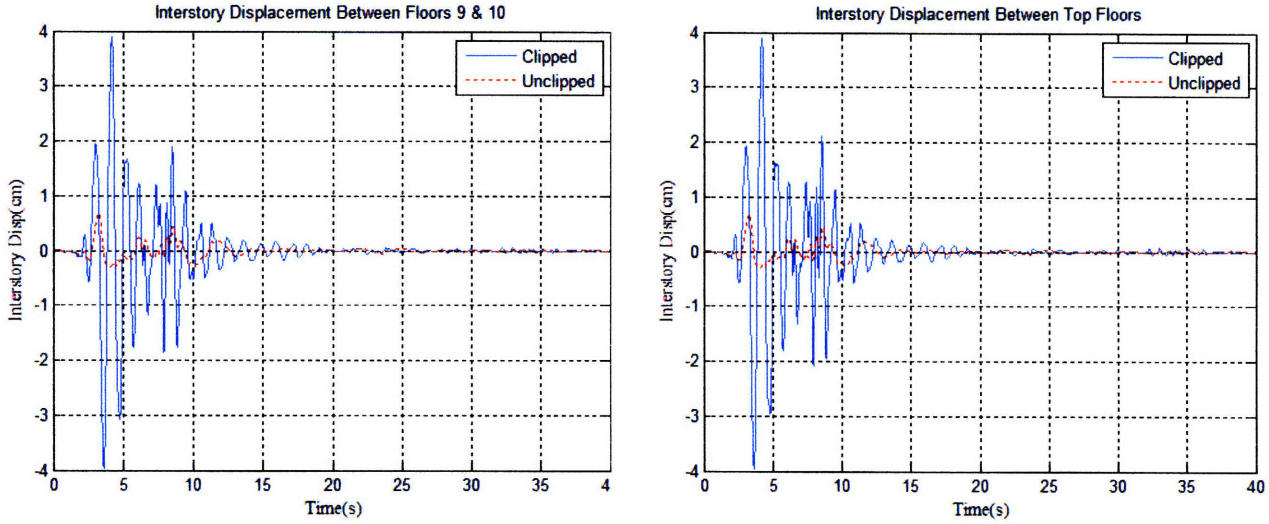


**Figure 131: Interstory Drift Floors 9-10 & 10-11 due to Pacoima earthquake: Remain unclipped**

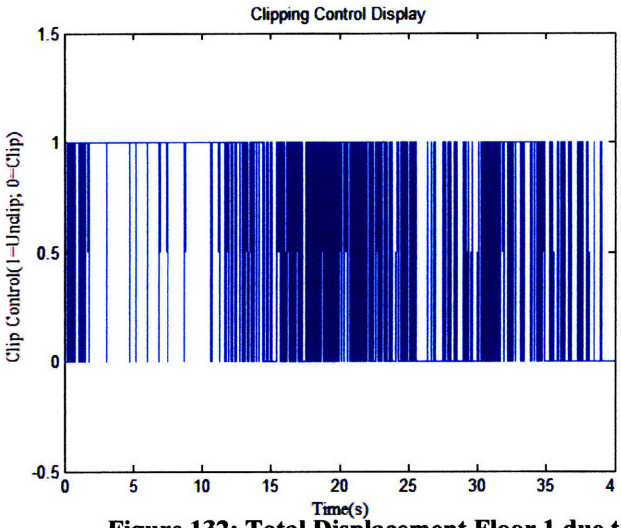


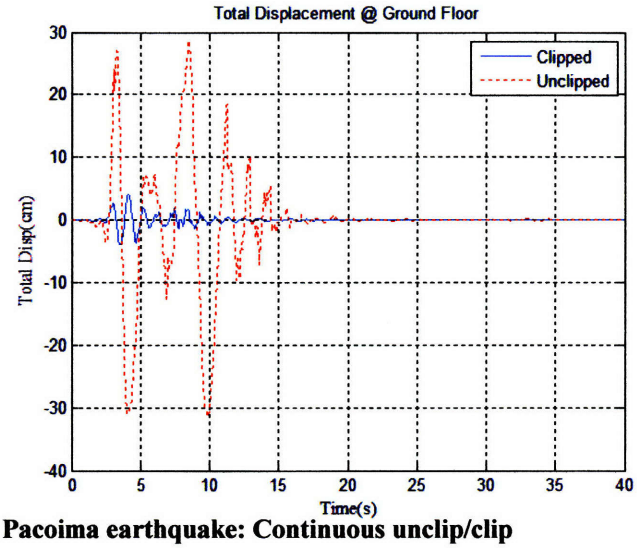


**Figure 132: Total Displacement Floor 1 due to Pacoima earthquake: Continuous unclip/clip**

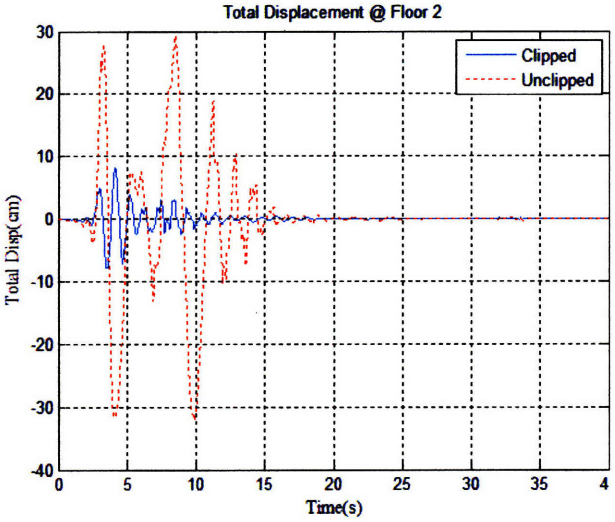


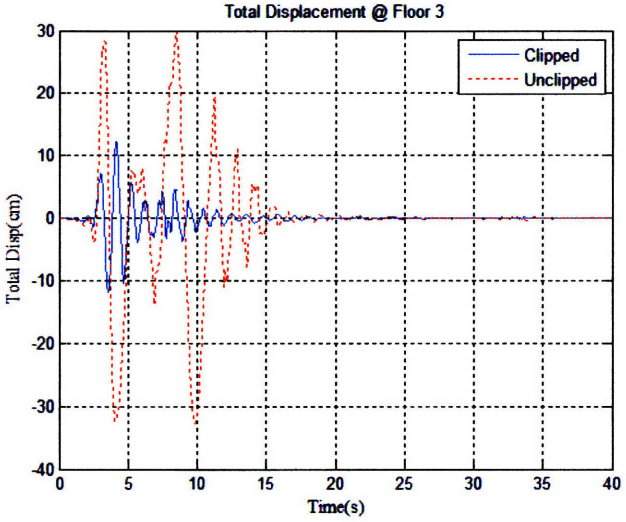


**Figure 133: Total Displacement Floors 2 & 3 due to Pacoima earthquake: Continuous unclip/clip**

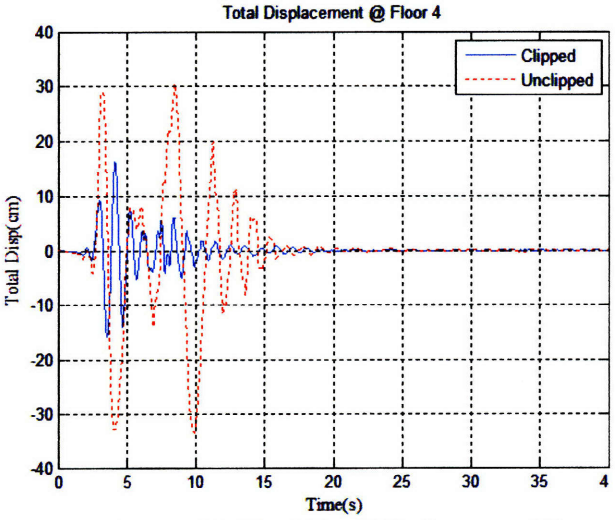


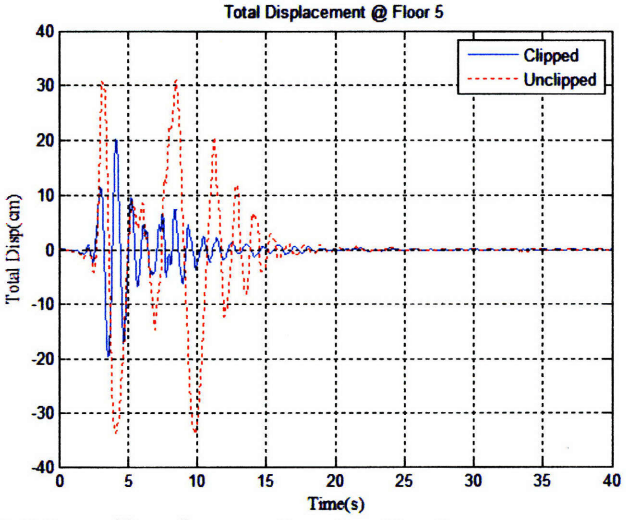


**Figure 134: Total Total Displacement Floors 4 & 5 due to Pacoima earthquake: Continuous unclip/clip**

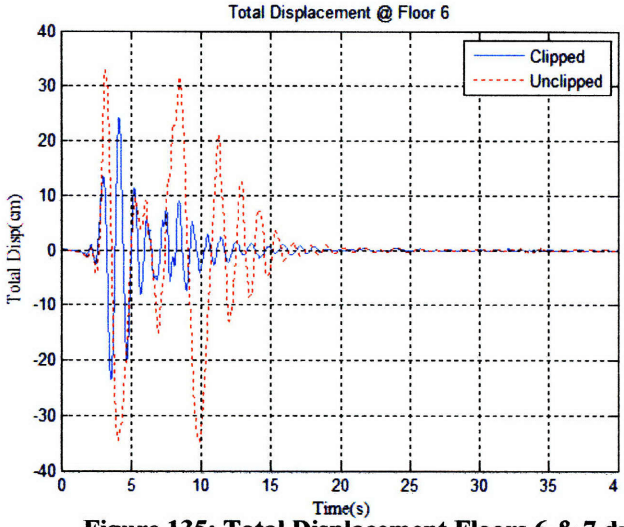


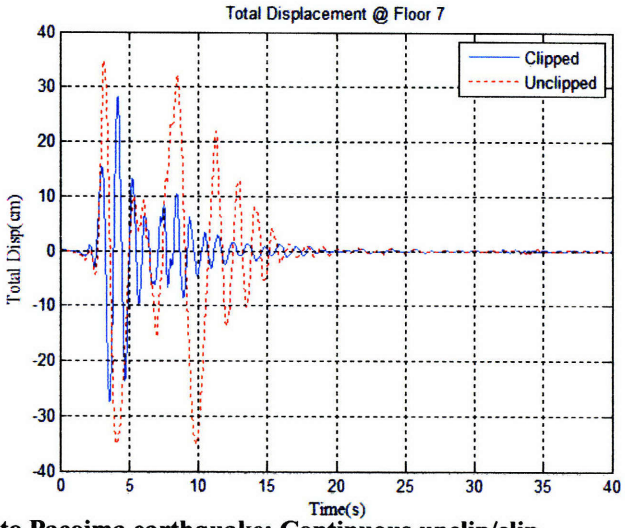


**Figure 135: Total Displacement Floors 6 & 7 due to Pacoima earthquake: Continuous unclip/clip**

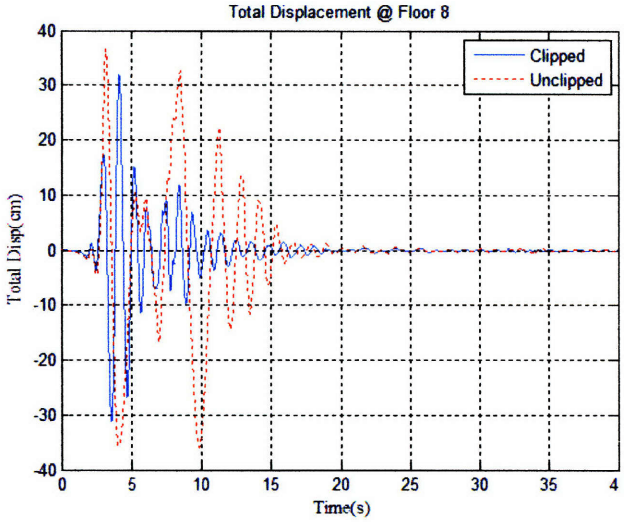


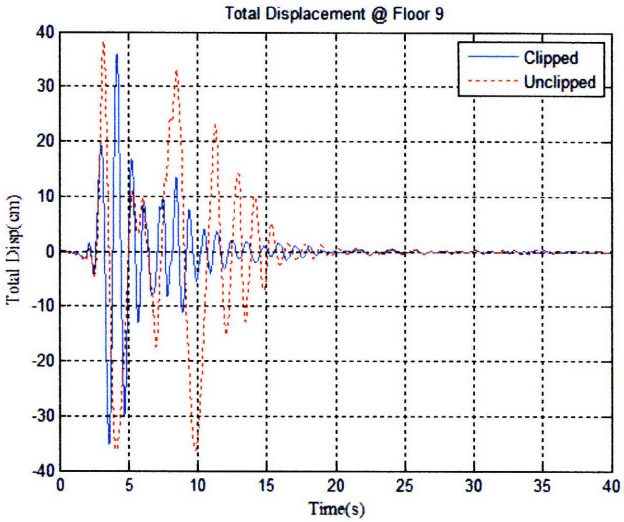


**Figure 136: Total Displacement Floors 8 & 9 due to Pacoima earthquake: Continuous unclip/clip**

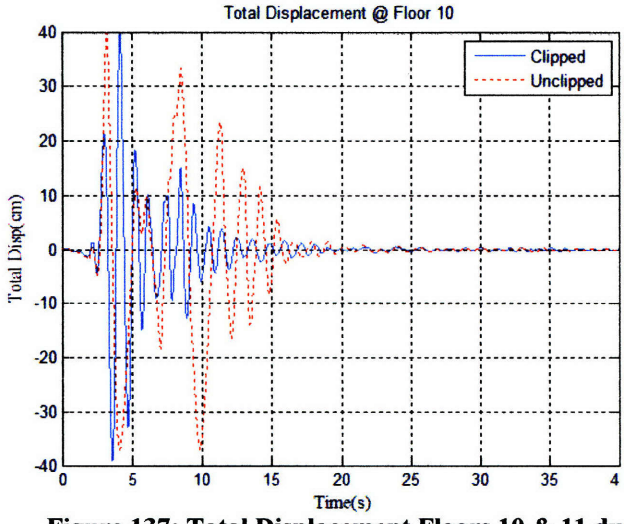


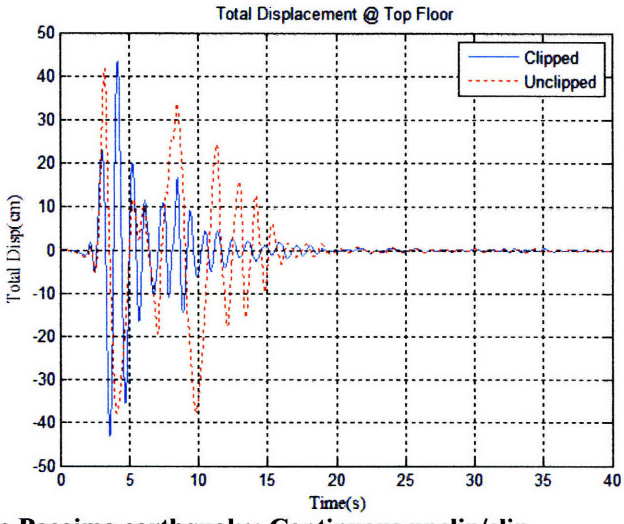


**Figure 137: Total Displacement Floors 10 & 11 due to Pacoima earthquake: Continuous unclip/clip**

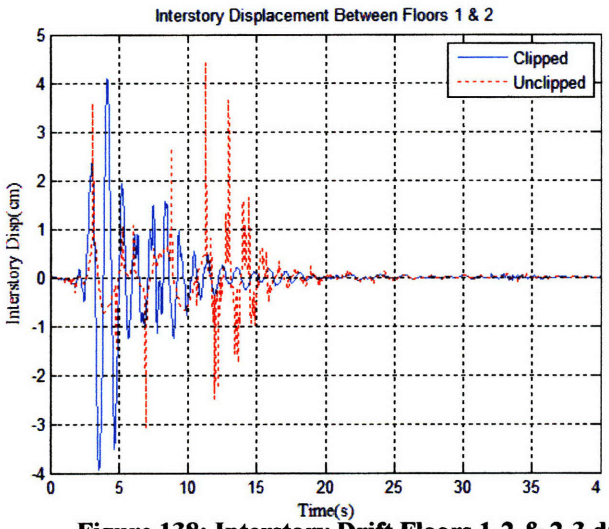


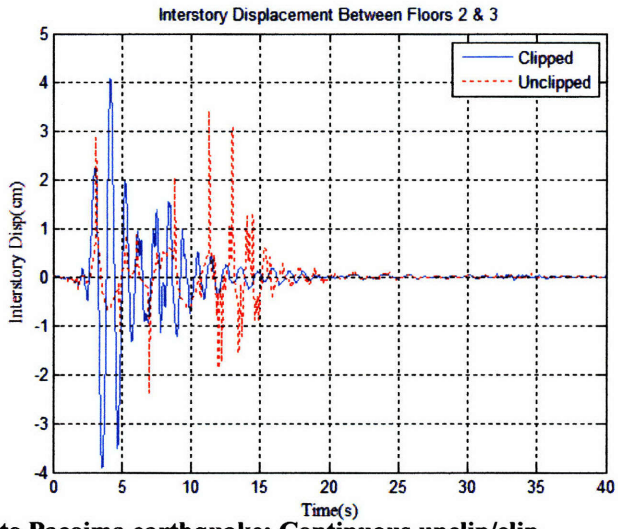


**Figure 138: Interstory Drift Floors 1-2 & 2-3 due to Pacoima earthquake: Continuous unclip/clip**

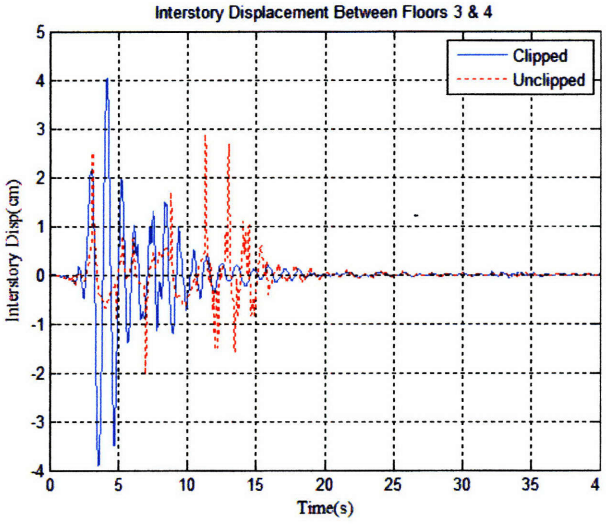


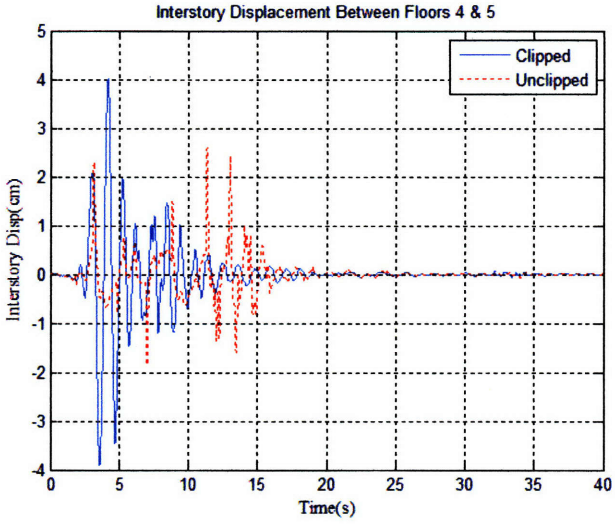


**Figure 139: Interstory Drift Floors 3-4 & 4-5 due to Pacoima earthquake: Continuous unclip/clip**

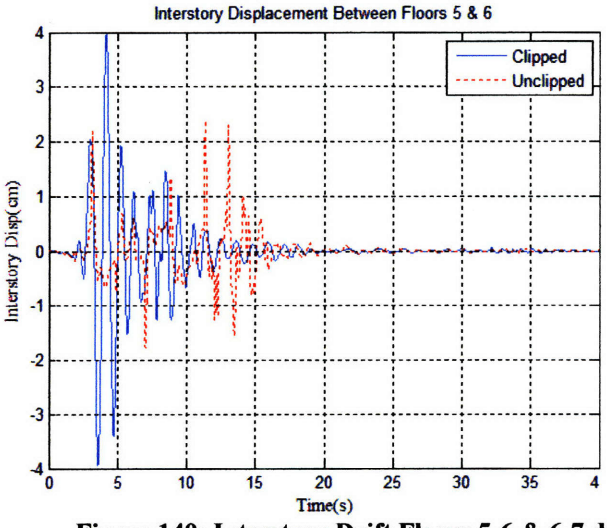


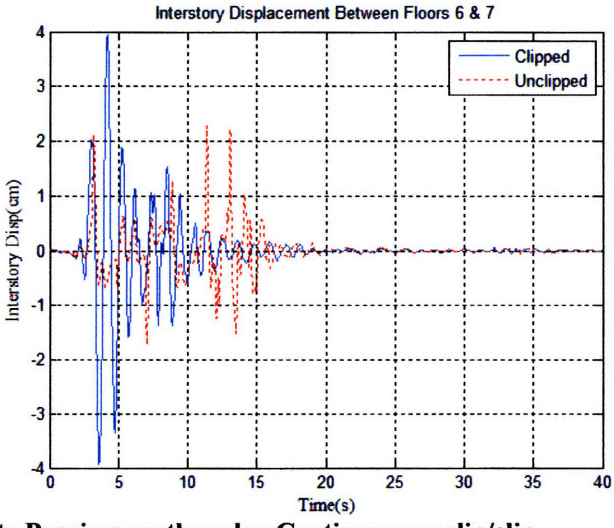


**Figure 140: Interstory Drift Floors 5-6 & 6-7 due to Pacoima earthquake: Continuous unclip/clip**

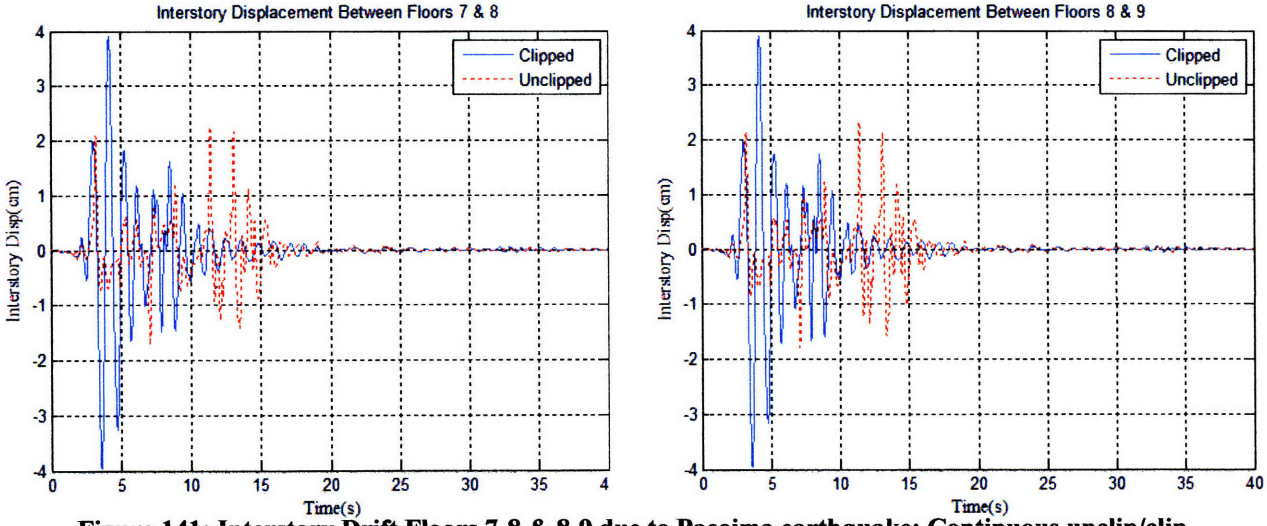


**Figure 141: Interstory Drift Floors 7-8 & 8-9 due to Pacoima earthquake: Continuous unclip/clip**

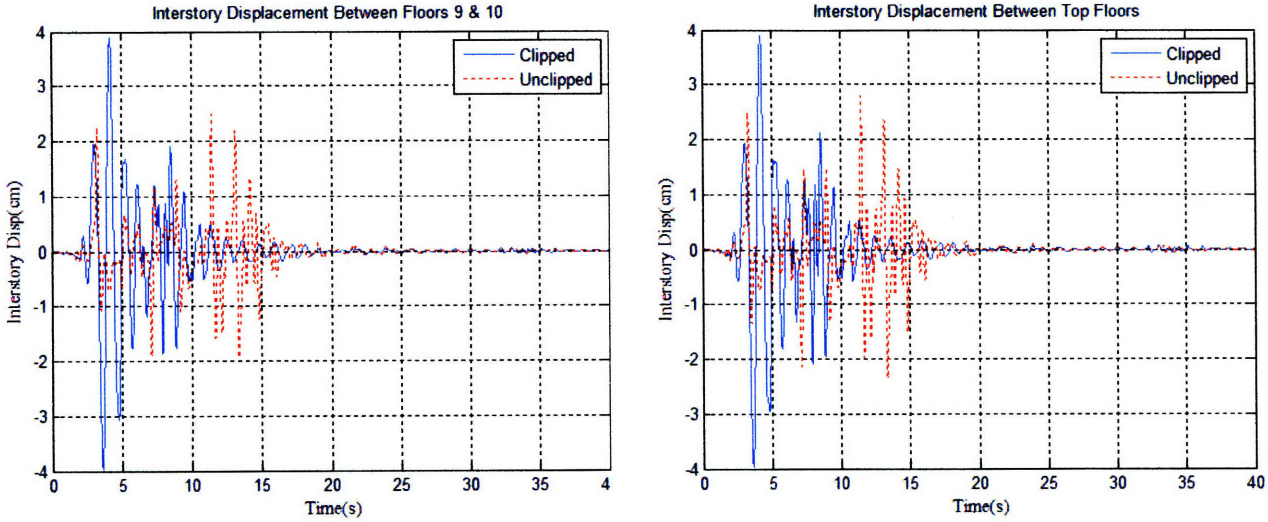


**Figure 142: Interstory Drift Floors 9-10 & 10-11 due to Pacoima earthquake: Continuous unclip/clip**

Appendix H: Wind Response

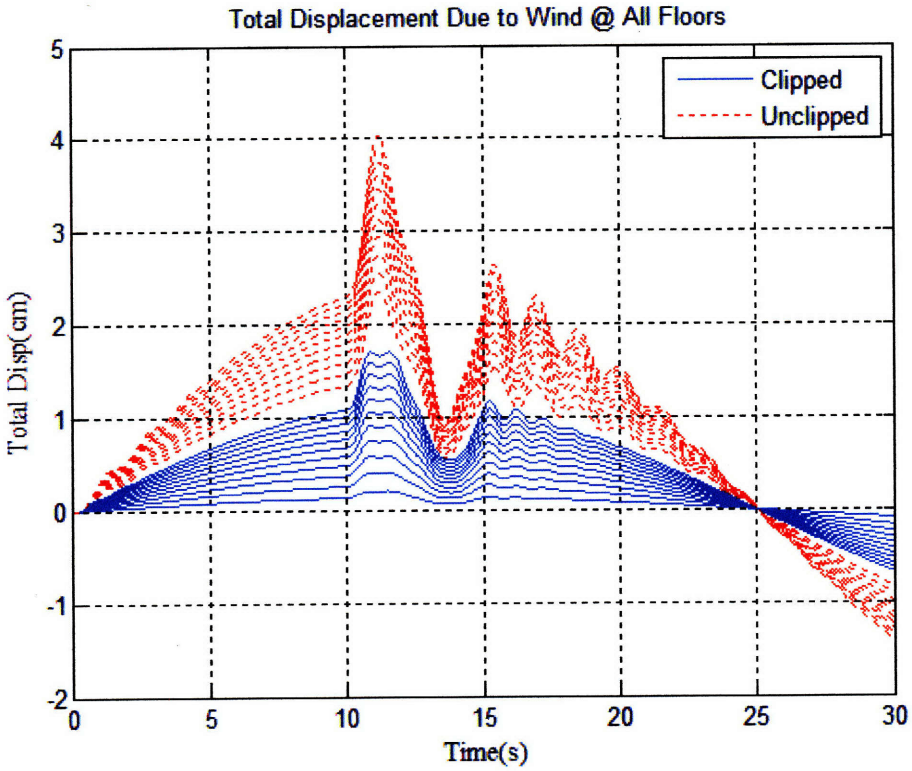


**Figure 143: Total displacement due to wind for all floors**

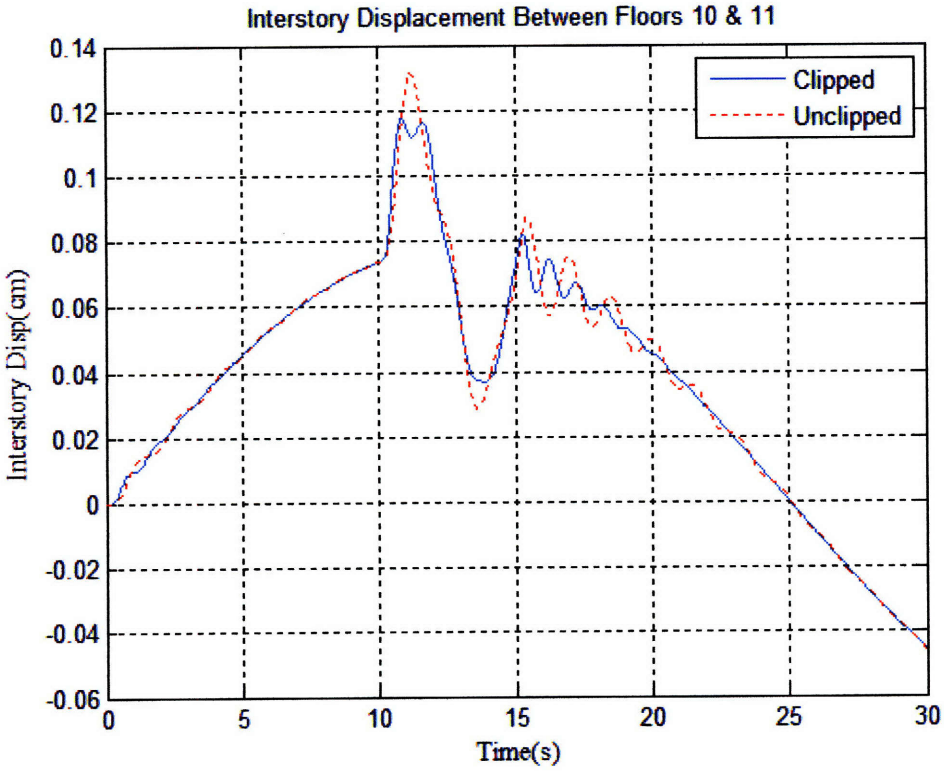


**Figure 144: Interstory displacement due to wind between floors 10 and 11**